Titre: Title:	Broadband Quasi-Phase-Matched Wavelength Converters
Auteur: Author:	Amirhossein Tehranchi
Date:	2010
Type:	Mémoire ou thèse / Dissertation or Thesis
Référence: Citation:	Tehranchi, A. (2010). Broadband Quasi-Phase-Matched Wavelength Converters [Ph.D. thesis, École Polytechnique de Montréal]. PolyPublie. https://publications.polymtl.ca/329/

URL de PolyPublie: PolyPublie URL:	https://publications.polymtl.ca/329/
Directeurs de recherche: Advisors:	Raman Kashyap
Programme: Program:	Génie Électrique

UNIVERSITÉ DE MONTRÉAL

BROADBAND QUASI-PHASE-MATCHED WAVELENGTH CONVERTERS

AMIRHOSSEIN TEHRANCHI

DÉPARTEMENT DE GÉNIE ÉLECTRIQUE

ÉCOLE POLYTECHNIQUE DE MONTRÉAL

THÈSE PRÉSENTÉE EN VUE DE L'OBTENTION

DU DIPLÔME DE PHILOSOPHIÆ DOCTOR (Ph.D.)

(GÉNIE ÉLECTRIQUE)

JUIN 2010

UNIVERSITÉ DE MONTRÉAL

ÉCOLE POLYTECHNIQUE DE MONTRÉAL

Cette thèse intitulée:

BROADBAND QUASI-PHASE-MATCHED WAVELENGTH CONVERTERS

Présentée par: TEHRANCHI, Amirhossein

en vue de l'obtention du diplôme de : PHILOSOPHIAE DOCTOR

a été dûment acceptée par le jury d'examen constitué de :

M. CALOZ, Christophe, Ph.D., président

M. KASHYAP, Raman, Ph. D., directeur de recherche

M. WU, Ke, Ph.D., membre

M. HAUGEN, Harold K., Ph.D., membre

To My Mother

(In Memory of My Father)

ACKNOWLEDGMENTS

Greatest thanks to my supervisor, Prof. Raman Kashyap, who has been an invaluable source of direction and support for my project. Without his encouragement, patience and guidance I could never have accomplished this research and would never have gained what I did from it.

I would like to express my deep gratitude to Prof. K. Wu, the director of the Center of Research in Radiofrequency Electronics (CREER) and Poly-Grames Research Center for his encouraging and helpful suggestion on my research proposal in pre-doc exam.

I thank the other two members of my thesis defense committee, Prof. C. Caloz and Prof. H. K. Haugen.

I would like to thank Prof. J. Yao, from the Microwave Photonics Lab, University of Ottawa, for fruitful discussions on my research proposal in pre-doc exam.

I would like to acknowledge Prof. C.-Q. Xu, from the Department of Engineering Physics, McMaster University, for helpful suggestion.

I am also thankful to Prof. N. Granpayeh from the Department of Electrical Engineering, K. N. Toosi University of Technology, with whom I first started the research on nonlinear fiber optics during my Master program.

I would like to thank my friends and colleagues in Advanced Photonics Concept Laboratory (APCL) and Poly-Grames Research Center for their friendship, help and discussions.

I thank all friends specially Ebrahim Mortazy, Ramin Deban, Alireza Hassani, Hamidreza Memarzadeh and Meenu Meenu for their encouragement and help.

I would like to thank my parents for the sacrifices they have made to help me pursue my interests, my beloved sister Gita, and my dear fiancée Azadeh for love and support.

RÉSUMÉ

Cette thèse propose de nouveaux concepts dans la conversion de fréquence optique à large bande dans les dispositifs à ondes guidées par quasi-accord de phase (*QPM*). Ces dernières années, la *QPM* a été appliquée avec succès à l'aide des réseaux de domaines inversés en matériaux non linéaires comme le niobate de lithium, en inversant le signe du deuxième ordre coefficient non linéaire, pour tirer parti le plus fort coefficient non linéaire de la génération seconde harmonique (*SHG*), la génération fréquence somme (*SFG*) et la génération fréquence différence (*DFG*). Toutefois, une structure périodique a un impact négatif de limiter la bande passante.

Même si une structure apériodique contribue à augmenter la bande passante, elle apporte des ondulations sur l'efficacité de conversion réduite, ce qui limite des applications. Néanmoins, une modification de la structure basée sur le quasi-accord de phase semble prometteuse pour fournir une large bande passante avec l'efficacité, et l'ondulation voulue. Il a été démontré pour la première fois dans cette thèse que l'utilisation de la technique de l'apodisation des réseaux apériodiques modifiée "*apodized step-chirped gratings (ASCG)*", la bande passante d'un doubleur de fréquence, basé sur la *SHG* en guide d'ondes du niobate de lithium, peut être élargie volontairement et les ondulations peuvent être réduites (< ±0.05dB). Cela signifie également que le dispositif peut être utilisé comme une source sur une large gamme de température. Il a été vérifié que l'utilisation de l'*ASCG*, la bande passante large (> 50 nm) est suffisamment contrôlable ; et la grande largeur de domaine et les étapes de *chirp* facilitent la fabrication des dispositifs. Ces dispositifs à large bande peuvent premièrement être utilisés pour la conversion de longueur d'onde variable dans les futurs réseaux optiques. Deuxièmement, ils mènent à l'avenir pour la réalisation de convertisseurs de fréquence à haute efficacité pour les écrans.

Toutefois, l'efficacité de la *SHG* pour un dispositif avec l'*ASCG* est plus faible que celle du réseau uniforme avec la même longueur. Il est démontré pour la première fois qu'il est possible d'accroître l'efficacité de la *SHG* d'un dispositif avec l'*ASCG*, en utilisant un guide d'onde à faible perte avec petite surface effective et avec la résonance des harmoniques fondamentales, ce qui

permet de réaliser très efficace doubleurs de fréquence à large bande. Le dispositif efficace avec l'*ASCG* permet également du doublement de fréquence d'une source à large bande pour des nouvelles applications telles que la tomographie par cohérence optique (*OCT*), étant donné que la résolution axiale pour la lumière à large bande en longueurs d'onde plus courte est plus satisfaisante.

D'autres configurations modifiées ont également été proposées dans cette thèse, celles-ci conduisent à élargir la bande passante et l'amélioration de l'efficacité des convertisseurs de longueurs d'onde, fondées sur la génération de fréquence somme et différence en cascade (*SFG + DFG*) avec un seul passage et doubles passages, qui utilisent quasi-accord de phase dans les guides d'ondes du niobate de lithium. Néanmoins, en augmentant la différence de longueur d'onde des pompes de la *SFG + DFG* en cascade, la bande passante peut être améliorée, mais avec une variation notable sur la réponse de l'efficacité pour les plus grandes différences de longueur d'onde des pompes, qui convertit le signal des canaux de façon inégale.

Deux solutions différentes à savoir, le désaccord de longueur d'onde d'une pompe et en utilisant "*step-chirped gratings (SCG)*", ont été proposées pour résoudre ce problème aux configurations avec un seul passage et doubles passages. Il est montré que, si la longueur d'onde de la pompe ou la période de la *SCG* est augmentée légèrement, les désaccords de phase de la *SFG* et la *DFG* sont diminuées différemment, ce qui conduit à un aplatissement de la variation de la réponse.

Pour la première fois, il est démontré que, pour la même longueur et la même puissance, l'amélioration de l'efficacité attendue, en raison de l'utilisation de la configuration avec les doubles passages plutôt que le seul passage, est terminée pour une perte de guide d'ondes. En outre, il est établi dans cette thèse que la configuration avec les doubles passages en utilisant guide d'onde à faibles pertes, est capable d'améliorer l'efficacité de conversion, tandis que l'aplatissement de la réponse de l'efficacité ($< \pm 0.05$dB) est accompli en augmentant le désaccord de la longueur d'onde d'une pompe ou bien en utilisant la *SCG*.

Pour les systèmes du multiplexage en longueur d'onde (*WDM*) de l'avenir, le 3-dB bande passante des convertisseurs de longueur d'onde doit être suffisamment large pour couvrir la fenêtre de fibre optique à 1,55 μm. Il conviendra si les pompes sont fixées aux longueurs d'onde hors de la fenêtre optique qui est au moins de 75 nm de large, tandis que nous avons besoin de réponses à

plat avec l’efficacité de conversion élevée. Par conséquent, pour différents dispositifs avec un seul passage et doubles passages, des schémas de conception pour le choix de la longueur de guide d'ondes à faible perte et le choix de la puissance des pompes sont présentés pour atteindre l'efficacité, l’ondulation et la bande passante souhaitée.

ABSTRACT

This thesis proposes new concepts in broadband optical frequency conversion in quasi-phase matched guided-wave devices. Quasi-phase matching (QPM) using domain-inverted gratings in nonlinear materials such as lithium niobate (LN) by reversing the sign of the second-order nonlinear coefficient, has been successfully applied in recent years to take advantage of the highest nonlinear coefficient for second harmonic generation (SHG), sum frequency generation (SFG) and difference frequency generation (DFG). Nevertheless, the periodic quasi-phase matched structure has a negative impact by limiting the bandwidth of frequency up-conversion.

Although an aperiodic quasi-phase matched structure can help to increase the bandwidth, it may cause ripples to appear in the reduced conversion efficiency response, which has detrimental implications for applications. However, an *engineered* quasi-phase matched structure seems to be a promising route to achieving a wide bandwidth with a desired efficiency, and tailored ripple. In this dissertation, it has been demonstrated for the first time that using the technique of *apodization* with *chirped* gratings, the bandwidth of frequency doublers based on SHG in lithium niobate waveguides can be broadened at will, and the ripple damped out ($< \pm 0.05$dB) to be low enough so as to be considered almost flat. A consequence of this technique is that the guided wave device may be used as a source over a wide unregulated temperature range, for the first time. It has been shown that using the *apodized step-chirped gratings* (ASCG) approach, the wide spectral conversion efficiency profile (> 50 nm) is suitably controllable. The large domain-widths and chirp-steps ease device manufacture. The impact of this design is clearly very high as firstly, this broadband wavelength converter can be used for variable waveband wavelength conversion in future all-optical networks, as the device based on the cascaded second harmonic generation and difference frequency generation (SHG + DFG), should be a broadband frequency doubler. Secondly, for displays it may lead to the realization of high-efficiency three-color frequency converters that do not change in intensity, even without the use of temperature control.

However, the SHG efficiency of an ASCG device is lower than that of the uniform grating with the same length. It is shown for the first time that it is possible to increase the efficiency of an ASCG device for broadband frequency doubling, by using a tight confinement in small-effective-cross-section low-loss waveguides, and with the resonance of fundamental harmonics in a singly pump-resonance waveguide. Another advantage of the efficient ASCG device is that it may allow frequency doubling of ultra-broadband light for novel applications such as dual-band optical coherence tomography (OCT) of tissues as the axial resolution length using wideband light at shorter wavelengths is more satisfactory. This OCT may have the advantage of higher penetration depth, providing additional phase and scattering information on the tissue sample examined.

The modified single-pass and double-pass configurations are also proposed in this dissertation lead to bandwidth broadening and efficiency enhancement of waveband wavelength converters based on quasi-phase matched cascaded sum frequency generation and difference frequency generation (SFG + DFG) in LN waveguides. It has been shown that increasing the pump wavelength difference in cascaded SFG + DFG devices, enhances the bandwidth, but with noticeable variation in efficiency response for larger pump wavelength differences, leading to uneven equal-input-power signal channel conversion.

Two different solutions have been suggested in this thesis to solve the problem in both single-pass and double-pass configurations, namely, detuning of a pump wavelength, and using a few-section step-chirped grating (SCG). It is shown that, if a pump wavelength is increasingly detuned, the SFG and DFG phase-mismatch decreases differently which leads to flattening of the conversion efficiency response. Alternatively, the period of a few-section SCG can also be increased slightly to arrive at a similar result.

Also, for the first time, it is shown that for the same length and power, the efficiency *enhancement*, expected due to the use of a double-pass configuration instead of a single-pass one, is lost for a particular waveguide loss. Further, it is demonstrated that a double-pass configuration with a low-loss waveguide is capable of improving the conversion efficiency while the efficiency response flattening ($< \pm 0.05$dB) is accomplished by two schemes namely increasing the wavelength detuning of one pump or alternatively using the SCG structure.

The role of these schemes is very important as wide waveband converters can be used for the wavelength division multiplexing (WDM) systems, in which the 3-dB bandwidth of the device should be broad enough to cover the 1.55 μm optical window. For this purpose, the pumps are set at wavelengths out of the optical window which is 75-nm wide, whilst we obtain flat responses with high conversion efficiency. For different single-pass and double-pass configurations using pump detuning or the SCG, design diagrams for the choice of low-loss waveguide length, and the assignment of pump powers of to achieve the desired efficiency, ripple and bandwidth are presented.

CONDENCÉ EN FRANÇAIS

Ces dernières années, il ya eu un grand intérêt pour les convertisseurs de longueur d'onde basée sur le quasi-accord de phase (*QPM*) dans les guides d'ondes optiques non linéaires, car la conversion de longueur d'onde peut être fait dans différentes bandes dans la région de la transparence du milieu par une conception appropriée de domaines inversée.

La *QPM* a été appliquée avec succès à l'aide des réseaux de domaines inversés en matériaux non linéaires, en inversant le signe du deuxième ordre coefficient non linéaire, pour tirer parti le plus fort coefficient non linéaire de la génération seconde harmonique (*SHG*), la génération fréquence somme (*SFG*) et la génération fréquence différence (*DFG*).

Aujourd'hui, le niobate de lithium est le matériel ferroélectrique dominant utilisé en optique non linéaire intégrée. Construits en niobate de lithium polarisé périodiquement (*PPLN*) avec guides d'ondes, des convertisseurs de longueur d'onde ont attiré une attention considérable en raison de leurs excellentes propriétés. Ils ont été largement étudiés et trouvés de nombreuses applications dans les communications et le traitement du signal dans la dernière décennie. Ils présentent à haute vitesse, petite taille, haute efficacité, faible bruit, haute transparence pour le format de modulation du signal.

Toutefois, une structure périodique a un impact négatif de limiter la bande passante. Même si une structure apériodique contribue à augmenter la bande passante, elle apporte des ondulations sur l'efficacité de conversion réduite, ce qui limite des applications. Néanmoins, une modification de la structure basée sur le quasi-accord de phase semble prometteuse pour fournir une large bande passante avec l'efficacité, et l'ondulation voulue.

Cependant, il ya eu un intérêt particulier pour réaliser des convertisseurs à large bande basés sur la génération seconde harmonique dans les guides d'ondes non linéaires comme il ya plusieurs applications. Pour la communication optique, une demande importante de la *SHG* à large bande

est dans la conversion variable de longueur d'onde basée sur la génération seconde harmonique et la génération de la fréquence différence en cascade (*SHG* + *DFG*) qui a besoin d'un doubleur de fréquence à large bande. Dans les anciens schémas, la bande passante de la pompe est étroite et donc les signaux peuvent être convertis en longueurs d'onde limitée qui se traduisent par l'inflexibilité du convertisseur variable de longueur d'onde.

Une autre application est dans la transformation des signaux optiques ultrarapides dans lequel le problème est associé à générer des impulsions ultra-courtes pour la seconde harmonique, aux réseaux périodiques de *PPLN*. Aussi, le convertisseur à large bande est bon pour la tomographie par cohérence optique (*OCT*), une technique utilisée pour diagnostiquer divers troubles médicaux.

Dans ce cas, dispositifs à large bande agirent comme une source de la lumière à large bande pour des longueurs d'onde plus courte. La raison de l'utilisation de la source à large bande dans un système *OCT* est la relation inverse entre la largeur de bande de la lumière et de la résolution axiale. La source de lumière à large bande dans le proche infrarouge est utilisée parce que la résolution axiale est aussi proportionnelle au carré de la longueur d'onde de la lumière.

Néanmoins, le problème lié à la conversion de longueurs d'onde fondée sur la *SHG* dans *PPLN* est la bande passante étroite, comme la bande passante dépend de l'inverse de la longueur du réseau de *PPLN*. Une solution simple consiste à utiliser un guide d'ondes courtes de *PPLN* pour obtenir une bande passante large. Toutefois, cela ne fonctionne pas ainsi que d'atteindre une efficacité raisonnable, il a besoin de très forte puissance d'entrée qui ne peut pas être tolérée par le guide d'ondes dans *PPLN*.

Ainsi, le réseau à pas variable a été proposé d'élargir la bande passante en changeant la période des domaines inversés en fonction de la longueur. Grâce à cette structure, élargissement de la bande passante de conversion est atteinte, mais avec une réponse fluctuée qui n'est pas acceptable pour les applications précitées. Il est également important qu'elle présente une bande passante plus large pour l'acceptation de la température que le réseau périodique (à pas constant) et fournit une plus grande stabilité du doublement de fréquence.

Toutefois, il existe trois problèmes en utilisant les réseaux à pas variable. Le premier problème pour la réalisation d'un dispositif à large bande est l'étroitesse du changement de période. Pour le réseau avec des variations linéaires de changement de la période qui est appelé *linear-chirp grating* (*LCG*), il est généralement d'environ 100 picomètres ou moins pour un convertisseur avec quelques nanomètres de largeur de bande.

Nous allons montrer pour la première fois que l'utilisation du réseau avec des variations comme étape pour le changement de la période qui est appelé *step-chirp grating* (*SCG*), il est possible d'augmenter le changement de période pour la commodité de fabrication alors que la bande passante et l'efficacité restent presque les mêmes par rapport à la *LCG*.

Le deuxième problème est la fluctuation considérable sur la réponse de l'efficacité de la *LCG* et *SCG*. La méthode pour aplatir la réponse de la *SHG* est d'utiliser *apodisation*. Ici, nous pouvons le faire en changeant le rapport entre la largeur du créneau et la période dans des régions polarisées, qui contribue à éliminer les ondulations et obtenir des réponses à plat.

Le troisième problème est lié à l'efficacité médiocre de la *SHG* pour la *SCG* apodisée (*ASCG*). L'efficacité peut être augmentée pour guides d'ondes avec la petite surface effective avec ou sans résonance. Néanmoins, il est démontré pour la première fois que l'utilisation du guide d'ondes avec la résonance de la pompe, forte amélioration de l'enveloppe de la réponse de l'efficacité de la *SHG* à large bande est possible.

Dans cette thèse, l'ingénierie des réseaux ou des domaines inversée, dans les guides d'ondes à faible perte qui est fabriqué par la diffusion du titane dans le niobate de lithium (*Ti:LN*), est présentée de telle manière à élargir la bande passante de la *SHG* de façon significative. Une formule de conception est proposée pour la première fois, de décider combien de segments on devrait utiliser comme une règle de conception, qui est dépendante de la bande passante requise. En outre, nous considérons une méthode de l'apodisation pour aplatir la bande passante de la *SHG* par la conception de l'augmentation et la diminution de domaines inversés dans les réseaux.

Il a été démontré pour la première fois dans cette thèse que l'utilisation de la technique de l'*ASCG*, la bande passante d'un doubleur de fréquence, basé sur la *SHG* en guide d'ondes du

niobate de lithium, peut être élargie volontairement et les ondulations peuvent être réduites (< ±0.05dB). Cela signifie également que le dispositif peut être utilisé comme une source sur une large gamme de température. Il a été vérifié que l'utilisation de l'*ASCG*, la bande passante large (> 50 nm) est suffisamment contrôlable; et la grande largeur de domaine et les étapes de *chirp* facilitent la fabrication des dispositifs.

Néanmoins, le concept proposé de l'*ASCG* peut être appliqué au quasi-accord de phase à large bande pour les autres matériaux non linéaires, avec ou sans guide d'ondes. Enfin, la bande passante de conversion de 50 nm (et même plus) peut être obtenu avec la conception spéciale de l'*ASCG* avec le 1-μm de largeur de ligne, pour nous fournir une réponse uniforme et de faciliter le processus de la fabrication.

Il est démontré que l'efficacité de la *SHG* pour l'*ASCG* dans guides d'ondes (*Ti:LN*) peut être améliorée en utilisant des guides d'ondes avec la petite surface effective. Pour atteindre cet objectif, guides d'ondes réalisés par échange protonique recuit (*APE*) sont utilisés en raison de la possibilité d'une différence d'indice plus élevé, des modes bien confinés en raison des petites surfaces des champs des modes.

En plus, pour la résonance de la pompe, il est démontré que, pour la pompe quasi continue il est possible d'augmenter efficacement l'enveloppe de l'efficacité de la conversion des modes de résonance axiale (surtout pour les faibles pertes), tandis que la bande passante de conversion reste à peu près les mêmes. Les valeurs optimisées de réflectivité pour une facette arrière et une puissance d'entrée ont aussi été présentées pour atteindre l'efficacité maximale, pour les pertes des guides d'ondes.

Il ya eu aussi un grand intérêt pour le développement des convertisseurs de longueur d'onde à large bande pour la bande de communication (*waveband*) basée sur $\chi^{(2)}$ en cascade, à savoir (*SHG* + *DFG*) en cascade, et la génération de la fréquence somme et différence en cascade (*SFG* + *DFG*) pour le futur système du multiplexage en longueur d'onde (*WDM*).

Pour les systèmes du *WDM* de l'avenir, le 3-dB bande passante des convertisseurs de longueur d'onde doit être suffisamment large pour couvrir la fenêtre de fibre optique à 1,55 μm. Il

conviendra si les pompes sont fixées aux longueurs d'onde hors de la fenêtre optique qui est au moins de 75 nm de large, tandis que nous avons besoin de réponses à plat avec l'efficacité de conversion élevée.

L'avantage le plus notable des dispositifs basés sur $\chi^{(2)}$ en cascade est la large couverture de longueur d'onde pendant que la pompe, signal et le signal converti sont dans la même bande. Ils peuvent offrir une bande passante large et une haute efficacité avec la puissance modérée de la pompe.

En plus de la fonction de conversion de longueurs d'onde, ces dispositifs peuvent effectuer des différents traitements de signaux optiques ultrarapides comme la commutation tout-optique, offrant des possibilités d'applications pour les réseaux photoniques ultrarapide basée sur le multiplexage temporel optique (*OTDM*).

Les convertisseurs de longueur d'onde fondée sur $\chi^{(2)}$ en cascade également offrent une variété de possibilités pour des applications dans le traitement du signal y compris la génération de *millimeter-wave/THz* et la radio sur fibre.

La *DFG* et *SHG* + *DFG* en guide d'ondes dans *PPLN*, a déjà été montrée à la fois théoriquement et expérimentalement avec plusieurs applications. Pour la conversion de longueurs d'onde dans une bande de communication, un avantage de la *SHG* + *DFG* en cascade par rapport à la *DFG* est qu'une pompe avec la longueur d'onde dans la même bande du signal peut être utilisée. Toutefois, il est difficile d'obtenir une haute efficacité avec une pompe de faible puissance dans la *SHG* + *DFG* en cascade avec un seul passage.

Pour résoudre ce problème, la *SHG* + *DFG* en cascade avec des doubles passages est une bonne technique pour accroître l'efficacité, mais avec une petite perte de bande passante. Néanmoins, l'inconvénient de la *SHG* + *DFG*, par exemple pour les systèmes *WDM*, est que plusieurs canaux doivent être sacrifiés parce que la longueur d'onde de la pompe doit être fixée au centre de la bande de conversion occupant les places des canaux possibles.

Une technique intéressante de conversion de longueurs d'onde fondée sur la *SFG* + *DFG* en cascade, a été démontrée théoriquement et pratiquement dans les guides d'ondes *PPLN* et a

trouvé de vastes applications y compris la conversion de longueur d'onde à large bande, la conversion des canaux sélectionnés et multiples et la conversion de format. Pourtant, la bande passante de 3 dB de ces convertisseurs devrait être suffisamment large pour couvrir la fenêtre optique en 1,55 μm. Il conviendra pour des applications pratiques si nous pouvons définir les pompes hors de la fenêtre optique qui est au moins 75 nm, alors que nous avons besoin de réponses à plat avec l'efficacité élevée de conversion.

En utilisant cette technique, en augmentant la différence de longueur d'onde de pompe, la bande passante pourrait être améliorée. Toutefois, la moyenne de l'efficacité de conversion dépend de la longueur d'onde de la pompe et celle-ci est diminuée en augmentant la différence de longueur d'onde de pompe.

Deux solutions différentes à savoir, le désaccord de longueur d'onde d'une pompe et en utilisant la *SCG*, ont été proposées pour résoudre ce problème. Pour compenser la réduction de l'efficacité, la *SFG* + *DFG* en cascade avec des doubles passages a été proposée qui est également capable de filtrer les longueurs d'onde de pompe résiduelle à la sortie.

Cependant, pour la longueur d'onde de pompe, le quasi-accord de phase de la *SFG* est parfaitement respecté tandis que le désaccord de phase de la *DFG* est grand lorsque le signal est loin de la pompe. Ainsi, le désaccord augmente la variation de la conversion pour la grande différence de la longueur d'onde des pompes, qui convertit le signal des canaux de façon inégale.

Bien que la *SFG* + *DFG* en cascade a été principalement étudiée, la recherche sur la façon de définir exactement les pompes ou encore la façon de concevoir les réseaux pour améliorer les propriétés de conversion reste toujours et il est de grande importance. Les solutions au problème sont proposées pour la première fois, en dispositifs avec un seul passage et des doubles passages en utilisant le désaccord de la longueur d'onde de pompe, ou en utilisant alternativement la *SCG*. Nous montrons que, si la longueur d'onde de la pompe ou l'étape de *chirp* de la *SCG* est légèrement augmentée, les désaccords de phase de la *SFG* et *DFG* sont réduits ce qui conduit à un aplatissement de la variation de la réponse.

Dans cette thèse, nous évaluons et comparons numériquement les propriétés de la *SHG + DFG* et *SFG + DFG* en cascade lorsque la différence de longueur d'onde de pompe est 0 nm et 75 nm, respectivement, et nous montrons que pour la même longueur, l'adoption de la *SFG + DFG* améliore encore la bande passante avec une légère diminution de l'efficacité et une augmentation de l'ondulation.

En outre, nous présentons les critères de sélection de la longueur du guide d'ondes et la puissance de pompe pour obtenir l'efficacité, l'ondulation et la bande passante requise. Nous montrons que l'augmentation du désaccord de longueur d'onde d'une pompe, dans le dispositif avec le seul passage, supprime l'ondulation avec une pénalité sur l'efficacité moyenne.

L'introduction de la structure de la *SCG* avec une conception appropriée, elle offre presque la même bande passante et de la planéité avec moins de pénalité de l'efficacité par rapport au dispositif avec le désaccord de la pompe. Nous aussi présentons les diagrammes de conception du dispositif avec le seul passage pour la sélection de la longueur et la puissance pour obtenir l'efficacité, l'ondulation et la bande passante requise.

En plus, les propriétés de la *SHG + DFG* et *SFG + DFG* en cascade avec des doubles passages sont évaluées et comparées numériquement lorsque la différence de longueur d'onde de pompe est de 0 nm et 75 nm, respectivement. Il est démontré que, pour la même longueur de guide d'ondes à faible perte, l'adoption des dispositifs avec des doubles passages, en utilisant le désaccord de la pompe ou alternativement de la *SCG*, améliore encore les performances d'efficacité avec une petite réduction de la bande passante, par rapport à celles des dispositifs avec un seul passage.

Il est démontré que, pour la même longueur et la puissance, l'amélioration de l'efficacité attendue, en raison de l'utilisation des dispositifs avec des doubles passages au lieu d'un seul passage, est finalement interrompue pour une perte de guide d'ondes. Nous présentons les diagrammes de la conception des dispositifs avec des doubles passages, pour le choix de la longueur et la puissance pour obtenir l'efficacité, l'ondulation et la bande passante nécessaire.

LIST OF PUBLICATION RELATED TO THE DISSERTATION

Journals

1. A. Tehranchi, and R. Kashyap, "Wideband wavelength conversion using double-pass cascaded $\chi^{(2)} : \chi^{(2)}$ interaction in lossy waveguides," Opt. Commun., vol. 283, pp. 1485-1488, 2010.

2. A. Tehranchi, and R. Kashyap, "Response flattening of efficient broadband wavelength converters based on cascaded sum- and difference frequency generation in periodically poled lithium niobate waveguides," IEEE J. Quantum Electronics, vol. 45, 9 pp. 1114-20, 2009.

3. A. Tehranchi, and R. Kashyap, "Efficient wavelength converters with flattop responses based on counterpropagating cascaded SFG and DFG in low-loss QPM $LiNbO_3$ waveguides," Optics Express, vol. 17, 21, pp. 19113–19119, 2009.

4. A. Tehranchi, and R. Kashyap, "Improved cascaded sum and difference frequency generation-based wavelength converters in low-loss quasi-phased-matched lithium niobate waveguides," Applied Optics, vol. 48, 31, pp. G143-7, 2009.

5. A. Tehranchi, and R. Kashyap, "Novel designs for efficient broadband frequency doublers using singly pump-resonant waveguide and engineered chirped gratings," IEEE J. Quantum Electronics, vol. 45, 2, pp. 187-94, 2009.

6. A. Tehranchi, and R. Kashyap, "Engineered gratings for flat broadening of second-harmonic phase-matching bandwidth in MgO-doped lithium niobate waveguides," Optics Express, vol. 16, 23, pp. 18970-75, 2008.

7. A. Tehranchi, and R. Kashyap, "Design of novel unapodized and apodized step-chirped quasi-phase matched gratings for broadband frequency converters based on second harmonic generation," IEEE J. Lightwave Technol., vol. 26, 3, pp. 343-49, 2008.

Patents

1. R. Kashyap, and A. Tehranchi, "Design of novel unapodized and apodized step-chirped quasi-phase matched gratings for broadband frequency converters based on second harmonic generation," USPTO Application # 61233230, Filed on August 2009.

Short Technical Reviews

1. A. Tehranchi, and R. Kashyap, "Efficient wavelength conversion with flattop response based on double-pass cascaded $\chi^{(2)}$ in periodically poled $LiNbO_3$ waveguides," Photons, vol. 7, 2, pp. 23-5, 2010.

Conferences (Presenter underlined)

1. A. Tehranchi, and R. Kashyap, "Pump-detuned double-pass cSFG/DFG-based wavelength converters in lossy PPLN waveguides," In Proceedings of 2010 Bragg Gratings, Photosensitivity and Poling in Glass Waveguides (BGPP) and Nonlinear Photonics (NP), NTuC21, 21-24 June, 2010, Karlsruhe, Germany. (**Received a CIPI travel award**)

2. A. Tehranchi, and R. Kashyap, "Flattop broadband wavelength converters based on double-pass cascaded SFG + DFG in quasi-phase matched waveguides," In IEEE Proceedings of the 22nd Annual Lasers and Electro Optics Society (LEOS) Meeting, ThY4, pp. 819-20, October 4-8, 2009, Antalya, Turkey.

3. A. Tehranchi, and R. Kashyap, "High-efficiency pump-resonant quasi-phase-matched frequency doublers with flat broadband responses," In Proceedings of the International Symposium on SPIE Photonic Devices + Applications, vol. 7420, August 2-6, 2009, San Diego, USA. (**Received an SPIE scholarship**)

4. Invited Paper: R. Kashyap, A. Tehranchi, and C.-Q. Xu, "Efficient broadband frequency conversion using engineered apodized $\chi^{(2)}$ gratings and fundamental harmonic resonance," In Proceedings of the 14th OptoElectronics and Communications Conference (OECC 2009),TuG6, 13-17 July, Hong Kong.

5. A. Tehranchi, and R. Kashyap, "Analysis of improved cascaded SFG+DFG wavelength converter in quasi-phase matched lithium niobate waveguide," In Proceedings of Photonics 2008 Conference, WC2.3, 13-17 December, New Delhi, India.

6. A. Tehranchi, and R. Kashyap, "Novel step-chirped quasi-phase matched gratings for flatly broadband frequency doublers with high efficiency in nonlinear-optic waveguides," In Proceedings of XXIXth General Assembly of the International Union of Radio Science (URSI 2008), D02a.5, 7-16 August 2008, Chicago, USA. (**Won the best student paper award from the Canadian National Committee**)

7. A. Tehranchi, and R. Kashyap, "A new design of apodized step-chirped gratings for broadband wavelength converters," In Proceedings of 2007 Bragg Gratings, Photosensitivity and Poling in Glass Waveguides (BGPP) and Nonlinear Photonics (NP), JMD30, 2-6 September, Quebec City, Canada.

LIST OF RELATED SCHOLARSHIPS AND AWARDS

The 2010 John Kiel Scholarship ($10,000) from SPIE - The International Society for Optics and Photonics- in May 2010.

The Travel Award from the Canadian Institute for Photonic Innovations (CIPI) for attendance at NP in June 2010.

The SPIE Scholarship in Optical Science and Engineering in May 2009.

The Charles Baskin Scholarship from École Polytechnique de Montréal in February 2009.

The URSI Student Award from the Canadian National Committee (CNC) of the International Union of Radio Science (URSI) in May 2008.

TABLE OF CONTENTS

LIST OF TABLES

LIST OF FIGURES

LIST OF ACRONYMS

ALCG	Apodized Linearly Chirped Grating
APE	Annealed Proton Exchange
aPPLN	Aperiodically Poled Lithium Niobate
ASCG	Apodized Step-Chirped Grating
BW	Bandwidth
CW	Continuous Wave
DFG	Difference Frequency Generation
EDFA	Erbium-Doped Fiber Amplifier
FH	Fundamental Harmonic
FWHM	Full-Width Half Maximum
LCG	Linearly Chirped Grating
LN	Lithium Niobate ($LiNbO_3$)
MgO	Magnesium Oxide
NLO	Nonlinear Optic
OCT	Optical Coherence Tomography
OTDM	Optical Time Division Multiplexing
PPLN	Periodically Poled Lithium Niobate
QPM	Quasi Phase Matching
SCG	Step-Chirped Grating
SFG	Sum Frequency Generation

SH	Second Harmonic
SHG	Second Harmonic Generation
THz	Terahertz
Ti:$LiNbO_3$	Titanium Indiffused Lithium Niobate (Ti:LN)
WDM	Wavelength Division Multiplexing
WG	Waveguide

LIST OF SYMBOLS AND NOTATIONS

A	Amplitude
a	Duty ratio
$a_1\Lambda_1$	Minimum line width (inverted domain)
BW	Device bandwidth
D	Depth of waveguide
d	Nonlinear coefficient
d_{eff}	Effective nonlinear coefficient
E	Electric field
j	$\sqrt{-1}$
k	Wavenumber
L'	Input apodized grating length
L''	Output apodized grating length
L	Unapodized grating length
L_i	Section (i) length (uniform grating)
L_t	Total grating length
L_c	Coherence length
n	Number of segments
N_ω	Effective index at ω
n_ω	Refractive index at ω
p'	Half number of apodized sections

p	Number of unapodized sections
P	Polarization
P_0	Input power
p_t	Total number of sections
r	Apodization ratio
R	Reflectivity
$r_{\text{p-p}}$	Peak-to-peak ripple
S_{eff}	Effective Area
T	Thickness of substrate
w	Mode width
W	Width of waveguide
α	Propagation loss
β	Propagation constant
$\delta\lambda$	Section bandwidth
$\Delta\lambda$	Total bandwidth
Δk	Phase-mismatch parameter
Δn	Refractive index difference
$\Delta\Lambda$	Chirp step
$\delta\nu$	Linewidth (resonant frequencies)
$\Delta\nu$	Mode spacing (resonant frequencies)
κ	Coupling factor
Λ	Period of inverted domain grating
τ	Round trip time

τ_p	Photon life time
ω	Angular Frequency
λ	Wavelength
λ_c	Central wavelength
ε_0	Permittivity of free space
μ_0	Permeability of free space
$\chi^{(i)}$	Susceptibility of order (i)

CHAPTER 1
INTRODUCTION

1.1 Motivation

Nonlinear optics (NLO) has found many applications in photonics. This is in part due to the availability of high quality nonlinear crystals such as lithium niobate (LN), and the access to the largest nonlinear coefficients using domain inversion by periodic poling. This technique, known as quasi phase-matching (QPM), ensures that the phases of the generated nonlinear waves remain synchronized with the fundamental input wave by reversing the sign of the nonlinearity at a period given by the dispersion of the material. There has been increasing interest in wavelength converters based on QPM in waveguides because wavelength conversion can be done in different wavelength bands within the transparency region of the medium by suitable design of domain-inverted gratings. Nowadays, LN is the dominant ferroelectric material used in nonlinear integrated optics. Built using periodically poled lithium niobate (PPLN) waveguides, quasi-phase matched wavelength converters have attracted considerable attention because of their excellent properties, having been extensively studied and found to have numerous applications in optical communications, optical signal processing and optical sensing in the past decade. They are intrinsically high speed, have a small size, high efficiency, low noise, high transparency to signal modulation format amongst other advantages. There is also a need for broadband quasi-phase matched wavelength converters in NLO waveguides, for ultrafast optical signal processing, ultrashort pulse compression, variable and broadcast wavelength conversion in optical communication, optical coherence tomography and displays. In this dissertation, new ideas for realizing such wideband wavelength converters are addressed.

1.2 Second-order NLO wavelength conversion

When intense optical waves pass through a NLO crystal, the response of the crystal cannot be considered linear [1]. The response generates optical waves at sum, difference and harmonic

frequencies. This mixing can be expressed using the relation between the dielectric polarization, P, and the applied electric field, E

$$P = \varepsilon_0 \left[\chi^{(1)} E + \chi^{(2)} E^2 + \chi^{(3)} E^3 + ... \right], \tag{1-1}$$

where $\chi^{(i)}$ is the i-order susceptibility tensor and ε_0 is the permittivity of free space. In Equation (1-1) the space coordinates are implicit in the susceptibility. The applied electric field is the driving term in the Maxwell's equation generates the polarization. The first term in the right-hand side of Equation (1-1) describes the first-order linear phenomena which are related to the phase velocity causing refraction, reflection, diffraction and dispersion. The second term expresses the first nonlinear response of the induced polarization, and is the second-order nonlinear effect, absent in materials with inversion symmetry, such as glass but can be present in non-centro-symmetric materials such as LN. The wavelength conversion in an NLO waveguide which is covered in this dissertation is defined by this effect. The third term describes the third-order nonlinear effects, present in all materials, and is responsible for effects such as self-phase modulation, soliton formation, cross-phase modulation, four-wave mixing and so on which are easily seen in optical fibers and have important implications in communications.

The most common second-order NLO effect used for wavelength conversion is second harmonic generation (SHG). In this case, the frequency (ω) of the input optical wave or fundamental harmonic (FH) is doubled to generate a second harmonic (SH) output wave if the condition is satisfied amongst the relevant phase components. Further, the second-order $\chi^{(2)}$ tensor of the NLO crystal must include an appropriate component to couple a FH wave to a SH wave. It is common to show the nonlinear coefficient d tensor instead of the $\chi^{(2)}$ tensor. Considering SHG in LN crystal, the Cartesian components of the polarization $P^{(2\omega)}$ are related to the components of the applied electric fields $E^{(\omega)}$ by [2]

$$\begin{bmatrix} P_x^{(2\omega)} \\ P_y^{(2\omega)} \\ P_z^{(2\omega)} \end{bmatrix} = 2\varepsilon_0 \begin{bmatrix} 0 & 0 & 0 & 0 & d_{31} & -d_{22} \\ -d_{22} & d_{22} & 0 & d_{31} & 0 & 0 \\ d_{31} & d_{31} & d_{33} & 0 & 0 & 0 \end{bmatrix} \begin{bmatrix} (E_x^{(\omega)})^2 \\ (E_y^{(\omega)})^2 \\ (E_z^{(\omega)})^2 \\ 2E_y^{(\omega)}E_z^{(\omega)} \\ 2E_x^{(\omega)}E_z^{(\omega)} \\ 2E_x^{(\omega)}E_y^{(\omega)} \end{bmatrix}, \tag{1-2}$$

where $d_{ml} = \chi_{ml}^{(2)} / 2$ are the nonlinear coefficients which are expressed in a 3 × 6 matrix; $d_{31} = d_{32} = d_{15} = d_{24} \approx -4.4\,\text{pm/V}$, $d_{22} = -d_{21} = -d_{16} \approx 2.4\,\text{pm/V}$ and $d_{33} \approx -25\,\text{pm/V}$.

The next second-order NLO wavelength conversion technique is difference frequency generation (DFG), which is of great importance as it can cover the entire transparency range of NLO crystals. The principle of operation is as follows: optical waves of two different frequencies are mixed in these devices to generate the third optical wave with a frequency which is the difference of the two input frequencies. Conversely, efficient generation of the sum-frequency occurs which is called parametric up-conversion or sum frequency generation (SFG) if the condition is satisfied amongst the relevant phase components.

1.3 Phase matching

SHG, DFG and SFG require phase matching to be efficient. For wavelength conversion, phase matching is essential for building up the NLO response constructively [3]. This means that a proper phase relationship between the interacting waves (for maximum wavelength conversion) is maintained along the propagation direction, so that the amplitude contributions from different locations to the resultant wave are all in phase. This leads to the condition that phase mismatch has to be zero.

For example using SHG, there is a driving field at a frequency ω generating linear polarization at ω and nonlinear polarization at 2ω. The phase-difference between the two oscillators (dipoles) separated in the propagation direction is found by the product of the oscillator's frequency and the time which the driving field needs to travel between them. This time is equal to the ratio of

the propagation distance and the phase velocity of light in the material at the driving field frequency. Therefore, the phase difference between the oscillators at ω is $k_\omega \Delta z$, where $k_\omega = \omega n_\omega / c$ is the wave-number of the FH, Δz is the distance between them, n_ω is the refractive index at ω and c is the light speed. Similarly, the phase difference between the nonlinear oscillations at 2ω is $2k_\omega \Delta z$. The SH field at 2ω generated by the nonlinear oscillator accumulates a phase of $k_{2\omega} \Delta z$ while traveling to get to the second oscillator where $k_{2\omega} = 2\omega n_{2\omega} / c$ is the wave-number of SH and $n_{2\omega}$ is the refractive index at 2ω.

If $n_{2\omega} = n_\omega$ is satisfied in a material, then the phase $k_{2\omega} \Delta z$ just compensates the phase difference of the nonlinear oscillations $2k_\omega \Delta z$ and the fields at 2ω generated by the two oscillators interfere constructively along the propagation direction resulting in growth of the SH power with propagation distance. However, satisfying $n_{2\omega} = n_\omega$ presents a problem as common NLO materials show normal dispersion, that is, $n_{2\omega} > n_\omega$. Therefore, dispersion commonly causes a non-zero phase mismatch ($\Delta k = k_{2\omega} - 2k_\omega \neq 0$) if no special measures are taken. To overcome this difficulty two main approaches have been used: birefringent phase matching and quasi-phase matching.

1.3.1 Birefringent phase matching

In NLO crystals, the refractive index depends on the polarization of the wave. This property can be utilized to compensate the refractive index difference between FH and SH resulting from normal dispersion. For example, considering SHG using uniaxial LN crystal, three orthogonal axes exist as shown in Figure 1-1, denoted *a*, *b*, and *c*. The refractive indexes for the polarized waves along the *a* and *b* axis are the same and called ordinary refractive index (n_o) whilst the refractive indexes for the polarized wave along the *c* axis is smaller than n_o and called extraordinary refractive index (n_e). Therefore, the light propagating along the *a*-axis of LN travels more slowly if it is linearly polarized along the *b*-axis than if it is linearly polarized along the *c*-axis. If we restrict the polarization of the FH wave to be along the *b*-axis and the polarization of the SH to be along the *c*-axis, the phase velocity difference due to dispersion can be compensated for by the phase velocity difference due to birefringence, so that $n_e(2\omega) = n_o(\omega)$ and $\Delta k = 0$ which results in the build-up of SH power as shown in Figure 1-2(a).

Although this configuration provides phase matching, it does not mean at once that it will efficiently generate the SH as the nonlinear tensor must include an appropriate component to couple a *b*-polarized FH to a *c*-polarized SH. An assessment of d_{ml}'s for the LN crystal in Equation (1-2) exhibits that the required component is d_{31}, which exists in LN. However, the largest nonlinear coefficient d_{33} for LN is still not phase-matchable as we can not use the *c*-polarized FH wave.

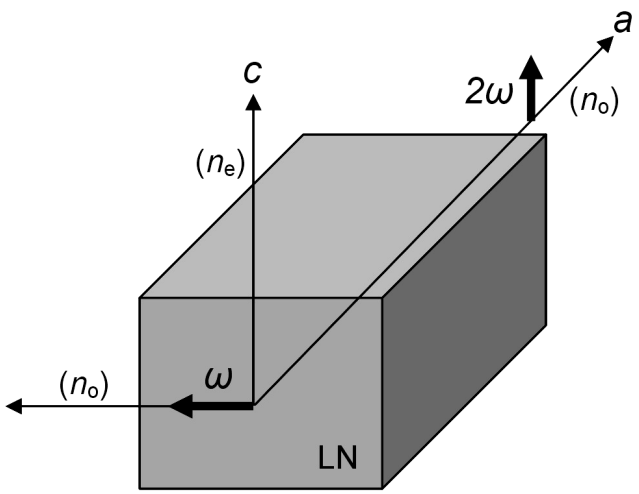

Figure 1-1 : A schematic view for using the LN crystal birefringence to obtain phase matching.

This technique may only work for a particular FH wavelength. For wavelengths below the FH wavelength, dispersion of LN exceeds the birefringence and for wavelengths above the FH wavelength, birefringence exceeds the dispersion. Nevertheless, as the involved refractive indexes change differently with temperature, temperature tuning can be used to achieve phase matching for some other wavelength. This is used to provide noncritical phase matching for the desired wavelength. The term "noncritical" is often used as this technique is relatively insensitive to the slight misalignment of beams. However, relatively high temperatures are required to obtain phase matching for SHG in practice and these high temperatures may be a disadvantage in some applications.

An alternative technique changes the direction of propagation rather than the temperature in order to achieve phase matching. Phase matching for SHG may occur for some direction of propagation in the *a*–*c* plane. In this arrangement, the SH is still polarized along the *c*-axis and experiences n_e, but the polarization of the FH in the *a*–*c* plane experiences the refractive index less than n_o and phase matching may be satisfied for special wavelengths and angles of beam propagation. However, this critical technique may also not be applicable to all wavelengths within the transparency range of materials [2].

1.3.2 Quasi-phase matching

Using birefringent phase matching, the phase mismatch for SHG given by $k_{2\omega} - 2k_{\omega}$ becomes zero and thus the condition $n_{2\omega} = n_{\omega}$ means that the FH at ω and the SH at 2ω travel through the nonlinear crystal at the same speed as the index of refraction is a measure of the speed (phase velocity). Phase matching ensures that SH contributions generated at each point along the crystal add in phase, maximizing the total generated SH power. Otherwise, there is a phase mismatch of $k_{2\omega} - 2k_{\omega}$ which leads to oscillations of the SH power as shown in Figure 1-2(b). In this case, the maximum SH power is limited to the power generated over a small interaction distance, $L_c = \pi/(k_{2\omega} - 2k_{\omega})$ called coherence length at which the phase mismatch is equal to π. However, the small coherence length is inadequate for efficient energy transfer to the SH component.

One solution to this problem was proposed in 1962 [4]. The technique, called quasi-phase matching (QPM) is based on the resetting of the phase mismatch to zero at each coherence length. After propagation in one L_c, the phase mismatch becomes π. If the sign of $\chi^{(2)}$ is changed at that position, an additional π phase shift is added to the nonlinear polarization, resetting the phase mismatch to zero. Therefore, reversing the sign of $\chi^{(2)}$ resets the mismatch to zero after a length L_c. Thus, QPM permits the phase mismatch to be annulled over long lengths. In such way, the power in the SH field is allowed to grow along the crystal, as shown in Figure 1-2(c).

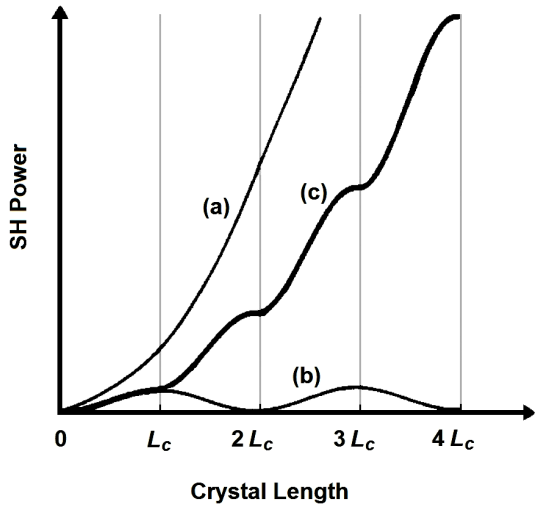

Figure 1-2 : SH power versus crystal length for (a) phase matching and (b) no phase matching and (c) quasi-phase matching schemes.

An important point here is that using birefringent phase matching in LN, it is not possible to exploit the largest nonlinear susceptibility element $\chi_{33}^{(2)}$ because it can be used only when all of the interacting waves are polarized along the *c*-axis, whilst QPM is not subject to such constraints because it depends on an externally imposed structure, rather than intrinsic dispersion properties of the material. Thus, QPM can be used in order to take advantage of the highest nonlinear coefficient in NLO materials.

QPM could not be realized at the time it was proposed as a concept, since appropriate fabrication techniques had not been developed, and was first made in 1970 [5]. By the development of advanced techniques for periodic poling to change the sign of $\chi^{(2)}$, QPM in bulk crystals and waveguides is widely used nowadays. QPM using periodic domain-inverted gratings in LN waveguide, as shown schematically in Figure 1-3, is used extensively for SHG in order to enhance the efficiency [6]-[7]. It offers several advantages such as phase matching at an arbitrary wavelength by the use of d_{33}, high conversion efficiency, and guided-mode harmonic output [8]. Nonetheless, most of the SHG-, DFG- and SFG-based devices use quasi-phase matched domain-inverted gratings (periodically poled structures) and channel waveguides in LN.

1.4 Poling and waveguide fabrication in LN

For fabrication of quasi-phase matched gratings, the most popular technique uses liquid electrodes and high-voltage pulse application [9]. In this method, a comb-shaped photo-resist pattern (6-μm SiO_2 layer) whose structure is the same as the poling period is formed on the surface of an LN substrate with a thickness of ($T \approx 0.5\,\text{mm}$) using a conventional photo or electron-beam lithographic technique. A liquid electrode consisting of saturated solution of lithium chloride is applied to both sides of the LN surface while insulation between them is preserved. The solution is confined within plastic frames sandwiching the crystal. A high-voltage pulse (~coercive field $21\,\text{kV/mm} \times T = 10.5\,\text{kV}$) is then applied to the LN substrate. This reverses the spontaneous polarization under the electrode.

For fabrication of waveguides, titanium in-diffusion and annealed proton exchange (APE) in LN are the most well known techniques [10]. Ti-diffused LN waveguides has been used in many integrated optic devices. The diffusion source is a Ti film with thickness of 50-100 nm deposited on the crystal surface. The source is thermally diffused into the crystal at ~1000ºC for several hours. These waveguides with an index difference of ~0.01 support both the TE and TM modes with very low propagation loss (as low as 0.1 dB/cm) at a wavelength of ~1.5 μm. However, APE waveguides may be preferred because of their resistance to photorefractive damages and the possibility of smaller mode fields due to tight confinement [11] but their losses are a little higher at 0.35 dB/cm at a wavelength of ~1.5 μm. For APE waveguide fabrication, a mask pattern of SiO_2 is first formed photo-lithographically on the LN substrate. Proton-exchanged lithium niobate optical waveguides are made by immersing the LN substrate at an elevated temperature (160 - 240 ºC) into a proton donor solution such as benzoic acid for several tens of minutes. Parts of the Li^+ ions in the substrate are exchanged for protons to obtain a thin (several microns thick) waveguide layer on the substrate. The proton-exchanged waveguides are thermally annealed (~350 ºC) to diffuse protons from the initial layer to a deeper region of the substrate to anchor the protons and stabilize the characteristics, reduce the relatively high propagation losses, and avoid a reduction in effective nonlinearity. The resulting waveguide's extraordinary refractive index is higher than that of the substrate with a difference of ~0.09, while the waveguide's ordinary

refractive index is lower than that of the substrate. Thus, the APE waveguides in *z*-cut LN (when the cut of the crystal is perpendicular to *c*-axis) support only TM modes.

1.5 SHG, DFG and SFG in PPLN waveguide

The basic structure of a *z*-cut PPLN waveguide for SHG is shown in Figure 1-3. For frequency doubling, the QPM condition for SHG is given by $2\beta_\omega + 2\pi/\Lambda_{\mathrm{SHG}} = \beta_{2\omega}$ and the period is $\Lambda_{\mathrm{SHG}} = 2L_c = (\lambda_\omega/2)/(N_{2\omega} - N_\omega)$ where β_i, N_i and λ_i are the propagation constants, effective indexes of guided waves and wavelengths of the FH and SH waves $(i = \omega, 2\omega)$, respectively. Moreover, an SHG bandwidth (BW) of a fraction of nm, inversely proportional to the length for a few-centimeter long PPLN waveguide is achieved [11].

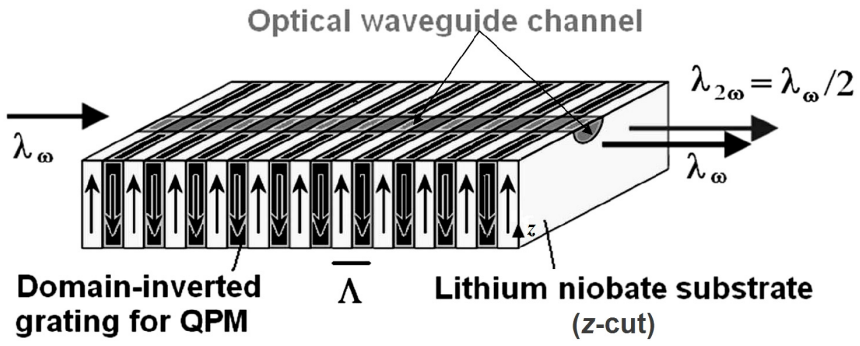

Figure 1-3 : A narrowband frequency doubler based on a uniform PPLN waveguide.

It is possible to utilize a PPLN waveguide for another second-order nonlinear mixing process which is DFG as shown in Figure 1-4(a). When a signal wave of angular frequency ω_s (wavelength λ_s) and a pump wave of $\omega_p = 2\omega_0$ (wavelength $\lambda_p = \lambda_0/2$) are mixed in a quasi-phase matched device, a difference frequency (converted signal or idler) wave of $\omega_c = \omega_p - \omega_s$ (wavelength $\lambda_c = (\lambda_p^{-1} - \lambda_s^{-1})^{-1}$) is generated. The difference frequency ω_c and the signal frequency ω_s are at points symmetrical to each other on the frequency axis with respect to the

half pump wave frequency, ω_0. Thus, the DFG device can be considered a wavelength converter from λ_s to λ_c. The QPM condition for DFG is given by $\beta_s + \beta_c + 2\pi / \Lambda_{\mathrm{DFG}} = \beta_p$ and the period is $\Lambda_{\mathrm{DFG}} = \left(N_p / \lambda_p - N_s / \lambda_s - N_c / \lambda_c \right)^{-1}$ where β_i, N_i and λ_i are the propagation constants, effective indexes of the guided waves and wavelengths of the signal and idler waves $(i = s, c)$ and pump frequency wave $(i = p)$, respectively.

Generally, DFG-based wavelength conversion has a large bandwidth, in which ω_c is near to ω_s (waveband conversion), but it is difficult to couple both the pump and signal into the waveguide as they are in different wavelength regions [11]. However, the use of cascaded $\chi^{(2)}$ namely SHG + DFG has been proposed to solve this problem. Consider a pump wave at $\omega_p = \omega_0$ and a signal wave of ω_s near to ω_0 coupled into the wavelength converter in which the QPM for SHG is satisfied. The generated SH mixes with the signal wave to give rise to an idler wave at $\omega_c = 2\omega_p - \omega_s$ when the QPM condition for DFG is satisfied. The configuration of the cascaded SHG + DFG wavelength converter is shown in Figure 1-4(b). For wavelength conversion within a communication band, an advantage of the cascaded SHG + DFG conversion is that the pump wave is in the same band of the signal and idler waves. This allows use of fiber and semiconductor lasers developed for optical communications instead of short wavelength lasers for pumps.

The conversion efficiency of the cascaded SHG + DFG, however, is lower than that of ordinary DFG for the same pump power. Although it is hard to obtain a high efficiency with a low-power pump wave, an erbium-doped fiber amplifier (EDFA) can be used to increase efficiency. Further, double-pass cascaded SHG + DFG has also been proposed to increase the conversion efficiency. By means of the cascaded SHG + DFG, wide waveband conversion of optical signal is possible.

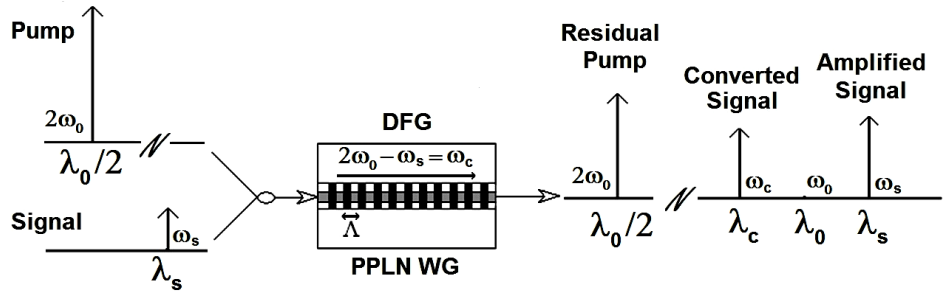

(a)

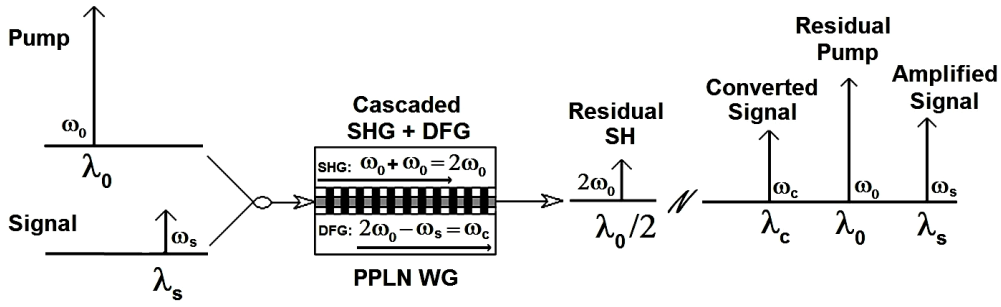

(b)

Figure 1-4 : (a) DFG scheme and (b) cascaded SHG + DFG scheme for broadband wavelength conversion.

It is also feasible to use a PPLN waveguide to achieve SFG. With the two pump wavelengths, λ_{p1} and λ_{p2}, the wavelengths of the sum frequency (SF) wave (λ_{SF}) is equal to $\lambda_{p1}\lambda_{p2}/(\lambda_{p1}+\lambda_{p2})$ provided that the QPM condition for SFG given by $\beta_{p1}+\beta_{p2}+2\pi/\Lambda_{\mathrm{SFG}}=\beta_{\mathrm{SF}}$ is satisfied. The QPM period for SFG thus is $\Lambda_{\mathrm{SFG}}=\left(N_{\mathrm{SF}}/\lambda_{\mathrm{SF}}-N_{p1}/\lambda_{p1}-N_{p2}/\lambda_{p2}\right)^{-1}$ where β_i, N_i and λ_i are the propagation constants, effective indexes of the guided waves and wavelengths of pumps

$(i = 1, 2)$ and SF wave $(i = \mathrm{SF})$, respectively. $\lambda_{\mathrm{SF}} \approx \lambda_0 / 2$, where λ_0 is approximately the mean wavelength of two pumps. By cascaded SFG + DFG, presenting advantageous feature including wider bandwidth, waveband conversion of optical signal is also possible.

In the next two Sections, several applications for the broadband SHG and cascaded $\chi^{(2)}$ are discussed and novel solutions to reach such wavelength converters are presented.

1.6 Wavelength conversion using broadband SHG (frequency doubling)

Broadband frequency doublers based on quasi-phase matched SHG in waveguides have several applications in optical communication and sensing [12]-[37]. Using broadband SHG, tunable generation of coherent radiation at wavelengths where no appropriate laser is available, will also be possible.

For optical communication, an important application of broadband SHG is in the variable and broadcast wavelength conversion based on the cascaded SHG + DFG which needs a broadband frequency doubler (SHG device) [15]. In earlier schemes, the pump bandwidth was narrow and therefore signals could only be converted to limited wavelengths which restricted the usefulness of the variable wavelength converter. Although, by imposing aperiodic quasi-phase matched structures for SHG a large wavelength tuning range for the converter can be achieved using multiple pumps, the pump wavelength channels are discrete and cannot be adjusted once the aperiodic structures are fabricated [55],[56]. However, using broadband SHG by the simultaneous use of Q pumps, R×Q wavelength broadcasting can be performed, in which each of R input optical signals can be converted to Q output wavelengths [43]. Nonetheless, a bandwidth more than 25 nm for broadband SHG is necessary to achieve a flexible broadcast wavelength conversion [15].

Another example is in ultrafast optical signal processing [36], [37] in which the problem is associated with generating ultrashort SH pulses in long quasi-phase-matched uniform gratings. To minimize dispersive walk-off, the traditional technique uses a short piece of uniform grating for large bandwidth but with only low efficiency. This works well when the input peak power is large. When the grating length is too long to provide sufficient SH conversion efficiency, the output SH pulses can be truncated and stretched in frequency and time domain, respectively due

to small conversion bandwidth. Nevertheless, the SHG of sub-picosecond pulses needs broadband frequency doublers, e.g., a 26-nm bandwidth is enough to convert the pulses down to ~100-fs duration [23].

Broadband SHG also seems promising in optical coherence tomography (OCT), a technique used to diagnose various medical conditions [44]. In this case, a broadband SHG device acts as a new broadband light source at shorter wavelengths. The reason for using the broadband source in an OCT system is the inverse relationship between the bandwidth of light and axial resolution length [45]. The use of the broadband light source in the near infrared is due to the fact that the axial resolution length is also proportional to the square of light wavelength [45]. On the other hand, for an OCT system a powerful light source is also required to achieve high detection sensitivity for deep imaging in tissues [47]. However, an approach which is being suggested is to use broadband frequency doublers to apply the broadband SH field simultaneously with the broadband FH, namely dual-band OCT, and thereby benefit from differential OCT which may be used to reveal otherwise unattainable data in one step [46].

Nonetheless, the problem associated with the PPLN-based frequency conversion is the narrowband feature of SHG, as the bandwidth is dependent on the inverse of the grating length. A simple solution is to use a short piece of PPLN waveguide to obtain wide bandwidth. To achieve reasonable efficiency it needs very high input power which may not be tolerated by the PPLN waveguide. Also, using an aperiodically poled lithium niobate (aPPLN), broadening (15 times) of the phase matching bandwidth is achieved due to the scrambling of the phases compared to that (0.3 nm) of a uniform grating with the same length [12]. However, the small bandwidth of the non-flat SHG response is not suitable for the aforesaid applications. Although there has been some work on waveguide structure to increase the bandwidth and tailored quasi-phase matched grating structures have been proposed in the literature to broaden the phase matching, e.g., two domain inverted building blocks and an aperiodic grating structure [26],[27], the bandwidths are still a few nanometer. Thus, a high conversion bandwidth e.g., > 25 nm, with high efficiency remains an unattainable goal. To solve this problem, the chirped grating scheme has been proposed to broaden the bandwidth by chirping the pitch of the inverted domains as a function of length [13]. Using this technique, broadening of the conversion bandwidth as a function of the

wavelength is achieved but with a fluctuated response, which is not acceptable for many applications as the spectral conversion response is not uniform. Figure 1-5 shows a schematic of the concepts of SHG bandwidth broadening in quasi-phase matched devices using a short uniform grating and a long chirped grating of inverted domains.

In this dissertation, we propose a good candidate for the realization of a novel broadband frequency doubler which is based on quasi-phase matched chirped gratings. In fact, the engineering of gratings in quasi-phase matched devices seems promising to solve problems, namely the broadband generation of SH optical wave with a desired spectrum and efficiency.

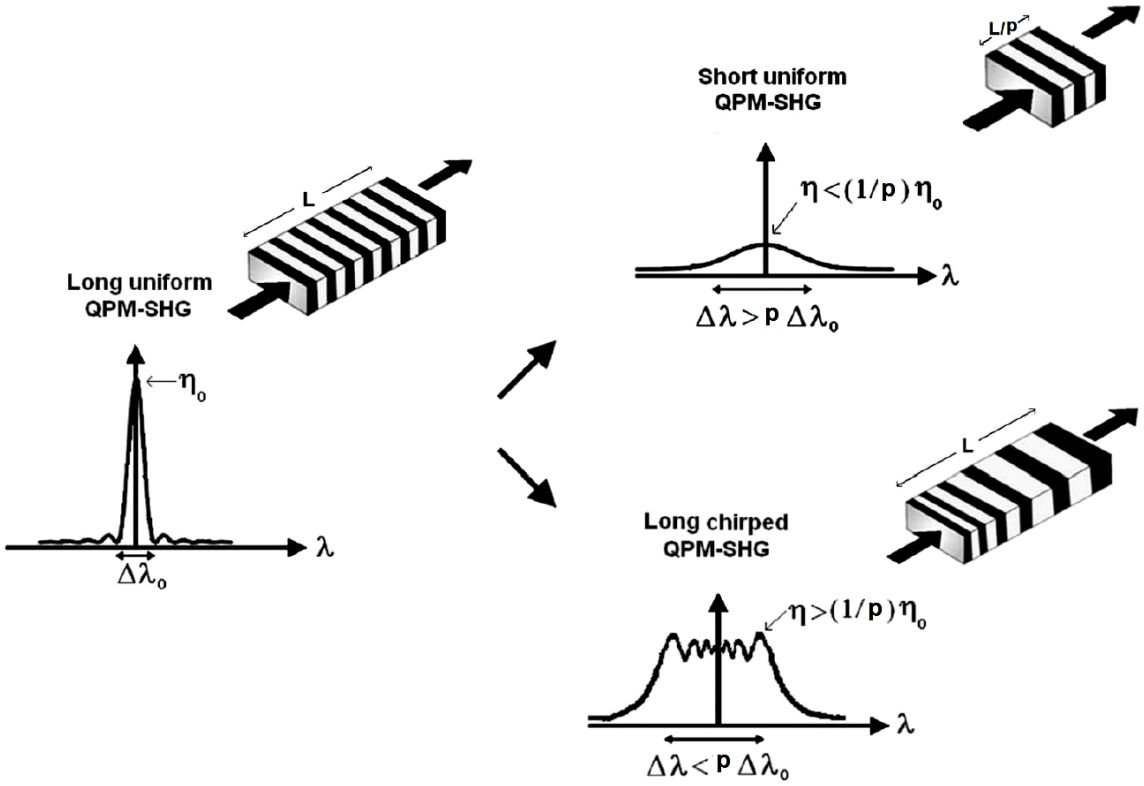

Figure 1-5 : Concepts of SHG bandwidth broadening in quasi-phase matched devices.

The potential of using chirped grating structures offers the advantage of obtaining larger bandwidths. It is also important that they remain significantly more temperature tolerant than the uniform gratings structures and provide a greater stability for frequency doubling. The potential of using chirped grating structure for broadening the bandwidth in SHG has already been theoretically analyzed [13]. However, there exist three problems using chirped gratings.

The first problem for realizing such broadband devices is the smallness of change in the linear-chirped grating (LCG) period, which is typically around 100 picometers or less for a converter with several nanometers of bandwidth. We will show for the first time that using the step-chirped grating (SCG) enables us to increase the step size period change for more convenient fabrication, while the bandwidth and efficiency remain almost the same in comparison to LCGs [38]. SCG first introduced to broaden and flatten the reflectivity in fiber Bragg gratings [51].

The second problem is the obvious ripple on the efficiency curves of the LCGs and SCGs. One method for flattening the SHG response is to use a grating structure with carefully located phase shifts [25]. The other approach to solve this problem is to use apodization [52]. Here, we have achieved this by changing the duty ratio of the poled regions, which removes the ripples and achieves a nearly flat response [39].

The third problem is related to the mediocre SH efficiency using the ASCG. The efficiency may be increased with small-effective-cross-section waveguides to increase the power density, with or without resonant structures [40]. Thus, it is demonstrated for the first time that using singly pump-resonant waveguides including ASCG, strong improvement in the SH conversion efficiency response envelope curve is possible.

1.7 Waveband wavelength conversion using broadband cascaded $\chi^{(2)}$

During the past years, there has been considerable work in research and development of all-optical wavelength conversion technology based on the cascaded $\chi^{(2)}$ effects namely SHG + DFG and SFG + DFG for future wavelength division multiplexing (WDM) systems in high-capacity optical communications. For true flexibility, the 3-dB bandwidth of these converters should be broad enough to cover the 1.55 μm optical window. For practical applications, it would be useful if one can position the pumps at wavelengths out of the optical window, which is at least 75 nm

wide and should have flat responses and high conversion efficiencies. In addition to the wavelength conversion function, these devices can perform different ultrafast optical signal processing such as all-optical switching, offering possibilities of applications in ultrafast photonic network systems based on optical time division multiplexing (OTDM) [41]. Cascaded $\chi^{(2)}$ wavelength converters also offer a variety of possibilities for applications in signal processing including millimeter-wave/THz generation and radio over fiber.

For optical communications, the most notable advantage of cascaded $\chi^{(2)}$ devices is the extremely wide wavelength coverage while the pump(s) and signal/idler are in the same band. The converters based on cascaded $\chi^{(2)}$ in PPLN waveguides are superior to others [42], as they can offer a high efficiency with a moderate pump power and can simultaneously convert a batch of broadband wavelengths or high-speed signals, with negligible signal-to-noise ratio (SNR) degradation. Another advantage as coherent wavelength converters, is full transparency to various signal formats. They can also perform bidirectional wavelength conversion. Compactness, compared to fiber devices and integration compatibility are among the other advantages of these devices.

DFG [75]-[81] and cascaded SHG + DFG in PPLN waveguides, has already been demonstrated both theoretically and experimentally as a wavelength conversion scheme in several applications [82]-[93]. For wavelength conversion within a communication band, an advantage of the single-pass cascaded SHG + DFG to DFG is that a pump wave with the wavelength in the same band of the signal and idler waves can be used. However, it is hard to obtain high efficiency with a low pump power in the single-pass cascaded SHG + DFG scheme. To solve this problem, the double-pass cascaded SHG + DFG is a good technique to increase the efficiency in comparison to that of the single-pass one but has a small bandwidth penalty [82],[83]. Nevertheless, the disadvantage of both SHG + DFG schemes e.g., for WDM systems is that several channels must be sacrificed because the wavelength of the pump light must be set at the centre of the conversion band occupying the place of possible channels. Furthermore, highly broadband SHG + DFG need gratings with complex structures, periodically distributed π-phase shifted domains or chirped optical superlattices [78],[79],[80].

Recently, an interesting wavelength conversion technique based on quasi-phase matched cascaded SFG + DFG has been demonstrated theoretically and practically in PPLN waveguides and found wide applications including broadband wavelength conversion, channel selective and multiple channel wavelength conversion, and format conversion [94]-[113]. By increasing the pump wavelength difference using this technique, the bandwidth can be enhanced [98]. However, the mean of the conversion efficiency depends on the wavelengths of the pumps and is decreased by increasing the pump wavelength difference. To overcome the efficiency reduction, a double-pass cascaded SFG + DFG scheme has been proposed, which is also able to filter out the residual pump wavelengths at the output [109]. Nonetheless, for wide pump wavelength difference, SFG is perfectly phase-matched whilst the DFG phase-mismatch is large when the signal is far from the pump wavelengths. Thus, the wide pump wavelength difference increases the variation of conversion efficiency, converting equal-power signal channels unevenly [115].

Although the cascaded SFG + DFG schemes have been principally investigated, the research on how to set the pumps exactly or alternatively to engineer the grating to improve the conversion properties still remain and are of great importance [114]. Solutions to the problem are proposed for the first time, in single-pass and double-pass devices using detuning of the pump wavelength [116], [117], or alternatively using step-chirped gratings. We show that, if the wavelength of a pump or the chirp step in the SCG is increased slightly, the SFG phase-mismatch decreases and the DFG phase-mismatch is also reduced, which leads to flattening of the variation in the response curve.

1.8 Overview of the dissertation

In Chapter 2, the engineering of quasi-phase matched chirped gratings including inverted domains for SHG in low-loss titanium in-diffused lithium niobate (Ti:LN) waveguides is presented in such a way as to broaden the bandwidth significantly. A design formula is proposed for the first time to help decide how many segments are needed as a design rule, dependent on the required bandwidth. In addition, we consider an apodization method to flatten the SH bandwidth by utilizing increasing and decreasing patterns of inverted domains into the quasi-phase matched gratings. More generally, the proposed concept of apodized step-chirped grating (ASCG) may be

applied to broadband QPM in other NLO materials, with or without a waveguide. Finally, the SH conversion bandwidth of > 50 nm may be designed with a special design of few-segment ASCG in LN with a 1-μm line width in such a way as to provide a flat response and also facilitate the poling and fabrication processes.

In Chapter 3, it is shown that the moderate SHG efficiency of the ASCG in Ti:LN waveguides can be boosted using small-effective-cross-section waveguides. To achieve this goal, APE waveguides are considered because of the possibility of higher index difference and smaller mode field cross section. Also, assuming a singly pump-resonant waveguide for broadband SHG using the ASCG, it is demonstrated that for the quasi-continuous FH it is possible to increase the conversion efficiency envelope of resonant axial modes effectively while the conversion bandwidth remains almost unchanged. Furthermore, it is shown numerically for an ASCG that by means of singly pump-resonant waveguides, the conversion efficiency of quasi-continuous waves shown with the envelope of responses increases substantially, especially for low propagation loss. The optimized values of back-facet reflectivity and input power to achieve the maximum efficiency, for several waveguide loss parameters are also presented.

In Chapter 4, we evaluate and compare numerically the properties of the single-pass cascaded SFG + DFG and SHG + DFG schemes when the pump wavelength difference is 75 nm and 0 nm, respectively and show that for the same device length, the adoption of the SFG + DFG device further improves the bandwidth performance with a small efficiency reduction and a slight ripple penalty. Moreover, we present the criteria for selection of the waveguide length and pump powers to obtain the required efficiency, ripple and bandwidth and show that increased wavelength detuning of a pump in the single-pass device, removes the ripple with a penalty on the mean efficiency. Further, introducing a few-section SCG device with the proper design, results in almost the same bandwidth and flatness, with less mean efficiency penalty compared to the counterpart pump-detuned device. Additionally, we present design diagrams for pump-detuned and SCG single-pass devices for selection of the length and pump powers to obtain the required efficiency, ripple and bandwidth.

In Chapter 5, the properties of the double-pass cascaded SFG + DFG and SHG + DFG schemes are evaluated and compared numerically when the pump wavelength difference is 75 nm and

0 nm, respectively. It is demonstrated that for the same device length, the adoption of the double-pass SFG + DFG in a low-loss waveguide device, with pump detuning or using a SCG, further improves the conversion efficiency with a small bandwidth reduction compared to the single-pass SFG + DFG device. Further, it is shown that for the same length and power, the efficiency enhancement advantage, expected due to the use of the double-pass device instead of the single-pass one, is lost when the waveguide loss reaches a particular value. Moreover, we present the design diagrams of pump-detuned and SCG double-pass devices for choice of the length and pump powers to obtain the necessary efficiency, ripple and bandwidth.

In Chapter 6, we conclude the work and propose some new ideas for future work.

CHAPTER 2
BANDWIDTH BROADENING AND FLATENNING OF QUASI-PHASE MATCHED SHG USING APODIZED STEP-CHIRPED GRATING

2.1 Overview

An important requirement for exploiting the second-order nonlinearity for harmonic generation and frequency conversion is phase matching to accumulate NLO response constructively. We have seen in the last Chapter that the QPM structure presents us with significant advantages. Nevertheless, the QPM bandwidth broadening for SHG has attracted considerable attention [12]-[37]. Modified quasi-phase matched structures have been proposed to broaden the phase matching and the segmented gratings have also been demonstrated for the SHG bandwidth broadening, however, the bandwidth was only broadened to 1.12 nm [21]. Although, there still exists a need for higher conversion bandwidth, e.g., more than 25 nm with flat conversion response, highly-broadband SHG in quasi-phase matched waveguides have not been achieved successfully.

The capability of using chirped grating structure, offers the benefit of obtaining large SHG bandwidth [13]. However, there exist three problems using chirped gratings for broadband frequency doubling. The first problem is the smallness of change in the linear-chirped grating (LCG) period. We show that a step-chirped grating (SCG) structure can solve the problem. Using SCG enables us to increase the period change for the convenience of fabrication while the bandwidth and efficiency remain almost the same in comparison to LCG. The second problem is the noticeable fluctuations on the broadband SH efficiency responses of chirped gratings. Our approach to solve this problem is the imposing of some apodization [52]. It can be done by changing the duty ratio of the poled regions in chirped gratings which helps to remove the ripples

and achieve flat responses. The third problem is related to conversion efficiency which will be addressed in Chapter 3.

In this Chapter, we propose the engineering of SCG in such a way to highly broaden the bandwidth with large chirp steps. A formula is proposed to decide how many segments one should use as a design rule dependent on the required bandwidth. Also, we consider an effective method to apodize and nearly flatten the SH bandwidth by considering increasing and decreasing patterns of inverted domains into the quasi-phase matched gratings, in low-loss lithium niobate waveguides with propagation loss around 0.1 dB/cm, e.g., Ti:LN [23], [34], [90], [101]. However, the proposed concept of apodized step-chirped grating can be applied to other kind of NLO materials and waveguides.

2.2 Modeling of step-chirped grating

For the frequency doublers based on SHG taking advantage of QPM, any phase mismatch between laser wavelength and gratings should be resolved. Uncertainty in the propagation constant, error in the fabrication process and fluctuation of the laser wavelength and temperature variations may increase the mismatch. Not only does a SCG provide a better means for fabrication of highly-broadband converters but also is able to solve the above problems by broadening the phase matching bandwidth.

A SCG structure is proposed as shown in Figure 2-1. In this structure, the total grating length (L) has been divided into p sections that each section consists of n constant periods Λ_i or n segments as a uniform grating with a 50% duty factor which is the ratio of the domain-inverted region to the period. Therefore, the section length is $(L_i = n\Lambda_i,\ i = 1, 2, ..., p)$. The period of the sections changes according to a function which we assume to be

$$\Lambda_i = \Lambda_1 + \Delta\Lambda\,(i-1), \tag{2-1}$$

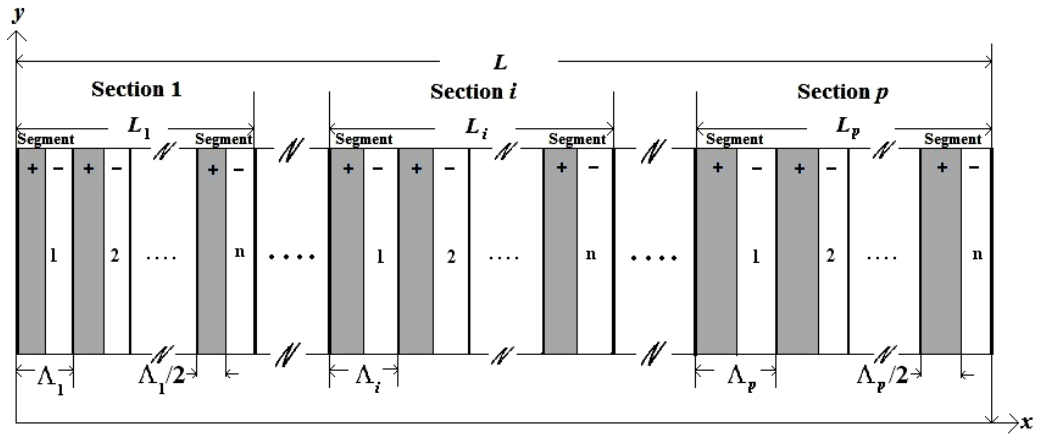

Figure 2-1 : Scheme of a domain-inverted SCG. The plus and minus signs refer to the sign of $\chi^{(2)}$ in gray and white regions, respectively.

where Λ_1 is the period of the first section, $\Delta\Lambda$ is the chirp step or period change between two adjacent section. To obtain the total SH wave amplitude and efficiency, we can consider p uniform gratings in PPLN. The calculations begin and cascade from the first section with the length L_1 to the last section with the length L_p, in which we use the nonlinear coupled mode equations [13]

$$\frac{d}{dx}A_{FH}(x) = -j\kappa^{*}A_{FH}{}^{*}(x)A_{SH}(x)e^{-j\Delta kx} - \tfrac{1}{2}\alpha_{FH}A_{FH}(x), \tag{2-2}$$

$$\frac{d}{dx}A_{SH}(x) = -j\kappa\left[A_{FH}(x)\right]^{2}e^{+j\Delta kx} - \tfrac{1}{2}\alpha_{SH}A_{SH}(x), \tag{2-3}$$

to describe SHG in each section which are solved numerically to take into account pump depletion. (A_{FH},α_{FH}) and (A_{SH},α_{SH}) are the amplitudes and losses of the FH and the SH waves, respectively and Δk is the phase mismatch parameter of each section defined as

$\Delta k = \beta_{2\omega} - 2\beta_{\omega} - 2\pi / \Lambda_i$ where $\beta_{\omega} = 2\pi N_{\omega} / \lambda_{\omega}$ and $\beta_{2\omega} = 2\pi N_{2\omega} / \lambda_{2\omega}$ are the mode propagation constants of the FH and SH waves, respectively. Moreover, $(N_{\omega}, \lambda_{\omega})$ and $(N_{2\omega}, \lambda_{2\omega})$ are the effective refractive indexes and wavelengths for the FH and SH waves, respectively. Also, the coupling factor can be shown as [11]

$$\kappa = \varepsilon_0 \sqrt{\frac{(2\omega)^2}{2(N_{\omega})^2 N_{2\omega}} \left(\frac{\mu_0}{\varepsilon_0}\right)^{3/2} \frac{d_{eff}^2}{S_{eff}}}, \tag{2-4}$$

where μ_0 is the permeability of free space, $d_{eff} = (2/\pi) d_{33}$ is the effective nonlinear coefficient for 50% duty ratio and the effective area is [11]

$$S_{eff} = \frac{\iint |E_{2\omega}(y,z)|^2 dydz \left[\iint |E_{\omega}(y,z)|^2 dydz\right]^2}{\left[\iint [E_{2\omega}(y,z)]^* [E_{\omega}(y,z)]^2 dydz\right]^2}. \tag{2-5}$$

where $E_{\omega}(y,z)$ and $E_{2\omega}(y,z)$ are the normalized mode profiles for the FH and SH waves, respectively in a *z*-cut LN waveguide, which is assumed to have a uniform cross section and to be parallel to the optical axis *a* which is called here the *x*-axis. Equation (2-4) shows that the coupling factor is directly proportional to the effective nonlinear coefficient and inversely to the square root of the effective area. The effective area of a ~6 μm × 3 μm LN waveguide with the maximum index difference of 0.01 is $\cong 20\,\mu\text{m}^2$.

The phase mismatch parameter Δk of each section is calculated first by finding the extraordinary indexes for different wavelengths using the Sellmeier expression in LN

$$n_e^2 = 4.5820 + \frac{0.0992 + 5.2716\times10^{-8} F}{\lambda^2 - (0.21090 - 4.9143\times10^{-8} F)^2} - 0.021940\lambda^2 + 2.2971\times10^{-7} F, \quad (2\text{-}6)$$

where λ is the wavelength in μm and F = 894.75 at 26º C [11]; and second by applying the effective refractive indexes of the waveguide [10]. Finally, the SHG conversion efficiency is defined as

$$\eta = \left|A_{SH}(x=L)\right|^2 / \left|A_{FH}(x=0)\right|^2 \ . \quad (2\text{-}7)$$

2.2.1 Bandwidth of a section in a step-chirped grating

We can now obtain an approximate expression for the bandwidth of a section in an SCG. We choose the length L_1 of the uniform grating consisting of *n* segments of period Λ_1. For the loss-less case that the pump is also non-depleting, the efficiency is given as $\kappa^2 P_0 L_1^2 \left(\sin u / u\right)^2$ where $u = \Delta k L_1$ and $P_0 = A_{FH}{}^2(0)$ is the incident FH power. Neglecting the wavelength dependence of κ, the FWHM *bandwidth of a section* $\delta\lambda$ is attained (see later) when the efficiency drops to 0.5 where $u = \Delta k L_1 = 1.39$, then

$$\left[\frac{2\pi}{\lambda}\Delta N - \frac{\pi}{\Lambda_1}\right] L_1 = \pm 1.39, \quad (2\text{-}8)$$

where $\lambda = \lambda_c \pm \delta\lambda/2$ and $\Delta N = N_{2\omega} - N_{\omega}$. For $\delta\lambda < \lambda_c$, we have

$$\frac{\Delta N}{\lambda} \cong \frac{\Delta N}{\lambda_c \mp \frac{\delta\lambda}{2}} \cong \frac{\Delta N}{\lambda_c} \pm \Delta N \frac{\delta\lambda}{2\lambda_c^{\,2}}, \tag{2-9}$$

where we assumed $\Delta N(\lambda) \cong \Delta N(\lambda_c)$. Substituting Equation (2-9) in (2-8), we obtain

$$\frac{\delta\lambda}{\lambda_c} \cong \frac{1.39\,\lambda_c}{\pi\,\Delta N\,L_1} \cong \frac{2.78}{\pi}\frac{\Lambda_1}{L_1} \cong \frac{0.88}{n}. \tag{2-10}$$

Therefore, the bandwidth of a section in an SCG is approximately equal to the product of the central wavelength and the ratio of the period of the grating to the total length of the section. In other words, the bandwidth of a section decreases as the number of the segments increase, thus the SCG bandwidth will be smaller. Equation (2-10) is a basic rule for the bandwidth calculation of a section in a SCG structure. For example, using a 10-segment SCG device $(n = 10)$, a rough estimate of maximum bandwidth for each section is approximately calculated using Equation (2-10) as $\delta\lambda \approx 0.88\lambda_c / n \approx 135\,\text{nm}$ near 1550 nm. In the next Section, it will be studied how the SCG bandwidth varies with the change of the SCG fundamental parameters of *p*, *n* and $\Delta\Lambda$.

2.2.2 Design considerations of step-chirped grating

To understand how the SCG bandwidth changes for the different SCG fundamental parameters of *p*, *n* and $\Delta\Lambda$, several combinations are simulated. Figure 2-2 to Figure 2-5 show the efficiency of the SCG versus the FH wavelength for different *p*, *n* and $\Delta\Lambda$ parameters. Also, the FH input power is assumed 50 mW. Considering a 50-nm bandwidth around 1550 nm requires the grating length of ~10 cm where the period of SCG starts as $\Lambda_1 = 16881\,\text{nm}$ and therefore $n \times p \cong 6000$ is achieved. Thus, for $n = 10$, 600 sections exist and the chirp step around 1 nm is necessary to cover the 3-dB bandwidth of 50 nm which is shown in Figure 2-2. It is seen that for broadband SHG, interference among phase matching conditions causes large ripples on the conversion efficiency response with the peak-to-peak of around 3 dB.

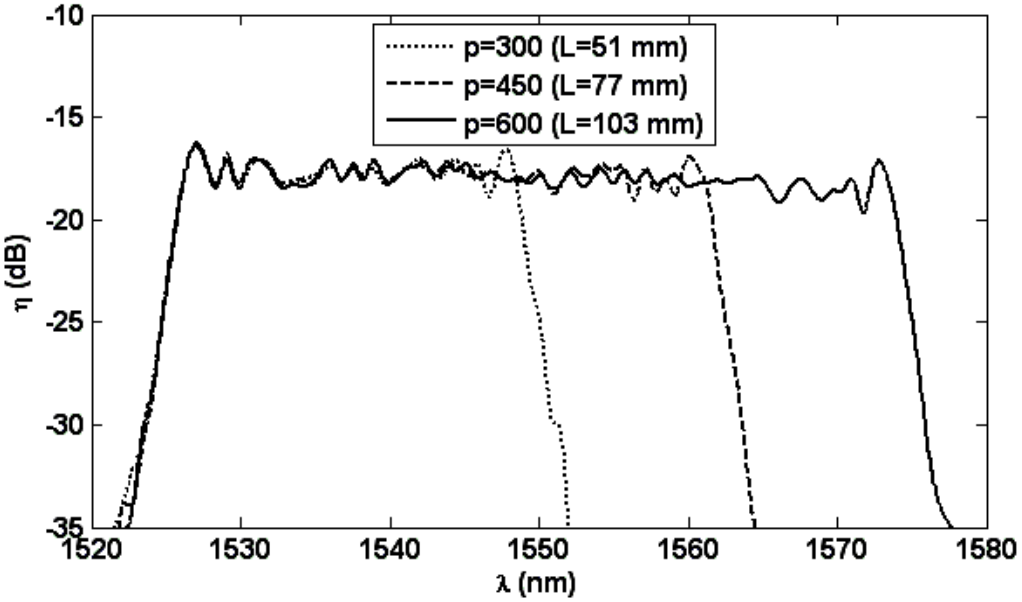

Figure 2-2 : SHG efficiency of SCG versus FH wavelength for different number of sections *p*, $n = 10$ and $\Delta\Lambda = 1\text{nm}$.

However, a shorter length results in a smaller bandwidth and a bandwidth of 25 nm for the SCG is achieved with about 300 sections where the average efficiency over the bandwidth is about -17.5 dB whilst using the uniform grating with the same length of ~5 cm, the bandwidth less than half a nanometer and the efficiency near 0 dB can be achieved.

In Figure 2-2, the SCG structure needs a total length more than 5 cm for the bandwidth greater than 25 nm which is hard to fabricate on LN substrates. To attain the bandwidth of 50 nm with a < 5-cm-long SCG, one possibility is to decrease *n*. In other words, at the expense of losing efficiency we reach the same bandwidth with the shorter SCG which is suitable for fabrication. This case for $n = 5$ is depicted in Figure 2-3. Actually, the conversion efficiency of the new SCG is almost 3-dB lower than that of Figure 2-2 because of the length of each section has been decreased to half.

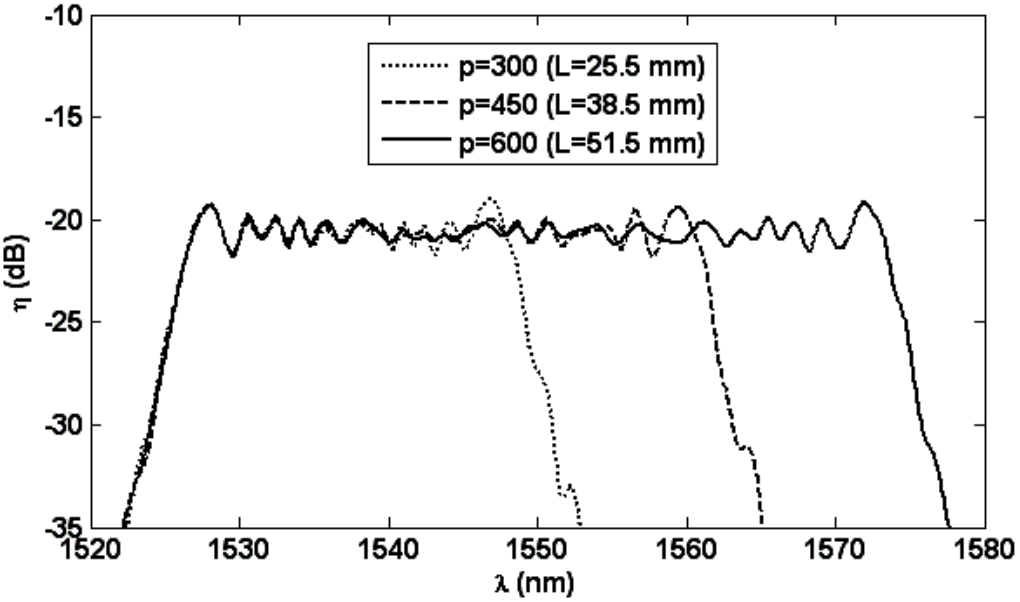

Figure 2-3 : SHG efficiency of SCG versus FH wavelength for different number of sections *p*, $n = 5$ and $\Delta\Lambda = 1\,\text{nm}$.

Another possibility to achieve the maximum bandwidth of 50 nm with a shorter SCG length, is to increase the chirp step. Figure 2-4 illustrates the efficiency for $n = 10$ and $\Delta\Lambda = 2\,\text{nm}$. It is obvious that the efficiency drops by almost 3 dB when the chirp step is doubled, with increased fluctuation on the efficiency response in comparison with Figure 2-2. Also the average efficiency is more slanted as a function of wavelength. So, there is an upper limit for increasing the period as it leads to a sloping response with wavelength and reduces the bandwidth.

Noteworthy conclusion results from the comparison of Figure 2-3 and Figure 2-4 with Figure 2-2, which is useful for understanding the importance of the SCG structure. For a constant length, doubling the sections (e.g. halving the segments), nearly doubles the bandwidth and halves the efficiency. On the other hand, doubling the chirp step $\Delta\Lambda$, also roughly doubles the bandwidth and halves the efficiency.

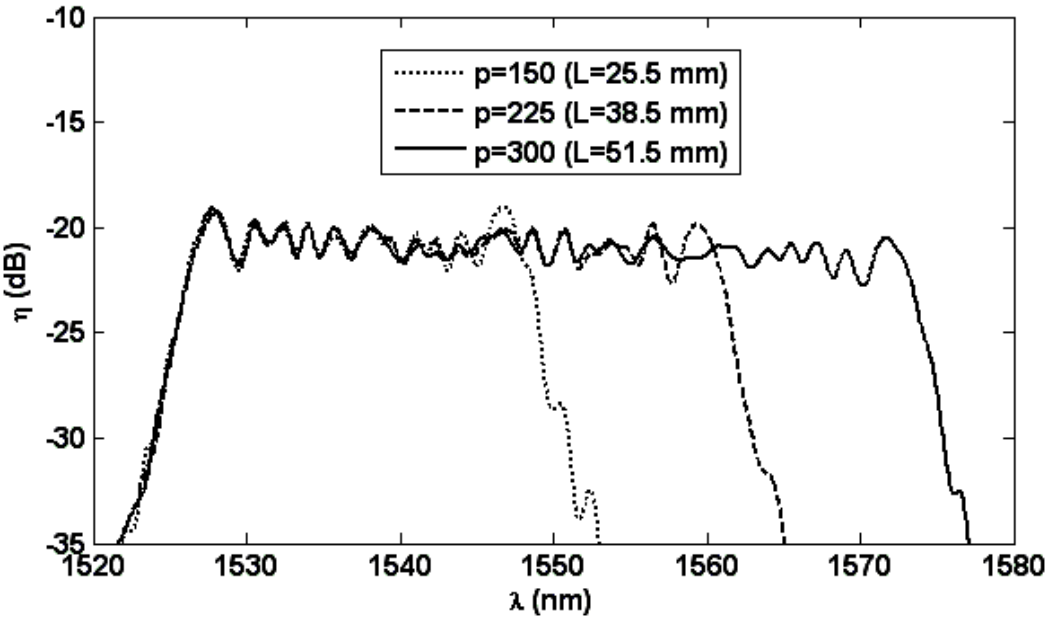

Figure 2-4 : SHG efficiency of SCG versus FH wavelength for different number of sections *p*, $n = 10$ and $\Delta\Lambda = 2\,\text{nm}$.

Figure 2-5 shows the efficiency for $n = 5$ and $\Delta\Lambda = 0.5\,\text{nm}$. The result is almost the same as Figure 2-2. Consequently, doubling the sections and halving the chirp in Figure 2-2 gives approximately the same result as seen in Figure 2-5. Following the same approach, if the chirp changes to one-tenth and the sections tenfold (segments changes to one-tenth), the result remains approximately as Figure 2-2. So, to achieve the same result, the LCG structure needs a smaller period difference in comparison to the SCG structure. Then, to achieve almost the same bandwidth and efficiency, instead of a smooth linear chirp, using a step chirp increases the difference in periods which is convenient for fabrication.

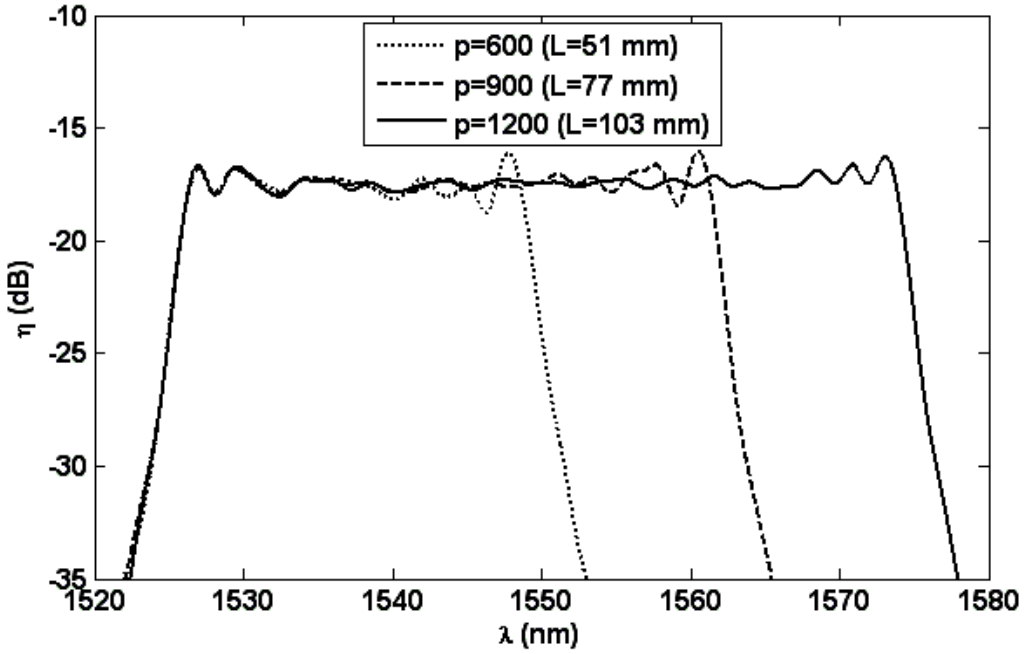

Figure 2-5 : SHG efficiency of SCG versus FH wavelength for different number of sections *p*, $n = 5$ and $\Delta\Lambda = 0.5\,\text{nm}$.

By examining the results of the previous SCG structures, it appears that for $\Delta\Lambda = 1\,\text{nm}$, the number of sections required for an acceptable unit bandwidth in nm from the grating is also a constant, i.e. 12 sections. To study the significance of the chirp step, we note that the approximate FWHM bandwidth of a section with period Λ is given by Equation (2-10) and noting the total bandwidth $\Delta\lambda$ and length *L* in meters and $p \approx 12\,\Delta\lambda / \Delta\Lambda,$ we get the bandwidth of the section which is equal to $\delta\lambda \approx 10\,\Lambda\,\lambda_c\,\Delta\lambda / (L\Delta\Lambda)$. Thus, using the total length of around 5 cm, the central frequency at 1550 nm and the chirp step of 1 nm, the bandwidth of each section is related to the SCG bandwidth by

$$\delta\lambda \approx 5.4\,\Delta\lambda. \qquad (2\text{-}11)$$

The interesting conclusion is that for the constant length of 5 cm, the bandwidth of each section of the SCG should be greater 5.4 times the total bandwidth. If we need to design a 50-nm-bandwidth SCG with the length of around 5 cm and $\Delta\Lambda = 1\,\mathrm{nm}$, according to Figure 2-1, $n \approx L / p\Lambda_{p/2}$ and the SCG will be realized with the number of segments equal or less than 5 (see Figure 2-3).

Additionally, fewer sections in the same length of the SCG give better efficiency because they have more segments. By examining Figure 2-2 and Figure 2-3 we understand that the 50-nm bandwidth can be achieved in both (600 sections: 10 segments) and (600 sections: 5 segments) schemes, but in the latter the length and the average efficiency are almost halved.

2.3 Apodized chirped gratings

In the preceding Section, it was found that the chirped grating enables us to broaden at will the phase matching bandwidth of SHG. However, the technique results in some non-uniformity in the broadband conversion efficiency response of frequency doublers. The ripple feature of SCGs in Figure 2-2 to Figure 2-5 is created by the interference among the constituent phase matching spectra originating from different positions in the gratings. In the following, we consider it more precisely how to remove those noticeable ripples.

The wave equation governs the electric field $E(x,t)$ propagation in the presence of nonlinear polarization $P_{NL}(x,t)$ in the nonlinear medium where the polarization is only a perturbation to the system. Assuming that both the electric field and nonlinear polarization are scalar plane waves and invoking the slowly varying envelope approximation, it can be described as follows [1]

$$\frac{\partial^2}{\partial x^2}E(x,t) - \mu_0\varepsilon\frac{\partial^2}{\partial t^2}E(x,t) = \mu_0\frac{\partial^2}{\partial t^2}P_{NL}(x,t). \tag{2-12}$$

The wave equation is derived in the frequency domain by taking the Fourier transform of Eq. (2-12) given by

$$\frac{\partial^2}{\partial x^2}\tilde{E}(x,\omega)+\mu_0\varepsilon\omega^2\tilde{E}(x,\omega)=-\mu_0\omega^2\tilde{P}_{NL}(x,\omega). \tag{2-13}$$

Describing the fields in complex notation as $\tilde{E}(x,\omega)=\frac{1}{2}\left\{\mathcal{E}(x,\omega)e^{-jk(\omega)x}+\mathcal{E}^*(x,-\omega)e^{jk(-\omega)x}\right\}$, and assuming the slowly varying envelope approximation, Equation (2-13) can be simplified approximately as

$$\frac{\partial}{\partial x}\mathcal{E}(x,\omega)\approx -j\frac{\mu_0\omega c}{2n_{(\omega)}}\mathcal{P}_{NL}(x,\omega)e^{jk(\omega)x}. \tag{2-14}$$

It is possible to define the spectrum of nonlinear polarization leading to SH field with the relation

$$\mathcal{P}_{NL,2\omega}(x,\Omega)=\varepsilon_0 d_{eff}\left\{(\mathcal{E}_\omega e^{-jkx})\otimes(\mathcal{E}_\omega e^{-jkx})\right\} \tag{2-15}$$

where $\otimes$ stands for convolution. Thus, Equation (2-14) gives the equation governing the SH field as

$$\frac{\partial}{\partial x}\mathcal{E}_{2\omega}(x,\Omega)\approx -j\kappa' d_{eff}\left\{\int_0^\infty \mathcal{E}_\omega(\omega')\mathcal{E}_\omega(\Omega-\omega')e^{j\Delta k(\Omega,\omega')x}d\omega'\right\}, \tag{2-16}$$

where $\kappa'=\omega_0/n_{2\omega}c$ and $\Delta k(\Omega,\omega')=k(\Omega)-k(\omega')-k(\Omega-\omega')$ which is a function of the frequencies at the SH (Ω) and FH (ω'). By integrating Equation (2-16) over the total length, the SH spectrum at the output of the converter of length L is

$$\mathcal{E}_{2\omega}(L_t,\Omega) = -j\kappa'\left\{\mathcal{E}_{\omega}\otimes\mathcal{E}_{\omega}(\Omega)\right\}\int_{over\,L} d_{eff}(x)\,e^{j\Delta k(\Omega)x}dx\,. \tag{2-17}$$

In Equation (2-17), the phase matching spectrum can be engineered by controlling the effective nonlinear coefficient, $d_{eff}(x)$. Here, we are only interested in the SH power spectrum. In other words, the effort should be focused to create a broad power spectrum controlling $d_{eff}(x)$ while we change the grating period, such that every local period $\Lambda(x)$ contributes to a constituent phase matched spectrum. In other words, the efficiency curve of the chirped structure versus wavelength is associated with sharp edges in the effective nonlinear coefficient. This is also true for an SCG with a constant $d_{eff}(x)$. This problem can be solved by introducing some form of apodization on the effective SHG coefficient. Therefore, proposing the apodized SCG, the effective nonlinear coefficient is engineered to flatten the efficiency curve of broadband SHG. A reduction in the ripple on the efficiency response of broadband LCG and SCG frequency doublers by tailoring the duty ratios of inverted domains is thus predicted.

2.3.1 Design of step-chirped grating with apodization

In this Section, we propose the apodization of SCGs to flatten the broadband SHG efficiency response. Evolution of conversion bandwidth and the reduction of ripple on efficiency response of SHG-based wavelength conversion by increasing the duty ratio of inverted domains are demonstrated. Figure 2-6 shows the model of the typical grating with several periodically increasing and decreasing inverted domains added at the beginning and the end of SCG shown in Figure 2-1 to form an ASCG structure.

These two parts are periodically poled in each section and aperiodically poled over the whole length. In this ASCG structure, the first and second grating with lengths L' and L'' have been divided into equal $p' = p''$ sections such that each section has the length $(L_i' = n\Lambda_i',\ L_i'' = n\Lambda_i'',\ i = 1,2,...,p')$ consisting of n segments with constant periods Λ_i' and Λ_i''. The periods of the sections in L' and L'' change according to a function which we assume to be $\Lambda_i' = \Lambda_1' + \Delta\Lambda\,(i'-1)$ and $\Lambda_i'' = \Lambda_1'' + \Delta\Lambda\,(i''-1)$ where Λ_1' and Λ_1'' are the periods of the first

sections of the first and second grating structures, respectively. The period relations of these two parts (Figure 2-6) which are settled in the right and left side of the SCG structure (Figure 2-1) described as $\Lambda_1 = \Lambda'_{p'} + \Delta\Lambda$ and $\Lambda''_1 = \Lambda_p + \Delta\Lambda$. Moreover, the effective nonlinear coefficient of the region within a grating period with the duty ratio of a_i is $d_{i(\mathrm{eff})} = (2d_{33}/\pi)\sin(a_i\pi)$ [13]. Thus, in each section we have a uniform grating but with slightly different $d_{i(eff)}$ from its adjacent section by changing the duty ratio which denotes the ratio of one gray region to the period. Consequently, this model of the typical domain-inverted quasi-phase matched gratings has increasing and decreasing duty ratios and effective nonlinear coefficients, at the beginning and at the end of the structure. According to Figure 2-1 and Figure 2-6, $r = L_{apod}/L_t \approx 2p'/p_t$ is the apodization ratio or the ratio of the total length with varying effective nonlinear coefficients $L_{apod} \approx 2L'$ to the total length of the device $L_t = L + 2L'$. The total length is $L_t \cong (p + 2p')n\Lambda_{p/2} = p_t n\Lambda_{p/2}$ where $\Lambda_{p/2}$ is the period of the central section (See Figure 2-1 and Figure 2-6).

Figure 2-7 depicts the normalized effective nonlinear coefficient versus the grating length for different *r* parameters. $r = 0$ illustrates a straight line implying an unapodized device while $r = 1$ depicts a half-cycle sine curve showing a totally apodized device. However, between these two numbers, one can find partially apodized devices.

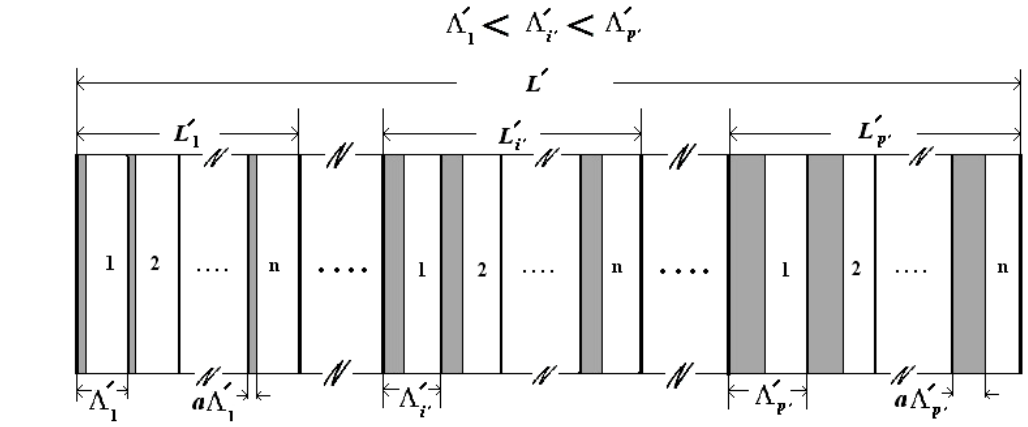

(a)

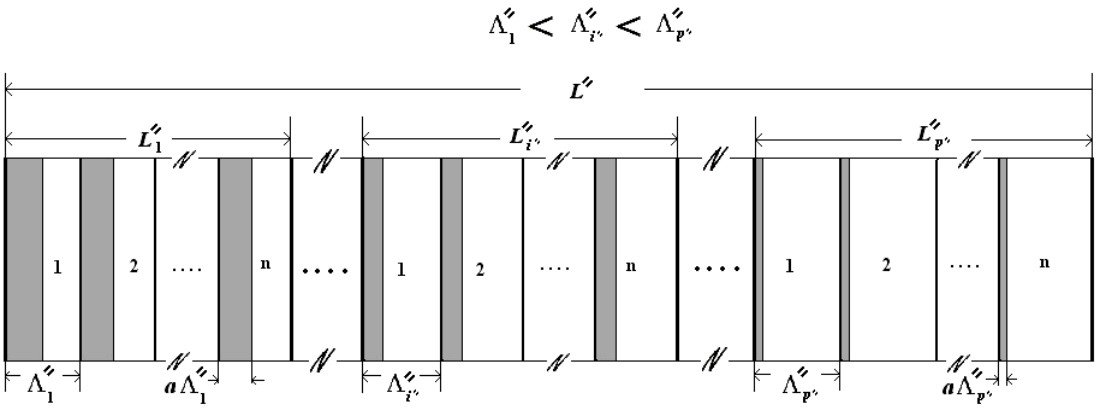

(b)

Figure 2-6 : Model of imposed quasi-phase matched grating structures with (a) increasing and (b) decreasing parts of inverted domains. The ASCG structure begins with (a) at the left side and ends with (b) at the right side of the SCG structure shown in Figure 2-1 where $\Lambda_1 = \Lambda'_{p'} + \Delta\Lambda$ and $\Lambda''_1 = \Lambda_p + \Delta\Lambda$.

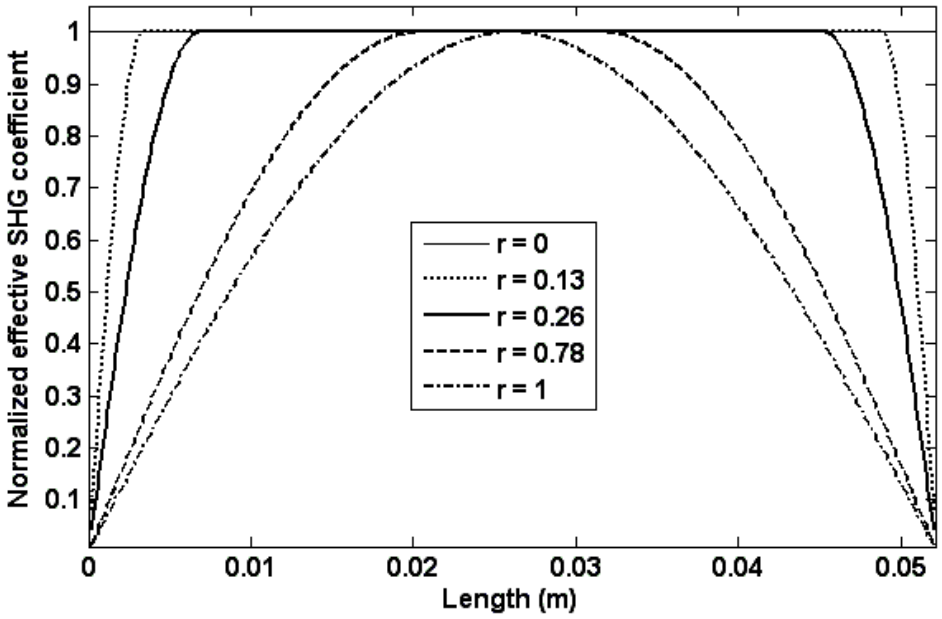

Figure 2-7 : Different apodization functions versus length for different apodization ratios, with $np_t = 3000$.

Efficiency curves versus the FH for the unapodized and apodized SCG structure, based on related apodization functions shown in Figure 2-7, are plotted in Figure 2-8 for $p_t = 300$, $n = 10$, $\Lambda_1' = 17193\,\text{nm}$ and $\Delta\Lambda = 1\,\text{nm}$, where the total length of all the gratings is about 5 cm and FH input power is 50 mW. According to Figure 2-8, enhancement of conversion efficiency and reduction of the ripples in the efficiency response of SHG-based wavelength converter by increasing and decreasing the duty ratio of inverted domains at the beginning and end parts of quasi-phase matched gratings are demonstrated. For a small apodization ratio $r = 0.13$, the efficiency is nearly ripple-free except for the two residual "ears" at the edges. Further suppression of these spectral ears can be achieved by introducing longer apodization regions. For $r = 0.26$, the nearly flat bandwidth of about 23 nm and a maximum flat efficiency of about -17.5 dB can be achieved. It is seen that with increasing *r,* it is possible to obtain improved and different forms of efficiency curves with decreased bandwidths.

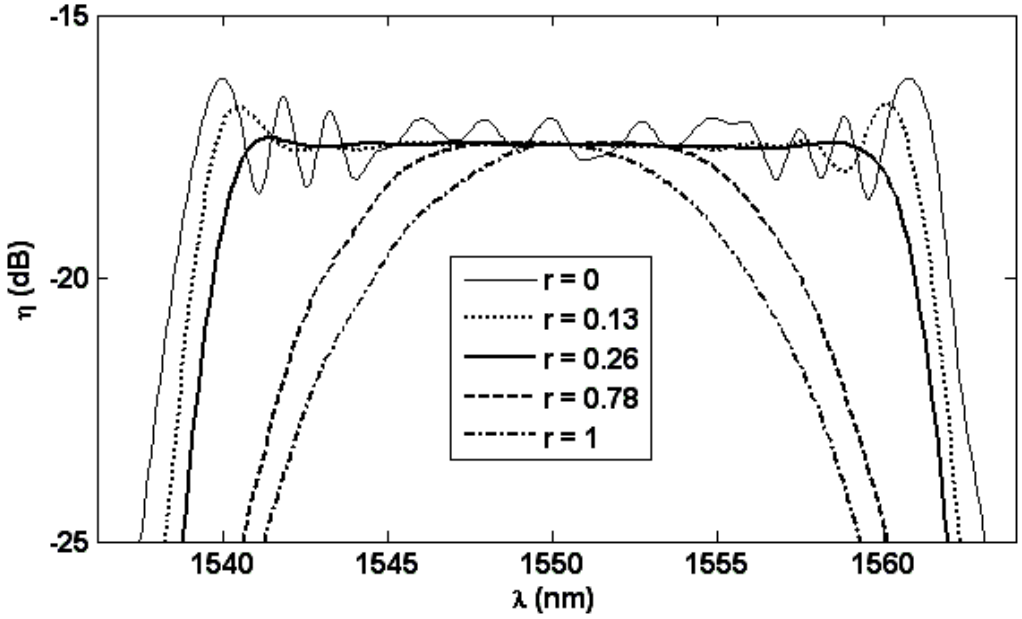

Figure 2-8 : SHG efficiency of SCG and ASCG for the different apodization ratios with $n=10$, p_t=300, $\Lambda_1'=17193\,\text{nm}$ and $\Delta\Lambda=1\,\text{nm}$.

Figure 2-9 shows the efficiency of the unapodized $r=0$ and apodized gratings structure for $p_t=600$, $n=5$, $\Lambda_1'=16881\,\text{nm}$ and $\Delta\Lambda=1\,\text{nm}$. For $r=0.26$, a flat bandwidth of about 44 nm and the maximum flat efficiency of about -20.5 dB can be obtained.

Figure 2-10 gives a comparison between SCGs ($n=10$) and LCGs ($n=1$) when the steps in the periods are 1 nm and 0.1 nm, respectively. Following the approach presented in Section 2.2.2, if the chirp changes to one-tenth and the sections increase tenfold (which changes the SCG into the LCG structure), the results are approximately the same. Thus to achieve the same result, the apodized LCG needs smaller chirp step in comparison to the apodized SCG.

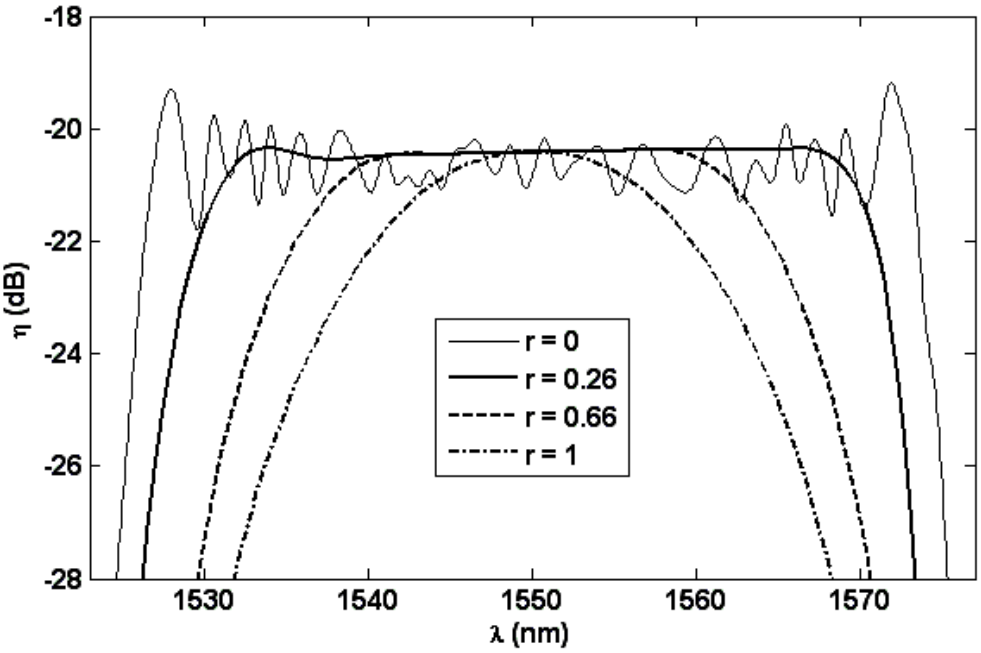

Figure 2-9 : SHG efficiency of SCG and ASCG for the different apodization parameter with $n = 5$, p_t=600 , $\Lambda_1' = 16881m$m and $\Delta\Lambda = 1$nm .

Therefore, to obtain almost the same bandwidth and efficiency of the ALCG, ASCG increases the chirp step, at the price of more segments. On the other hand, for the same length, the ASCG scheme reduces the number of sections and therefore increases the changes in the width of the poled region or the duty factor. Thus, increasing the chirp step and duty-factor change makes the ASCG more convenient for fabrication. The curves in the inset of Figure 2-10 show details of how the ripples and spectral ears of the ASCG structure can be suppressed with increasing apodization ratios. Also, the slight slope between the ears in ALCG is basically a result of nonlinear wave number variation $2\pi / \Lambda(x)$, although the QPM period $\Lambda(x)$ is linear.

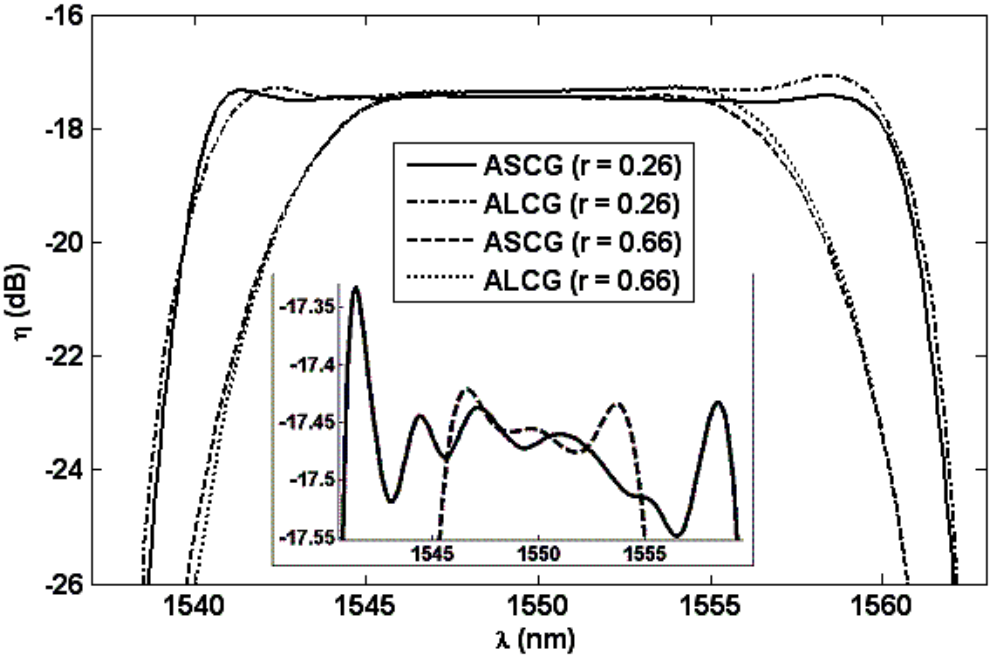

Figure 2-10 : SHG efficiency comparison of ALCG and ASCG for the same length, with a high resolution detail in the inset.

2.4 Few-segment ASCGs in MgO-doped LN

MgO-doped LN waveguides, suggested for the future fabrication, have the advantage of higher optical damage threshold, and can also operate at room temperature [118]. Therefore, the inverted domains in the form of few-segment ASCG in MgO-doped LN waveguides are designed so that the bandwidth is broadened to > 50 nm with a smaller number of segments and larger step chirp.

Using the MgO-doped PPLN information provided by the fabricator including the extraordinary refractive index as

$$n_e^2 = 4.5583 + \frac{0.091806}{\lambda^2 - 0.048086} - 0.032068\lambda^2, \tag{2-18}$$

leads to the period of 18.85 μm around 1550 nm. Based on the procedure of Section 2.2.2, the number of sections required for a unit bandwidth (in nm) from the 5-cm SCG in MgO-doped LN is calculated to be roughly 8.5 sections for the chirp step of 2 nm and thus $p_t \approx 17\,\Delta\lambda / \Delta\Lambda$. Therefore, for a 50-nm-bandwidth SCG with the length of 5 cm and the chirp step of 2 nm it is necessary to have the number of segments equal or less than 6 using $n = L_t / p_t \Lambda_{p/2}$. Thus, for maximum conversion efficiency, a 6-segment ASCG is designed to provide the 50-nm flattop bandwidth with apodization ratio of $r = 0.40$. Also, the minimum line width $(a_1\Lambda_1)$ is considered to be 100 nm.

Figure 2-11 shows the SHG efficiency of the 6-segment ASCG versus FH wavelength, assuming different large chirp steps, waveguide length and input power parameters. Figure 2-11 demonstrates that keeping the chirp step around 2 nm leads to a nearly flat response and the enhancement of the chirp step leads to a slanted response with increasing bandwidth, and a decrease in efficiency. Nevertheless, slight slopes are seen in the response for $\Delta\Lambda = 2.5\,\text{nm}$ and 3 nm. Moreover, the noteworthy feature of the ASCG is that when the input power is halved (25 mW), the efficiency is also halved and the bandwidth is nearly unchanged. On the other hand, decreasing the waveguide length to one half (25 mm), decreases the bandwidth to almost one half while the efficiency remains the same. The reasons for this are based on the ASCG structure which consists of several unchirped sections with nearly equal lengths (due to chirped structure the periods change between sections and therefore they are different in length, e.g., about 12-nm length difference between two adjacent sections for 6-segment ASCG), each of which produces almost the same efficiency for the phase-matched wavelength of that section (and this is proportional to the squared length of the section) and a similar bandwidth with a small shifted central wavelength. Thus, as we increase the sections with a small chirp step between them, we consequently increase the length and the equivalent bandwidth of the whole SCG while the mean efficiency remains almost unchanged. At the same time as the length of each section is very small, its efficiency changes linearly with power, as in unchirped phase matching. Therefore, the results show that the bandwidth and efficiency are almost linearly proportional to the length and input power, respectively. Further, there is another notable point which is useful for controlling the flat-top bandwidth of the phase matching response of the ASCG. Figure 2-11 shows for a

constant length, raising the chirp step, increases the bandwidth (and the slant in the response) and decreases the efficiency.

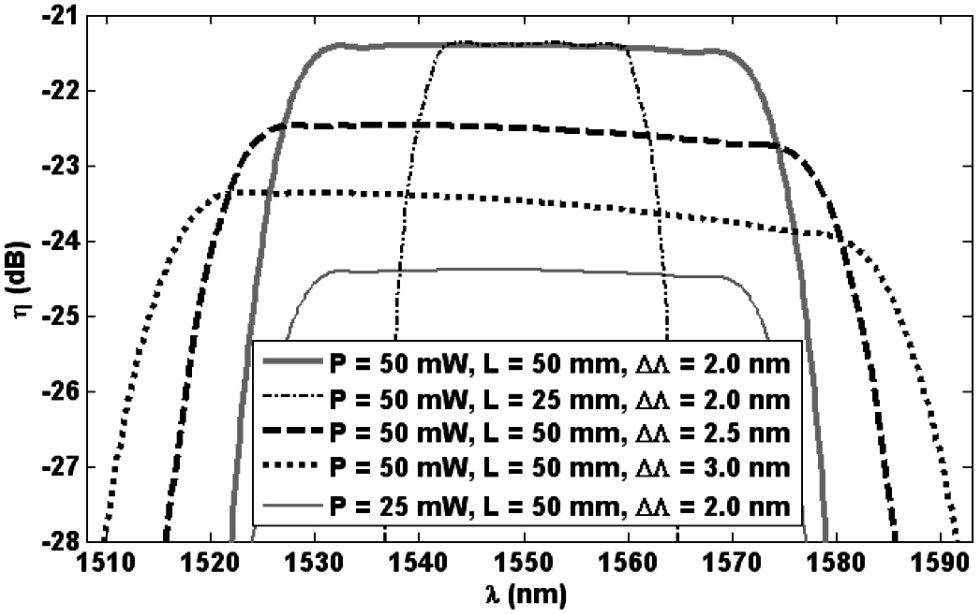

Figure 2-11 : SHG efficiency versus FH wavelength for 6-segment ASCGs with $r = 0.40$ and different parameters.

One challenge in the previous design is the smallness of the minimum width of line in the apodized parts, which is assumed 100 nm. As the 100-nm size is difficult to fabricate, in order to examine the effect of enhancing the minimum line width, we consider a 1000-nm line width, to ease the fabrication. Nonetheless, increasing the minimum line width in the ASCG, it is still possible to attain almost the same efficiency responses with a small price of a slight increase in the non-uniformity of conversion efficiency over the bandwidth in the benefit of facilitating the poling and fabrication processes.

Figure 2-12 illustrates the efficiency curves versus input wavelength for the 5-, 6- and 7-segment ASCG for the apodization ratio of 0.4, length of ~5 cm and input FH power of 50 mW. It shows

that using $a_1\Lambda_1 = 1\mu m$ introduces a small fluctuation in the response of ±0.15 dB. Nonetheless, increasing the minimum line width also makes the fabrication of the few-segment apodized step-chirped gratings with the large chirp steps more convenient.

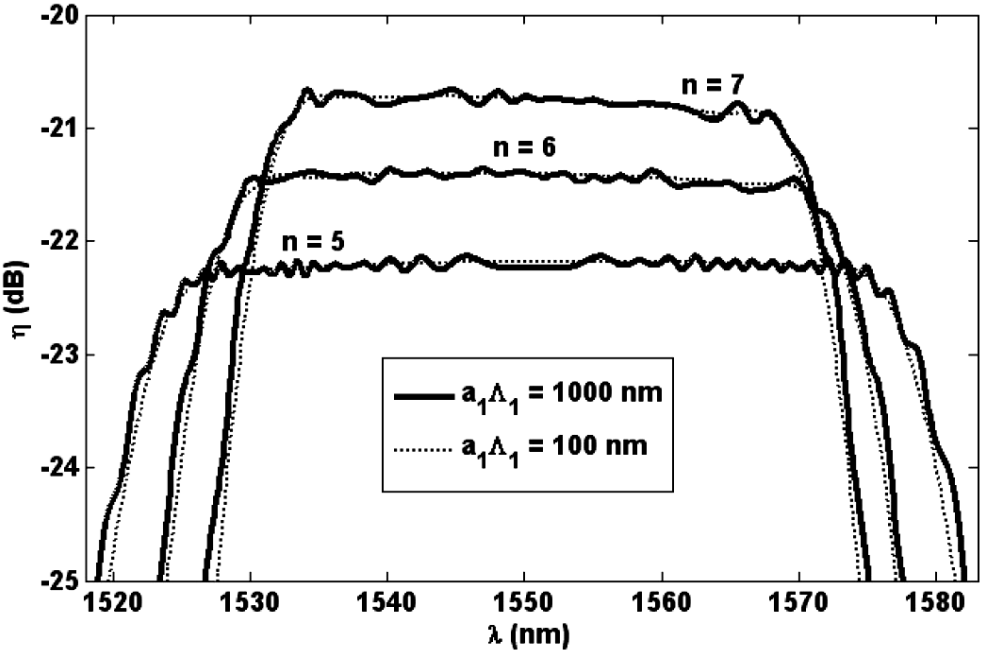

Figure 2-12 : SHG efficiency versus FH wavelength with $r = 0.40$ for 5-, 6- and 7-segment ASCGs when $L_t \approx 50\,\text{mm}$.

On the other hand, Figure 2-12 demonstrates that decreasing the number of segments for the same length, increases the bandwidth and decreases the efficiency. Thus, it is possible to achieve higher bandwidth when there are fewer segments in more sections in the same length and it is a good technique to design highly-broadband frequency converters. Consequently, a bandwidth > 65 nm can be obtained for a 5-segment ASCG while the efficiency can be linearly increased with the enhancement of input FH power.

Table 2-1 shows the design parameter for the apodized SCG (6-segment) and apodized LCG (1-segment) structure with a ~5-cm MgO-doped LN waveguide and the central period of 18.85 μm around the central FH wavelength of 1550 nm (from uniform grating) with the bandwidth of around 50 nm and the mean efficiency of -22 dB (for 17 dBm input FH power) when the minimum width of line is 100 nm (fine) or 1000 nm (coarse).

Table 2-1 : Design parameters for different engineered chirped gratings to achieve almost the same mean efficiency and bandwidth.

	ASCG (Coarse)	**ASCG (Fine)**	**ALCG (Coarse)**	**ALCG (Fine)**
Min. line width $(a_1\Lambda_1)$	1000 nm	100 nm	1000 nm	100 nm
Ripple (dB)	±0.15 dB	±0.05 dB	±0.15 dB	±0.05 dB
Chirp step $(\Delta\Lambda)$	2 nm		0.3 nm	
Sections (p_t)	450		2700	
Segments (n)	6		1	

2.5 Conclusion

In this Chapter, we proposed the engineering of the step-chirped grating in such a way as to broaden significantly the QPM bandwidth of SHG with larger chirp steps in which we used a full model of FH pump depletion to solve the equations. Also, a formula was presented for the first time to determine the maximum number of segments one should use as a design rule dependent on the required bandwidth. Achievement of higher conversion bandwidth also was addressed with the special design of a few-segment engineered SCG in such a way as to provide us with a controllable broadband response. Tens of nanometer flat bandwidth is achieved with a 5-cm-long ASCG in LN waveguides for different number of segments whilst the counterpart uniform grating with the same length, has less than 0.5-nm bandwidth. An effective apodization technique is proposed to broaden and flatten the wavelength conversion bandwidth by engineering the patterns of inverted domains in increasing and decreasing forms. Further, by re-designing of the inverted domains in the form of few-segment ASCG in MgO-doped LN, the bandwidth broadened with a smaller number of sections and larger step chirp. The efficiency curves with the bandwidth as large as 65 nm (which can still be increased) were smoothed dramatically and flattened with the ripples being reduced to less than ±0.15 dB, even with a 1000-nm minimum width of line, and the spectral ears significantly suppressed at the cost of a 40% apodization ratio. Further, it was found that the bandwidth and efficiency are almost linearly proportional to the length and input FH power, respectively. However, the moderate efficiency can still be improved with some techniques, e.g., using the waveguides with smaller effective cross sections or resonance, which are further investigated in the next Chapter.

Summarizing, the use of the engineered ASCG with the larger minimum line width and chirp step is a highly flexible technique for design, and for easing the fabrication requirements of highly-broadband frequency doublers and the proposed concepts can be applied for broadband QPM to other NLO materials like polymers and semiconductors, with and without waveguide.

CHAPTER 3
EFFICIENCY ENHANCEMENT OF BROADBAND QUASI-PHASE MATCHED SHG USING SMALL EFFECTIVE-CROSS-SECTION WAVEGUIDE AND SINGLY PUMP-RESONANCE

3.1 Overview

In Chapter 2, it was shown that the SHG efficiency of the ASCG is diminished compared to the uniform grating with the same length. Nevertheless, the efficiency can be boosted with small-cross-section waveguides. This is because the coupling factor is inversely dependent on the square root of the waveguide effective cross section. Therefore, a smaller cross section may lead to higher efficiency. To achieve this goal, APE waveguides can be chosen because of the possibility of higher index difference and a smaller mode field cross section [11] but the reported loss of APE waveguides in LN is greater than that of Ti-indiffused waveguides in LN (e.g., > 0.1 dB/cm) [36], [105], [109]. However, Ti-indiffused waveguides cannot be used with high powers.

On the other hand, the SHG efficiency of ASCG for quasi continuous waves (CW) may be increased with resonant structures. There are several theoretical analyses and experiments on different types of bulk and waveguide resonant SHG devices [60]-[74]. A Fabry-Perot type cavity maybe constructed in a waveguide SHG device by placing cavity mirrors on waveguide facets. For waveguide devices, experimental study of narrowband SHG was done in phase-matched singly pump-resonant waveguide SHG devices and an increased efficiency was obtained with a matched resonator [74]. Also, a 40% enhancement of the efficiency for a quasi-phase matched SHG device by integrating two distributed Bragg reflector was achieved [66]. Moreover, a narrowband pump-resonant quasi-phase matched SHG device with uniform gratings and a factor of 8 higher conversion efficiency was demonstrated [70], [71].

Nonetheless, to increase the efficiency of ASCG in broadband wavelength conversion, using small-effective-cross-section waveguides with or without singly pump-resonance, a strong

improvement in the conversion efficiency response is anticipated. In this Chapter, we design an ASCG-based device including APE waveguides in LN in such a way as to broaden the bandwidth with the maximum efficiency while we consider an effective apodization to flatten the SHG bandwidth. Also, assuming a singly pump-resonant waveguide structure including the designed ASCG, we show that for the quasi-continuous FH it is possible to increase the conversion efficiency envelope of resonant axial modes effectively while the conversion bandwidth remains almost the same.

3.2 Design of efficient broadband SHG using APE waveguide

A scheme of apodized step-chirped grating in LN waveguide is shown in Figure 3-1(a). Using APE waveguides, it is possible to enhance the efficiency due to the smaller effective cross section. For this device, an optical waveguide is designed with the dimensions of ~ 3 μm × 1.25 μm to achieve the maximum confinement resulting to a tighter coupling coefficient between FH and SH. We consider the dimensions of the lithium niobate waveguide in such a way as to support one guided mode for both FH and SH waves [10]. The result for optical field distribution in the resultant single mode waveguide is depicted in Figure 3-1(b) and (c) in which 3.1 μm × 2.1 μm and 2.3 μm × 1.25 μm are the mode widths of FH and SH, respectively. These result in a small effective-cross- section of ~5 μm^2 which later leads to a higher coupling factor between the FH and SH waves and thus a higher SHG efficiency.

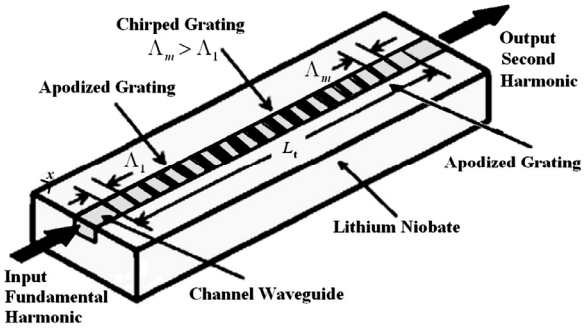

(a)

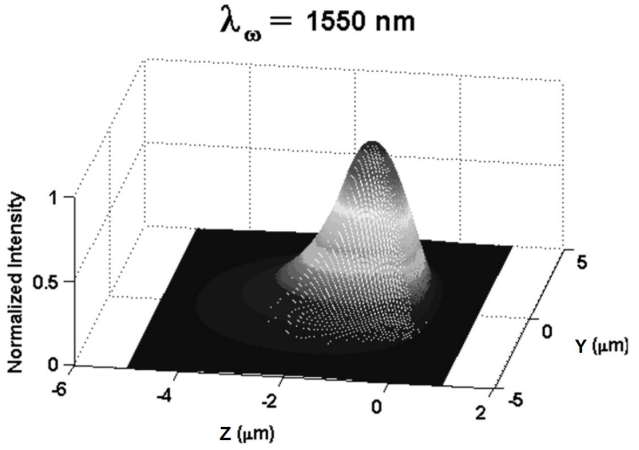

(b)

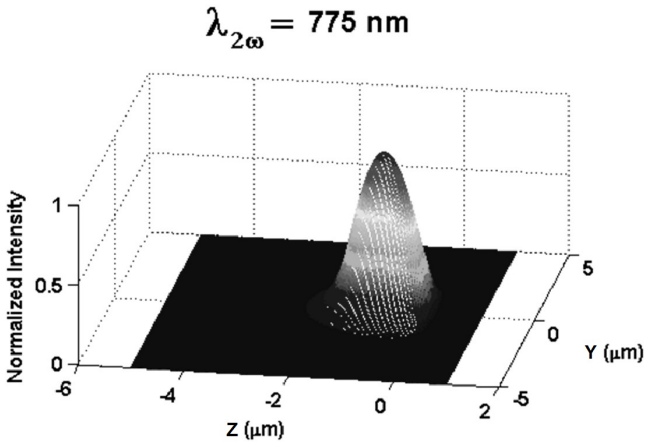

(c)

Figure 3-1 : (a) A Scheme of the proposed device. Optical field distribution for (b) FH (λ_ω = 1550 nm) and (c) SH ($\lambda_{2\omega}$ = 775 nm).

The exact form of the ASCG on top of the device in Figure 3-1(a) is depicted in Figure 3-2. Based on the procedure of Section 2.2.2, the number of sections required for a unit bandwidth (in nm) from the 5-cm SCG in LN is calculated to be roughly 10 sections for the chirp step of 0.75 nm and thus $p_t \approx 7.5\Delta\lambda / \Delta\Lambda$. Therefore, for a 35-nm-bandwidth SCG with the length of 5 cm and the chirp step of 0.75 nm, using $n = L_t / p_t \Lambda_{p/2}$, it is necessary to have the number of segments ≤ 10. Therefore, to achieve higher efficiency, we choose larger number of segments, namely 10. On the other hand, the central period for the central wavelength (for a PPLN at 1550 nm) is obtained to be around 14.43 μm. This rules that a ~5-cm grating can accept around 3500 periods. Thus, this results in having 350 sections, each of which has 10 segments. The period of the grating starts at $\Lambda_1 = 14303\,\text{nm}$ and finishes at $\Lambda_{350} = 14565\,\text{nm}$. The apodization ratio is kept around 0.4 to achieve the maximum bandwidth with flat response, which leads to using 140 apodized sections (i.e., r = 140/350) equally set in the beginning and the end of the structure. The parameters of the designed ASCG in detail are given in Table 3-1.

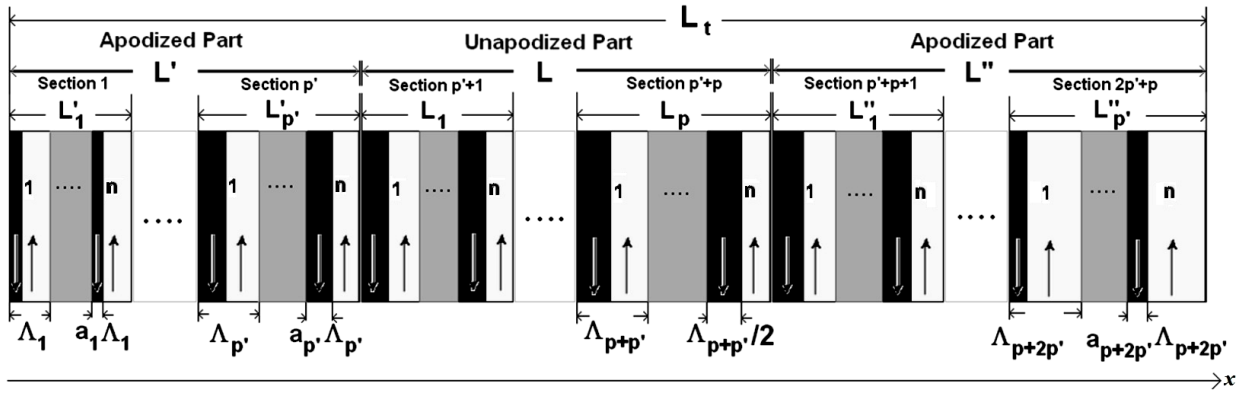

Figure 3-2 : Schematic of proposed ASCG structures (n > 1) with increasing and decreasing parts of inverted domains. For n = 1, it converts to an ALCG structure. The up and down arrows refer to the sign of $\chi^{(2)}$ in white and black regions, respectively.

Table 3-1 : Design parameters of the ASCG for broadband SHG ($r \sim 0.4$).

Parameter	value	Description
n	10	No. of periods in each section
p_t	350	Total no. of sections
$2p'$	140	Total no. of apodized sections
Λ_1'	~14.3 μm	Period of first section
$\Delta\Lambda$	0.75 nm	Step chirp
N_ω	~2.15	Effective index for FH
$N_{2\omega}$	~2.20	Effective index for SH
λ_c	1550 nm	FH central wavelength
L_t	~5 cm	Total length of gratings
d_{33}	25 pV/m	NLO coefficient of LN
Δn_e	0.09	Max. index difference
a_1	100 nm	Width of first poled region
W	3 μm	Waveguide width
D	1.25 μm	Waveguide depth
κ	~262 $W^{-1/2}m^{-1}$	Coupling factor

Figure 3-3 depicts the SHG efficiency of the SCG and ASCGs ($n = 10$) versus the FH wavelength and provides a comparison between them for different r parameters when the chirp step is 0.75 nm. Similar curves to Figure 2-8 with higher SH efficiency is achieved showing how the ripples of the ASCG may also be suppressed with increasing r. For a small apodization ratio

$r = 0.2$, the efficiency is nearly ripple-free with the bandwidth of ~32 nm, except for the two residual ears at the edges, and the maximum flat efficiency of about -12 dB can be achieved. Further suppression of these spectral ears can be achieved by introducing longer apodization regions. For $r = 0.4$, the nearly flat bandwidth of ~30 nm with the maximum flat efficiency of about -12 dB can be achieved showing almost 5.5 dB increase compared to that of Figure 2-8 with the same length and input FH power. It is seen that with increasing *r* up to 1, it is possible to obtain improved and different forms of efficiency curves with correspondingly smaller bandwidths.

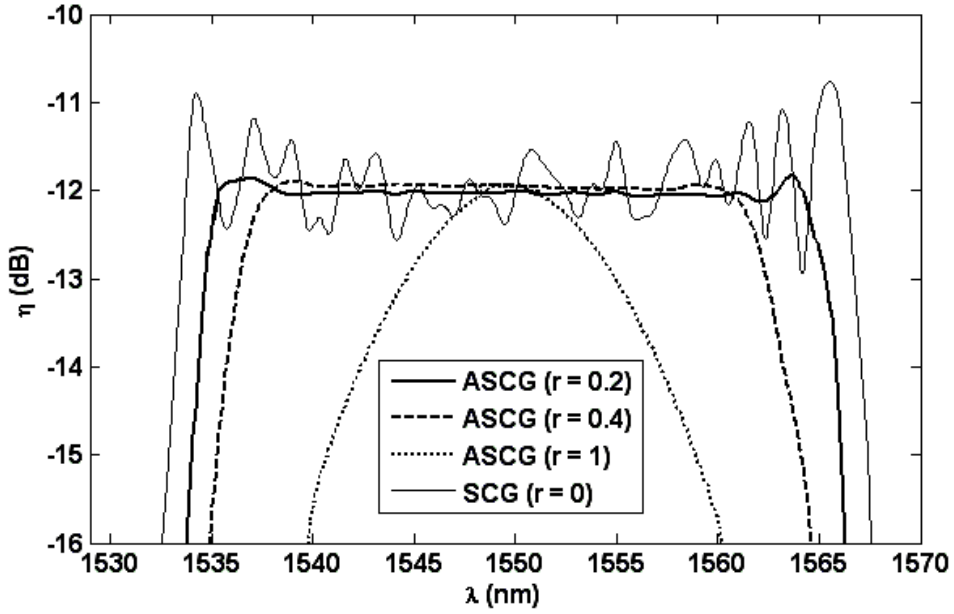

Figure 3-3 : SHG efficiency comparison of SCG and ASCGs for the different apodization ratios where $n = 10$ and $\Delta\Lambda = 0.75\,\text{nm}$.

Figure 3-4 illustrates the SHG efficiency of the LCG and ALCGs ($n = 1$) versus the FH wavelength when the chirp step is 0.075 nm. It provides a comparison between LCG and ALCGs for different *r* parameters so that different forms of efficiency curves with different bandwidths

can be achieved. Based on the approach, the enhancement of conversion efficiency and reduction of ripples in the SHG efficiency response of ALCGs by increasing and decreasing of the duty ratio of inverted domains at the beginning and end parts of LCG are demonstrated. It shows how the ripples and spectral ears of the ALCGs can be suppressed with increasing apodization ratios. Again, the slight slope seen between the ears in the ALCG is basically a result of nonlinear wave-number variation, although the QPM period changes linearly.

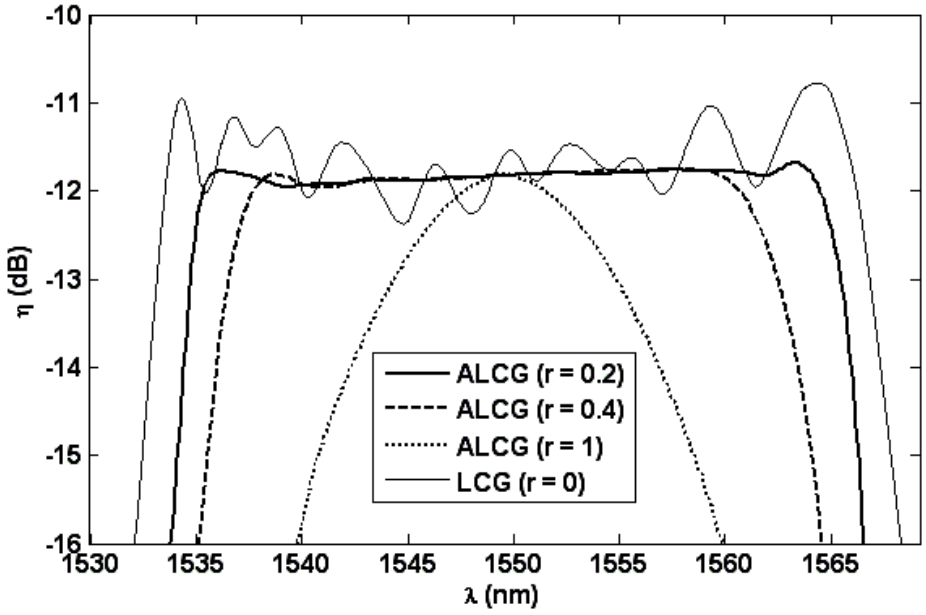

Figure 3-4 : SHG efficiency comparison of LCG and ALCGs for the different apodization ratios where $n = 1$ and $\Delta\Lambda = 0.075\,\text{nm}$.

A comparison between Figure 3-3 and Figure 3-4 shows that if the chirp period changes to one-tenth and the sections increase tenfold (which changes the SCG into the LCG structure), the results are approximately the same. Thus to achieve the same result, the apodized LCG needs smaller chirp period in comparison to the apodized SCG. Therefore, to obtain almost the same bandwidth and efficiency of ALCG, ASCG increases the chirp step, at a cost of more segments.

On the other hand, for the same length, the ASCG reduces the number of sections and therefore increases the changes in the width of the poled region or the duty cycle. Thus, increasing the chirp step and duty-cycle change makes the ASCG more convenient for fabrication.

Figure 3-5 illustrates the efficiency of the ASCG ($n=10$) and ALCG ($n=1$) structures versus the FH wavelength and gives a comparison between them for different r parameters when the steps in the periods are 0.75 nm and 0.075 nm, respectively. For $r=0.2$, the nearly flat bandwidth of about 32 nm with the ears at the edges and the maximum flat efficiency of about -12 dB can be achieved for both cases while ASCG suppress the slope of the efficiency in comparison to ALCG .

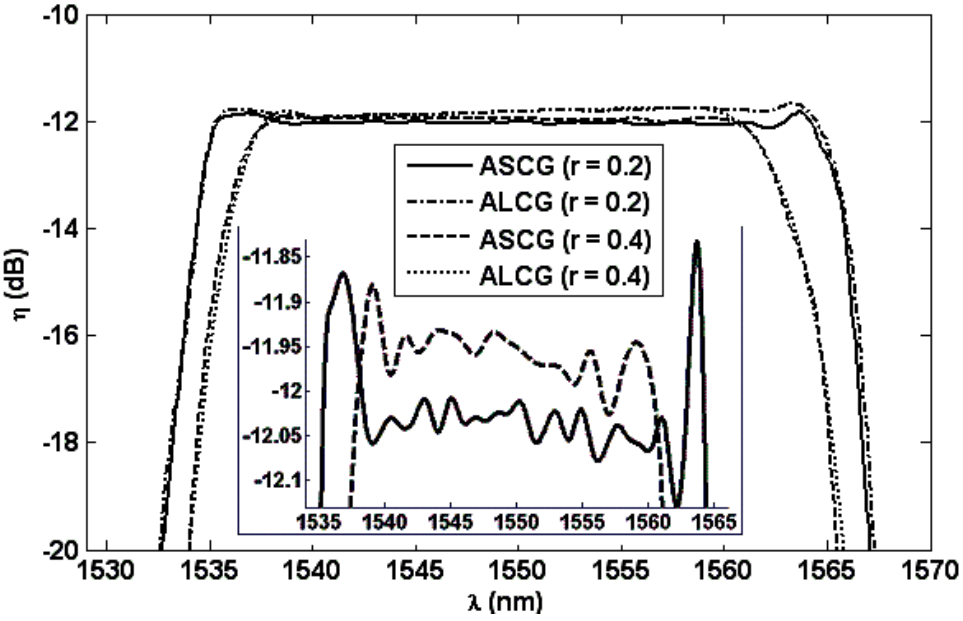

Figure 3-5 : SHG efficiency comparison of LCG and SCG, and ALCG and ASCG for the same length, with a high resolution detail in the inset.

The SHG efficiency of the small-cross-section waveguide improves around 5.5 dB due to the enhancement of the coupling coefficient in comparison to the large-cross-section waveguide in Figure 2-10. Also, the SHG bandwidth for the small-cross-section waveguide has a maximum of 10-nm increase due to the increment of p_t and decrement of $\Delta\Lambda$. The curves in the inset of Figure 3-5 show how the ripples of the ASCG may also be suppressed with increasing *r*. Also, further suppression of spectral ears can be achieved by introducing larger apodization ratio shown for $r = 0.4$.

3.3 Design of efficient broadband SHG using pump-resonant waveguides

With a simple arrangement, a Fabry-Perot type cavity enables the construction of a singly pump-resonant device including the designed ASCG achieved by imposing cavity mirrors on waveguide facets, to resonate the quasi-CW pump for SHG. A singly pump-resonant device for the proposed broadband frequency doubler is shown in Figure 3-6.

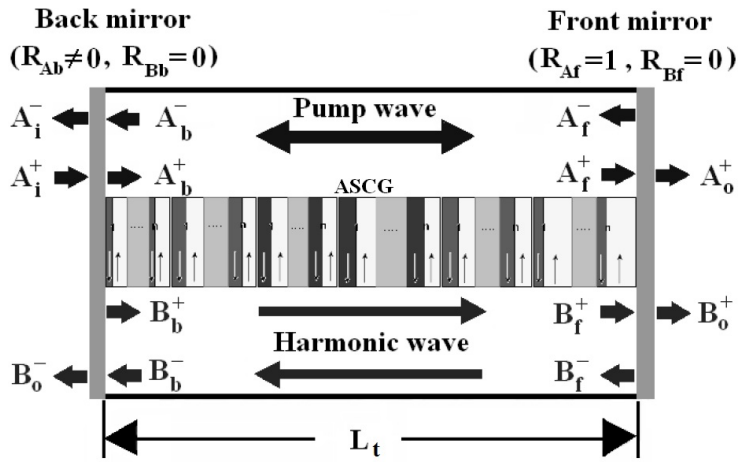

Figure 3-6 : Simple configuration of a singly pump-resonant waveguide for broadband ASCG-based frequency doubler.

Cavity mirrors are set to the front and back facets of the waveguide ASCG frequency doubler. A quasi-CW FH pump wave launched from the back side, propagates and resonates in the waveguide cavity. The SHG can occur in the waveguide, with an SH quasi-CW as the output. The power reflection coefficients for the FH and SH are described by R_{Ab} and R_{Bb} for the back-facet mirror and by R_{Af} and R_{Bf} for the front-facet mirror, respectively. Nevertheless, precise control of the grating position relative to the mirrors and that of cavity length, for realization of efficient SHG in resonant waveguide devices, are necessary. Further, for an efficient resonant converter, the phase matching condition for SHG and resonance conditions for the FH wave $(2\beta_{FH}L_t = 2m\pi)$ must be satisfied simultaneously. The latter means that the resonant longitudinal modes include the frequencies which satisfy the condition $\Delta\nu = 1/\tau \approx c/2N_\omega L_t$, where τ is the round trip time. This mode spacing is around 1.4 GHz (i.e. ~11 pm at a wavelength of ~1550 nm) for the structure. After a round trip, the power of the FH guided wave will be $R_{Af}R_{Ab}\exp(-2\alpha L_t)$ times the initial value where α is the loss for the FH. The inverse of photon life time can be expressed as $\frac{1}{\tau_p} = \frac{c}{N_\omega}(\alpha + \frac{1}{2L_t}\ln\frac{1}{R_{Ab}R_{Af}})$ and the linewidth can be written as $\delta\nu \approx 1/2\pi\tau_p$ showing that it depends on the present loss in the low finesse resonator [65]. Whilst the resonance condition is satisfied, the boundary conditions of a simple singly pump-resonant SHG device are $A_b^+ = \sqrt{1-R_{Ab}}A_i^+ + \sqrt{R_{Ab}}A_b^-$ and $A_i^- = \sqrt{1-R_{Ab}}A_b^- - \sqrt{R_{Ab}}A_i^+$ for the FH quasi-CW at the input facet of waveguide and $A_f^- = \sqrt{R_{Af}}A_f^+$ and $A_o^+ = \sqrt{1-R_{Af}}A_f^+$ for the FH quasi-CW at the output facet of the waveguide and $B_b^+ = 0$, $B_o^- = B_b^-$ and $B_o^+ = B_f^+$, $B_f^- = 0$ for the SH quasi-CW at the input and output facets of the waveguide, respectively. However, the singly pump-resonant SHG devices ($R_{Ab}R_{Af} \neq 0$ and $R_{Bb}R_{Bf} = 0$) are preferred to doubly resonant devices as the SH power build-up is not required in these devices [68].

To obtain series of high-efficiency axial-mode SH waves from a resonant quasi-CW FH waves shown by an envelope response, a simple singly pump-resonant structure including the previously-designed 10-segment ASCG in an APE LN waveguide as a broadband frequency doubler is considered here and numerically characterized assuming the different amounts of FH

loss where the reflectivities are taken invariant over the bandwidth. However, for a practical singly pump-resonant device, the exact efficiency can be obtained by subtracting the additional losses such as the reflection of the quasi-CW SH waves at the mirrors in dB from the efficiency result. Figure 3-7 shows the envelope of SHG efficiency responses of the singly pump-resonant waveguide with the ASCG, versus FH wavelength for different R_{Ab} when $R_{Af} = 1$ and the total waveguide FH loss of $\alpha L_t = 1\text{dB}$. Other parameters are the same as given for Figure 3-3. With increasing reflectivity of FH at the back facet mirror, the efficiency improves and reaches a maximum of $\approx -2.9\,\text{dB}$ for $R_{Ab} \approx 0.65$ and decreases again with the increasing R_{Ab}. Furthermore, using the resonant waveguide for the ASCG structure with $r = 0.4$, nearly the same 3-dB bandwidth of ~30 nm (i.e. ~3.75 THz) is obtained, which includes around 2700 axial modes with an 11.2 pm (~1.4 GHz) separation and a 1.6 pm (~0.2 GHz) FWHM linewidth, and in the best case, at least a 9-dB improvement in peak efficiency can be achieved in comparison to Figure 3-3.

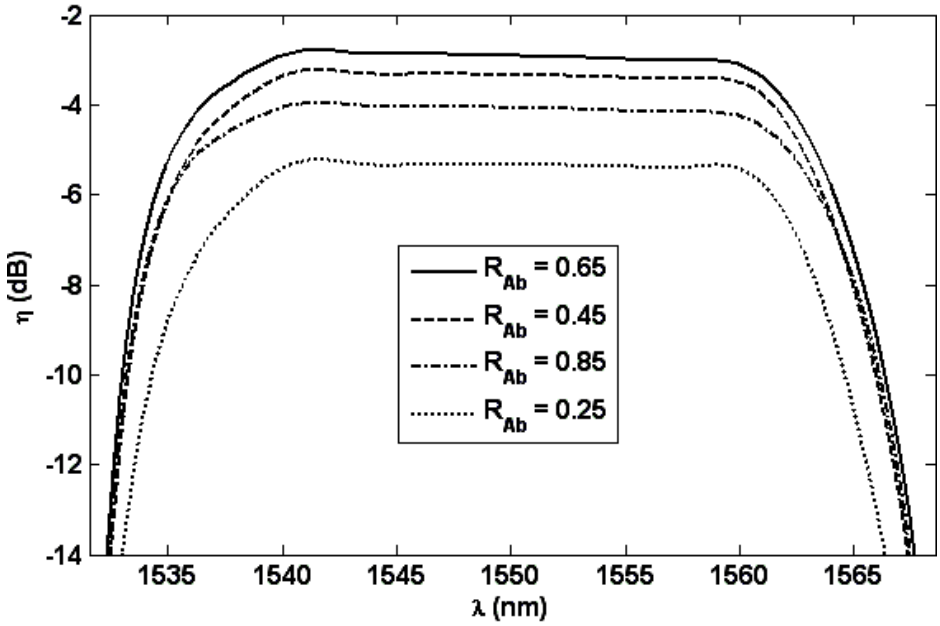

Figure 3-7 : The envelope of SHG efficiency responses of the singly pump-resonant ASCG versus FH wavelength, for $R_{Af} = 1$, $\alpha L_t = 1\text{dB}$ and $L_t \approx 5\,\text{cm}$.

Figure 3-8 depicts the envelope of SHG efficiency responses of the singly pump-resonant waveguide with ASCG, versus wavelength for different R_{Ab} assuming $R_{Af}=1$ and the total waveguide FH loss of $\alpha L_t = 3\,\text{dB}$ when other parameters of Figure 3-3 remain the same. In Figure 3-8, the maximum efficiency of about –7.2 dB is achieved for a lower back facet reflectivity of $R_{Ab}=0.45$ implying that more FH waveguide loss results in lower efficiency. Thus, in the case of a high-loss resonant waveguide, ~4.8-dB improvement in peak efficiency can be obtained in comparison to –12 dB for the non-resonant waveguide shown in Figure 3-3. Also, Figure 3-8 may predict the peak efficiency when the back facet reflectivity and FH loss are $R_{Af}=0.8$ and $\alpha L_t = 1\,\text{dB}$, respectively. In comparison to Figure 3-7 ($R_{Af}=1$ and $\alpha L_t = 1\,\text{dB}$), it shows that the reduction of the reflectivity of the front facet also deteriorates the efficiency even when the waveguide loss is constant.

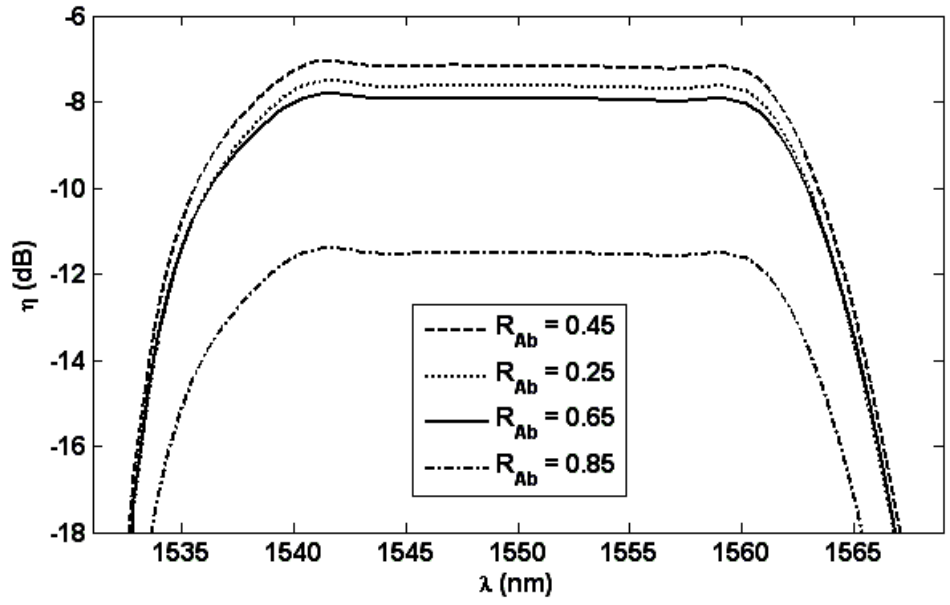

Figure 3-8 : The envelope of SHG efficiency responses of the singly pump-resonant ASCG versus FH wavelength, for $R_{Af}=1$, $\alpha L_t = 3\,\text{dB}$ and $L_t \approx 5\,\text{cm}$.

Figure 3-9 illustrates the maximum SHG efficiency versus R_{Ab} for different amounts of FH waveguide loss. It is clear that the highest efficiency is obtainable only for the lowest loss (i.e. lossless waveguide $\alpha L_t = 0$). Although the efficiency degrades due to loss, remarkable enhancement is still achieved in matched situations with the proper selection of R_{Ab}. The matching condition for singly pump-resonant structures represents that no pump power exits from the resonator, meaning that $A_i^- = (A_b^- / A_b^+ - \sqrt{R_{Ab}})A_b^+ / \sqrt{1-R_{Ab}}$ should be zero resulting in the matched situation as $A_b^- / A_b^+ = \sqrt{R_{Ab}}$. In fact, A_b^- is the altered amplitude obtained during a round trip in the resonator from the transmitted pump A_b^+ through the back mirror. A_b^- depends on the SHG pump depletion, waveguide loss and front mirror reflectivity.

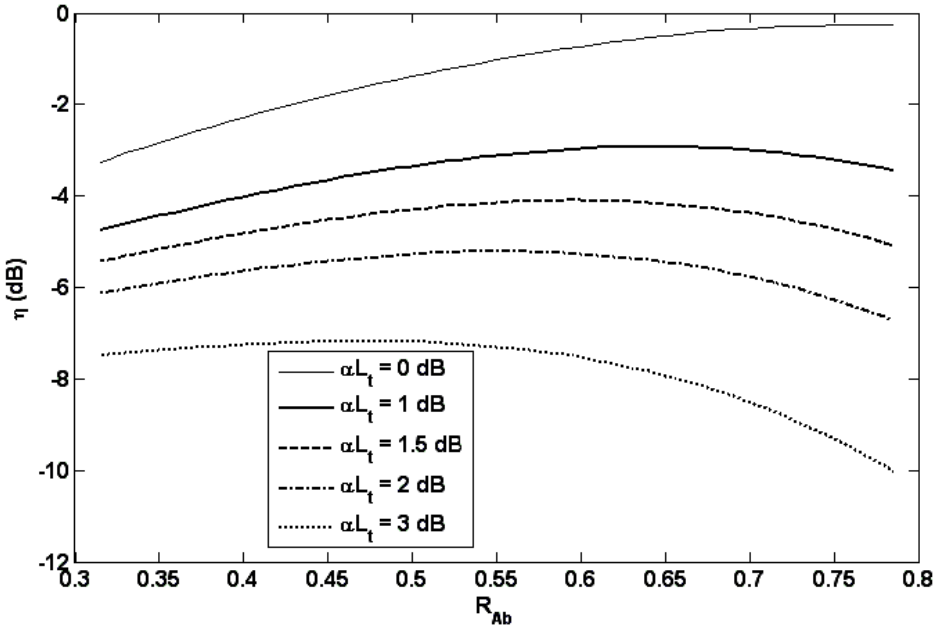

Figure 3-9 : Peak SHG efficiency of the singly pump-resonant waveguide with ASCG, versus R_{Ab} for different waveguide FH loss when $R_{Af} = 1$ and $L_t \approx 5\,\text{cm}$.

Consider a singly pump-resonant structure with low propagation loss and high reflectivity of the FH at the front facet mirror. Pump depletion and the efficiency are very low, mean $A_b^- \to A_b^+$ and R_{Ab} moves toward unity. On the other hand, for a moderate pump depletion and efficiency (non-resonant pump case), $A_b^+ \to A_i^+$ and $A_i^- \to A_b^-$, and R_{Ab} approaches zero. Thus, for a remarkably high pump depletion and efficiency in the resonator, the matching condition $A_b^- / A_b^+ = \sqrt{R_{Ab}}$ can be satisfied and the singly pump-resonant structures provide maximum efficiency for a given loss. It can be seen that the maximum efficiencies of around –2.9, –4.1, –5.2 and –7.2 dB can be achieved for the FH losses of –1, –1.5, –2 and –3 dB when the back-facet reflectivities are 0.65, 0.6, 0.55 and 0.45, respectively. Thus, to achieve the maximum efficiency for larger FH loss, the optimum value of back-facet reflectivity can be found at lower values of R_{Ab}. However, there is a compromise between the FH loss αL_t and the reflectivity R_{Ab} since for constant efficiency, the waveguide with the greater αL_t, may need a higher R_{Ab}. For instance, to achieve –4.1-dB efficiency, the waveguides with 1 dB and 1.5 dB losses require ~0.4 and ~0.6 reflectivities, respectively.

Figure 3-10 shows the dependence of the maximum SHG efficiency on the input FH power for different amounts of waveguide FH loss, and the reflectivity R_{Ab} for which the peak efficiency occurs in Figure 3-9. It is apparent that with increasing power, the efficiency increases rapidly in the low pumping region and decreases in the high pumping region. This is because the pump power build-up in the resonator is disabled by pump depletion due to intense SHG interaction.

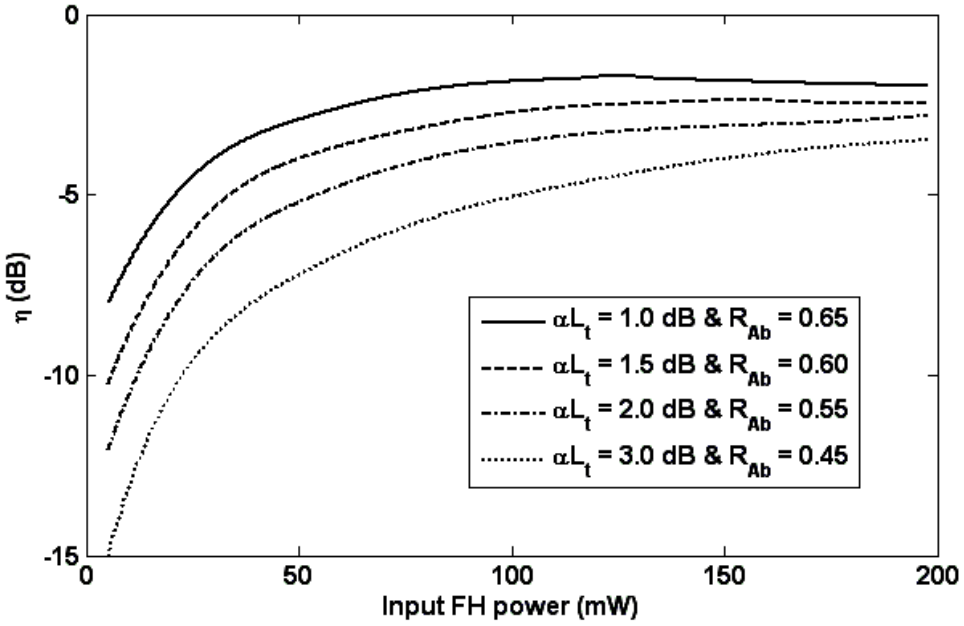

Figure 3-10 : Peak SHG efficiency of the singly pump-resonant waveguide with ASCG, versus input FH power for different waveguide loss and back-facet reflectivity when $R_{Af} = 1$ and $L_t \approx 5\,\text{cm}$.

However, the maximum efficiency of ~ –1.8 dB for 125 mW input FH power is achieved when the waveguide FH loss is 1 dB and the back-facet reflectivity is 0.65. It is also evident when the waveguide loss increases, the peak efficiency is achieved at higher input FH powers but the peak value is smaller than that of the low-loss waveguides. Thus, increasing the input power for enhancement of efficiency (before the peak point) is more useful for lossy waveguides. For example, increasing the input power from 50 to $125\,\text{mW}$ enhances the efficiency to 1.2 dB and 2.8 dB for waveguides losses of 1 dB and 3 dB, respectively.

3.4 Conclusion

A 10-segment ASCG device in a ~5-cm-long APE waveguide in LN with smaller effective area (~4 times) was designed to achieve a 30-nm bandwidth and a maximum SHG efficiency of -12 dB was obtained, showing a 5.5-dB improvement in efficiency compared to that of the same length previously designed in a Ti:LN waveguide. Also, by proposing a singly pump-resonant waveguide including the ASCG, we found that the conversion efficiency envelope of resonant axial modes for quasi-continuous FH increases substantially with the same bandwidth, especially for low loss waveguides. Considering the singly pump-resonance, a peak SHG efficiency of greater than -3 dB over a bandwidth of about 30 nm in a ~5-cm-long APE LN waveguide with 1-dB FH loss is achieved using the same 10-segment ASCG. Thus, the SHG efficiency of an ASCG increases dramatically for low-loss waveguides. For a 21-dBm input FH power in a 5-cm-long resonant waveguide with 1-dB FH loss and an optimized back-facet reflectivity of 0.65, the maximum efficiency of about -1.8 dB over the same bandwidth of 30 nm is obtained using a singly pump-resonant waveguide with the ASCG. Moreover, resonant devices with larger-bandwidth (e.g., 60 nm) can be simply designed using the ASCG with fewer segments (e.g., 5 segments) at the same length.

To sum up, we believe that combining the apodized step-chirped gratings in small-cross-section waveguides with the singly pump-resonant structures seems to be a highly flexible technique for designing and easing the fabrication requirements of special highly-efficient, broadband frequency doublers based on SHG. Although experimental demonstration of small chirp values may be difficult to implement, the nano-scale domain patterns have already been controlled by back-switched poling [53], [54]. We also note that a few nanometers of chirp between the poling periods of adjacent domain gratings have been demonstrated in multiple QPM devices [57], [58] and between the poling periods of adjacent domain gratings for DFG using apodized gratings [59]. Chirp below the accepted resolution of the electron-beam writing machine has also been previously demonstrated in linearly chirped fiber Bragg gratings [51]. We are therefore confident that the small change in the periods will be possible. It is thus expected that the demonstration of the ASCG structures will be possible in the near future.

CHAPTER 4
BANDWIDTH BROADENING BY SINGLE-PASS CASCADED SFG + DFG AND RESPONSE FLATENNING USING PUMP TUNING AND SCG

4.1 Overview

Recently, an interesting wavelength conversion technique based on quasi-phase matched cascaded sum frequency generation and difference frequency generation (SFG + DFG) has been demonstrated theoretically and practically in PPLN waveguides and found applications including broadband wavelength conversion, channel selective and multiple channel wavelength conversion, format conversion and cross-connection [94]-[108]. Using this technique, by increasing the pump wavelength difference, the conversion bandwidth can be enhanced [98]. However, the mean of conversion efficiency depends on the wavelengths of the pumps and is decreased by increasing the pump wavelength difference due to the response being non-uniform.

Although the single-pass cascaded SFG + DFG structure has been principally investigated, the research on how to set the pumps or alternatively to engineer the grating to improve the conversion properties still remain and are of great importance. For wide pump wavelength difference, the SFG is perfectly phase-matched whilst the DFG phase-mismatch is large when the signal is far from the pump wavelengths. Thus, it increases the variation of conversion response for larger pump wavelength difference, converting equal-power signal channels unevenly. In this Chapter, two different solutions to this problem are proposed firstly using detuning of the pump wavelength and secondly using step-chirped gratings. It is shown that, if a pump wavelength is increased slightly or alternatively periods of a few-section SCG are shifted with nanometer resolution, the SFG phase-mismatch is decreased a little and the DFG phase-mismatch is also reduced, which leads to a flattening of conversion efficiency response.

In this Chapter, we evaluate and compare numerically the properties of the single-pass cascaded SHG + DFG and single-pass cascaded SFG + DFG schemes and propose that for the same length

with or without waveguide loss, the adoption of a single-pass cascaded SFG + DFG, increases the bandwidth and ripple with a mean efficiency reduction, which can be easily compensated by increasing the input pump power. We also show that for the single-pass cascaded SFG + DFG, using a pump detuning or alternatively SCG, improves the efficiency response to achieve almost a flat bandwidth. Moreover, we demonstrate that for the same length of the single-pass cascaded SFG + DFG, using the SCG further improves the conversion efficiency performance with a smaller mean efficiency penalty compared to the pump detuning scheme. In addition, we present design diagrams of optimized single-pass devices for selection of the waveguide length and pump powers to obtain the required efficiency, ripple and bandwidth.

4.2 Single-pass cascaded SFG + DFG

In this section, wavelength converters based on quasi-phase matched single-pass cascaded SFG + DFG in LN waveguide are modeled and investigated theoretically. Figure 4-1 shows the scheme of the wavelength conversion based on the single-pass cascaded SFG + DFG.

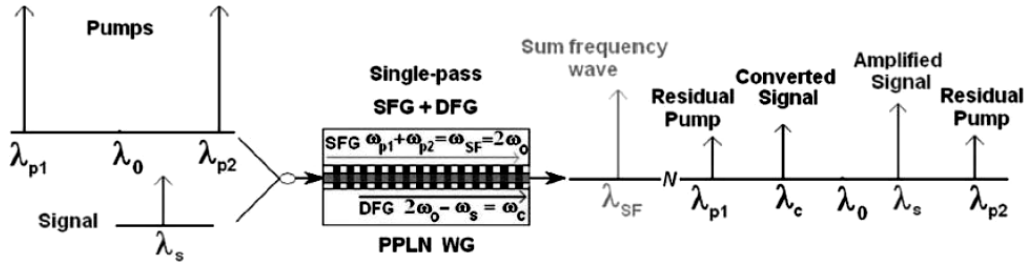

Figure 4-1 : Schematic description of single-pass cascaded SFG + DFG scheme.

With the two pump wavelengths λ_{p1} and λ_{p2}, and the signal wavelength λ_s, the wavelengths of the SF wave (λ_{SF}) and converted signal wave (λ_c) are equal to $\lambda_{p1}\lambda_{p2}/(\lambda_{p1}+\lambda_{p2})$ and $\lambda_s\lambda_{\mathrm{SF}}/(\lambda_s-\lambda_{\mathrm{SF}})$, respectively. $\lambda_{\mathrm{SF}} \approx \lambda_0/2$ where λ_0 is approximately the mean wavelength of the two pumps. The relation optimizing the two pumps is determined by $P_{p1}\lambda_{p1} = P_{p2}\lambda_{p2}$

according to the energy balance condition [110]. The single-pass cascaded SFG + DFG interaction can be described by the nonlinear coupled-mode equations [109]

$$\frac{d}{dx}A_{p1}(x) = -j\omega_{p1}\kappa_{\mathrm{SFG}}A_{p2}^{*}(x)A_{\mathrm{SF}}(x)\exp(-j\Delta k_{\mathrm{SFG}}x) - \tfrac{1}{2}\alpha_{p1}A_{p1}(x), \tag{4-1}$$

$$\frac{d}{dx}A_{p2}(x) = -j\omega_{p2}\kappa_{\mathrm{SFG}}A_{p1}^{*}(x)A_{\mathrm{SF}}(x)\exp(-j\Delta k_{\mathrm{SFG}}x) - \tfrac{1}{2}\alpha_{p2}A_{p2}(x), \tag{4-2}$$

$$\begin{aligned}\frac{d}{dx}A_{\mathrm{SF}}(x) = &-j\omega_{\mathrm{SF}}\kappa_{\mathrm{SFG}}A_{p1}(x)A_{p2}(x)\exp(j\Delta k_{\mathrm{SFG}}x)\\ &- j\omega_{\mathrm{SF}}\kappa_{\mathrm{DFG}}A_{s}(x)A_{c}(x)\exp(j\Delta k_{\mathrm{DFG}}x) - \tfrac{1}{2}\alpha_{\mathrm{SF}}A_{\mathrm{SF}}(x),\end{aligned} \tag{4-3}$$

$$\frac{d}{dx}A_{s}(x) = -j\omega_{s}\kappa_{\mathrm{DFG}}A_{\mathrm{SF}}(x)A_{c}^{*}(x)\exp(-j\Delta k_{\mathrm{DFG}}x) - \tfrac{1}{2}\alpha_{s}A_{s}(x), \tag{4-4}$$

$$\frac{d}{dx}A_{c}(x) = -j\omega_{c}\kappa_{\mathrm{DFG}}A_{\mathrm{SF}}(x)A_{s}^{*}(x)\exp(-j\Delta k_{\mathrm{DFG}}x) - \tfrac{1}{2}\alpha_{c}A_{c}(x), \tag{4-5}$$

where $\Delta k_{\mathrm{SFG}} = \beta_{\mathrm{SF}} - \beta_{p1} - \beta_{p2} - 2\pi/\Lambda$ and $\Delta k_{\mathrm{DFG}} = \beta_{\mathrm{SF}} - \beta_{s} - \beta_{c} - 2\pi/\Lambda$ are the SFG and DFG phase-mismatched parameters of the structure and $(A_{p1},\alpha_{p1},\beta_{p1})$, $(A_{p2},\alpha_{p2},\beta_{p2})$, $(A_{\mathrm{SF}},\alpha_{\mathrm{SF}},\beta_{\mathrm{SF}})$, $(A_{s},\alpha_{s},\beta_{s})$, $(A_{c},\alpha_{c},\beta_{c})$ are the amplitude, propagation losses and propagation constants of the first and second pumps, sum frequency, signal and converted signal (idler) waves, respectively and Λ is the QPM period. Moreover, $\kappa_{\mathrm{SFG}} = d_{eff}(2\mu_0/cS_{\mathrm{SFG}}N_{\mathrm{SF}}N_{p1}N_{p2})^{1/2}$ and $\kappa_{\mathrm{DFG}} = d_{eff}(2\mu_0/cS_{\mathrm{DFG}}N_{\mathrm{SF}}N_{s}N_{c})^{1/2}$ are the coupling coefficients, where $d_{eff} = (2/\pi)d_{33}$ is the effective value of the nonlinear coefficient of PPLN. N_{p1}, N_{p2}, N_{SF}, N_{s}, N_{c} are the effective

guided mode indexes for the first and second pumps, sum frequency, signal and converted waves, respectively. Also, S_{SFG} and S_{DFG} are the cross sections of channel waveguide in LN for SFG and DFG and are assumed to be $S_{\mathrm{DFG}} \approx S_{\mathrm{SFG}} \approx 30\,\mu\mathrm{m}^2$.

Equations (4-1) to (4-5) describing the single-pass cascaded SFG + DFG are solved numerically with a full model of depleted pumps and sum frequency waves. However, the conversion efficiency is defined as the power ratio of the output converted signal to the input signal as $\eta = |A_c(L)|^2 / |A_s(0)|^2$ where L is the waveguide length including the grating. The LN waveguide loss is assumed to be double for the sum frequency (SF) wave compared to the pump, signal and idler waves and for brevity the SF loss (α_{SF}) is only mentioned in the text and figures. Throughout this Chapter, typical values, $\alpha_{p1} = \alpha_{p2} = \alpha_s = \alpha_c = 0.35\,\mathrm{dB/cm}$ and $\alpha_{\mathrm{SF}} = 0.7\,\mathrm{dB/cm}$ are assumed for low-loss waveguides in the 1550-nm and 775-nm band, respectively [105].

4.2.1 Bandwidth broadening

For future WDM applications, the 3-dB conversion bandwidth of efficient wavelength converters should be broad enough to cover the 1.55 μm optical window [109]. It will be appropriate for practical applications if we can set the pumps at wavelengths out of the optical window which is at least 75 nm wide, whilst we need good efficiency with low ripple. To achieve these objectives, we consider the conversion efficiency, ripple and 3-dB bandwidth of the single-pass cascaded SFG + DFG with and without waveguide loss for two wavelength differences of the pumps ($\Delta\lambda_p = \lambda_{p2} - \lambda_{p1}$).

Figure 4-2 depicts the conversion efficiency of a 3-cm single-pass cascaded SFG + DFG device versus signal wavelength for lossless ($\alpha_{\mathrm{SF}} = 0$) and low-loss ($\alpha_{\mathrm{SF}} = 0.7\,\mathrm{dB/cm}$) cases for the wavelength differences of the pumps of $\Delta\lambda_p = 0$ and $\Delta\lambda_p = 75\,\mathrm{nm}$ for which the QPM periods of SFG are calculated to be $14.286\,\mu\mathrm{m}$ and $14.273\,\mu\mathrm{m}$, respectively. These are calculated by fitting the refractive indexes with the help of the Equation (2-6) for the crystal and subsequently finding the effective indexes of the waveguide. Also, the total pump power and signal power are 50 mW and 1 mW, respectively. For both $\Delta\lambda_p = 0$ and $\Delta\lambda_p = 75\,\mathrm{nm}$, the SFG is perfectly phase-matched

whilst in the former the DFG is phase-matched only at $\lambda_s = 1550\,\text{nm}$. In the latter case the DFG is phase-matched only at $\lambda_s = 1512.5\,\text{nm}$ and $\lambda_s = 1587.5\,\text{nm}$. For $\Delta\lambda_p = 0$ (shown with thin lines in Figure 4-2), we encounter the case with and without loss in which the two pump wavelengths are identical and set to $\lambda_{p1} = \lambda_{p2} = 1550\,\text{nm}$, resulting in an SF wave at $\lambda_{\text{SF}} = 775\,\text{nm}$. This is the degenerate condition for SHG. Thus, the single-pass cascaded SFG + DFG based wavelength conversion process in this condition turns out to be similar to the single-pass cascaded SHG + DFG. This means that as the two pump powers of the SFG + DFG are equal, each required pump power of the SFG + DFG is half that of the SHG + DFG to achieve the same conversion efficiency.

The problem with the single-pass cascaded SHG + DFG is that the pumps are within the signal bandwidth and as long as we set them farther apart, the ripple in efficiency grows gradually whilst the conversion bandwidth is enhanced. For $\Delta\lambda_P = 75\,\text{nm}$ (shown with thick lines in Figure 4-2), we consider two cases with and without loss in which the pumps are set at $\lambda_{p1} = 1512.5\,\text{nm}$ and $\lambda_{p2} = 1587.5\,\text{nm}$ under the power balance condition resulting in an SF wave at $\lambda_{\text{SF}} = 774.546\,\text{nm}$. In fact, in this case for a signal between two pumps, the SFG is perfectly phase-matched whilst the DFG is phase-matched only at two points around the pump wavelengths and phase-mismatched between them with the maximum at $2\lambda_{\text{SF}}$. This mismatch will increase as a function of the separation of the pump wavelengths causing greater efficiency variation since the efficiency corresponding to the larger phase-mismatch is low. Figure 4-2 shows that the conversion bandwidth is enhanced by setting the pumps farther apart but the efficiency curve develops large ripples. Moreover, assuming the loss ($\alpha_{\text{SF}} = 0.7\,\text{dB/cm}$), the mean efficiency drops 2.4 dB while the bandwidth and response variation remains almost the same for both $\Delta\lambda_p = 0$ and $\Delta\lambda_p = 75\,\text{nm}$ cases. Thus, the loss consideration is very important for a realistic design.

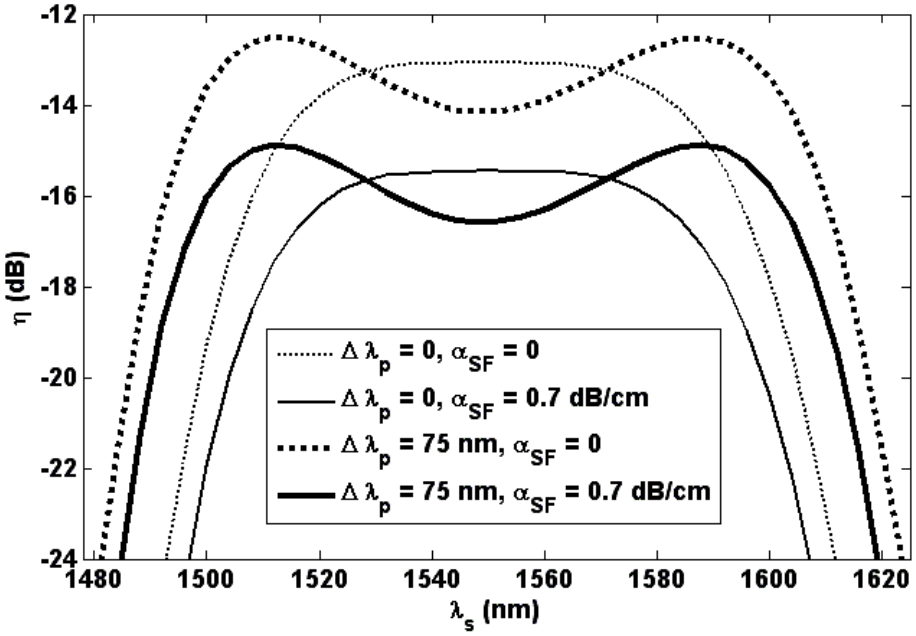

Figure 4-2 : Efficiency of single-pass cascaded SFG + DFG device versus signal wavelength with a waveguide length of 3 cm and 50-mW total pump powers for $\Delta\lambda_p = 0$ and $\Delta\lambda_p = 75\,\text{nm}$ with and without loss.

Figure 4-3 depicts the design diagram contour maps of efficiency, peak-to-peak ripple and bandwidth of the single-pass cascaded SFG + DFG device versus waveguide length and total pump powers where the pumps are set at 1512.500 nm and 1587.500 nm. The efficiency decreases considerably for $\alpha_{\text{SF}} = 0.7\,\text{dB/cm}$ compared to $\alpha_{\text{SF}} = 0$ especially for long devices while the peak-to-peak ripple and bandwidth contour maps are almost the same with and without loss. Figure 4-3 also shows that almost a constant bandwidth and ripple can be achieved using a fixed length and further reduction in the ripple can be achieved for shorter waveguides. For a 3-cm long waveguide, the bandwidth of 118 nm with less than 2-dB ripple is achieved in which -10-dB mean efficiency is possible for pump powers of 76 mW and 102 mW when $\alpha_{\text{SF}} = 0$ and $\alpha_{\text{SF}} = 0.7\,\text{dB/cm}$, respectively. Thus, there is a need for a supplementary 26 mW of power for the same efficiency to compensate for the loss. It is also seen that to achieve the higher efficiency for

the same length, the amount of the extra power to compensate the loss increases which can be easily predicted using the contour map.

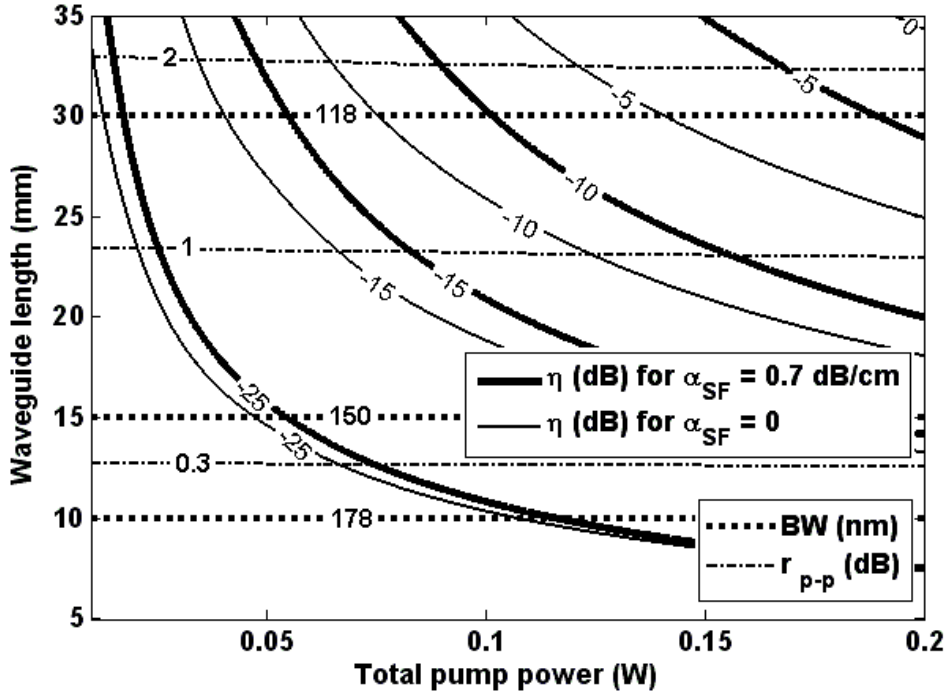

Figure 4-3 : Efficiency contour maps of single-pass cascaded SFG + DFG device versus waveguide length and total pump powers for $\alpha_{SF} = 0$ and $\alpha_{SF} = 0.7\,\text{dB/cm}$. Peak-to-peak ripple and bandwidth contour maps are the same with and without the low loss ($\alpha_{SF} = 0.7\,\text{dB/cm}$). The pumps are set at 1512.5 nm and 1587.5 nm.

4.2.2 Response flattening

To overcome the ripple in the conversion efficiency, we propose the use of increased detuning of the pumps or alternatively step-chirped grating for single-pass cascaded SFG + DFG for small but tolerable reduction in the bandwidth and mean efficiency.

4.2.2.1 Pump detuning

If one or both of the pump wavelength λ_{p1} or λ_{p2} are increasingly detuned, the conversion response will be changed due to different SFG and DFG phase-matching conditions. Here, we consider the increased detuning of the pump wavelength λ_{p2} while increased detuning of both pump wavelengths is possible. With increasing λ_{p2} the new phase-matching conditions are $\Delta k'_{\mathrm{SFG}} = \beta'_{\mathrm{SF}} - \beta_{p1} - \beta'_{p2} - 2\pi/\Lambda$ and $\Delta k'_{\mathrm{DFG}} = \beta'_{\mathrm{SF}} - \beta_s - \beta'_c - 2\pi/\Lambda$ for SFG and DFG, respectively. The phase-mismatch for the SFG and DFG are $\delta k_{\mathrm{SFG}} = \beta'_{\mathrm{SF}} - \beta_{\mathrm{SF}} - \beta'_{p2} + \beta_{p2}$ and $\delta k_{\mathrm{DFG}} = \beta'_{\mathrm{SF}} - \beta_{\mathrm{SF}} - \beta'_c + \beta_c$. When the second pump wavelength is detuned such that $\lambda'_{p2} > \lambda_{p2}$, the wavelength of the SF wave increases to λ'_{SF}. Thus, the reduction of β_{SF} to β'_{SF} is more than that of β_{p2} to β'_{p2} and β_c to β'_c, which leads to $\delta k_{\mathrm{SFG}} \approx \delta k_{\mathrm{DFG}} < 0$. For the single-pass cascaded SFG + DFG, the phase-matching conditions for signals between the wavelengths of the two pumps are $\Delta k_{\mathrm{SFG}} = 0$ and $\Delta k_{\mathrm{DFG}} > 0$. With detuning of the pump wavelength, $\Delta k_{\mathrm{SFG}} L$ and $\Delta k_{\mathrm{DFG}} L$ are reduced. However, conversion efficiencies near the pumps are decreased resulting in a flattening of the response.

Figure 4-4 illustrates the conversion efficiency of a 3-cm single-pass cascaded SFG + DFG device versus signal wavelength assuming lossless ($\alpha_{\mathrm{SF}} = 0$) and low-loss ($\alpha_{\mathrm{SF}} = 0.7\,\mathrm{dB/cm}$) waveguide for $\Delta\lambda_{p2} = 0$ and $\Delta\lambda_{p2} = 0.450\,\mathrm{nm}$ where $\Delta\lambda_{P2}$ is a small increase in the wavelength of the second pump. Also, we consider again $\Delta\lambda_p = 75\,\mathrm{nm}$, the total pump powers of 50 mW and signal power of 1 mW. As the second pump is detuned to $\Delta\lambda_{p2} = 0.450\,\mathrm{nm}$, the phase-matching parameters for both the SFG and DFG decrease and their two new matching points coincide, making the two peaks in the efficiency curve gradually move toward $2\lambda_{\mathrm{SF}}$. For $\Delta\lambda_{p2} = 0.450\,\mathrm{nm}$, the peak-to-peak ripple in the efficiency reduces from 1.7 dB to 0.2 dB with a mean efficiency penalty and bandwidth penalty of about 2.0 dB and 20 nm, respectively, for both low-loss and lossless waveguides. Moreover, the loss ($\alpha_{\mathrm{SF}} = 0.7\,\mathrm{dB/cm}$) decreases only the mean efficiency by around 2.4 dB for both $\Delta\lambda_{p2} = 0$ and $\Delta\lambda_{p2} = 0.450\,\mathrm{nm}$. On the other hand, comparison of Figure

4-2 and Figure 4-4 for both the lossless and low-loss waveguides shows that using the single-pass cascaded SFG + DFG device with a pump detuning ($\Delta\lambda_p = 75\,\text{nm}$) instead of the single-pass cascaded SHG + DFG one ($\Delta\lambda_p = 0$) increases the flattop bandwidth by about 10 nm for a mean efficiency penalty of around 1.8 dB, which can be easily compensated by increasing the input pump power. Although there are advantages using the single-pass cascaded SFG + DFG wavelength conversion technique instead of the single-pass cascaded SHG + DFG one, the drawbacks may be the need for a tunable laser, combiner and additional components.

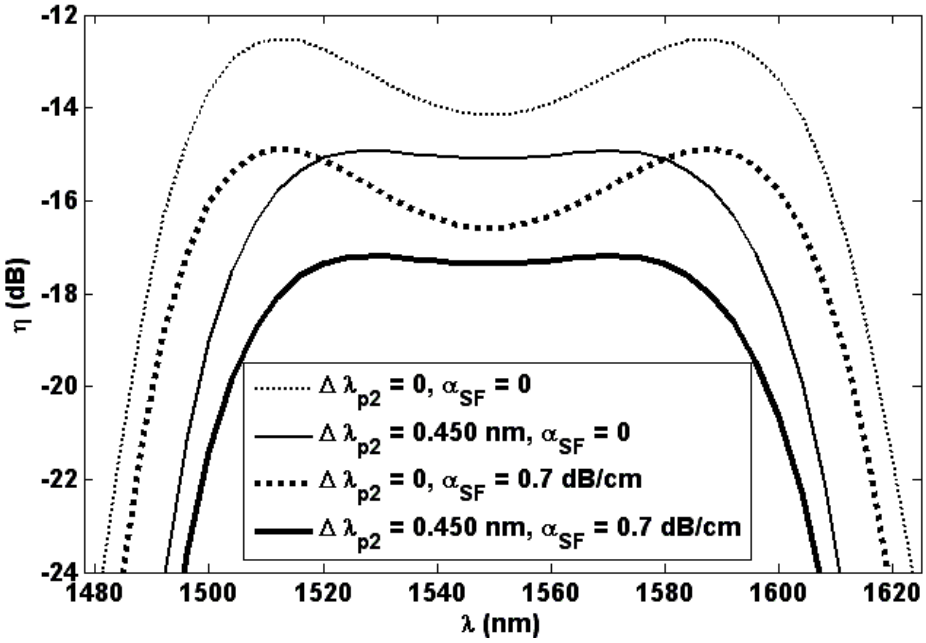

Figure 4-4 : Efficiency of single-pass cascaded SFG + DFG device versus signal wavelength for 3-cm lossless and low-loss waveguides when the pumps are set at 1512.5 nm and $1587.5 + \Delta\lambda_{p2}$ nm and the total pump powers is 50 mW.

Figure 4-5 illustrates the design diagram contour maps of efficiency, peak-to-peak ripple and bandwidth of the single-pass cascaded SFG + DFG device versus waveguide length and total pump power where the pumps are set at 1512.500 nm and 1587.950 nm. The efficiency decreases

considerably for $\alpha_{SF} = 0.7\,\text{dB/cm}$ compared to $\alpha_{SF} = 0$ especially for long devices while the peak-to-peak ripple and bandwidth contour maps are almost the same with and without loss.

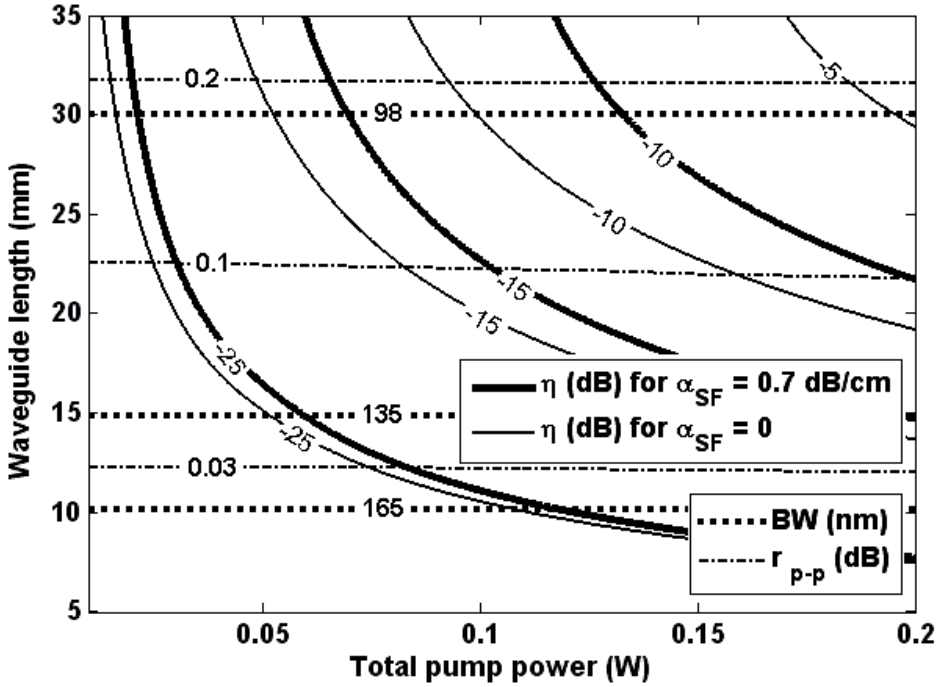

Figure 4-5 : Efficiency contour maps of the single-pass cascaded SFG + DFG versus waveguide length and total pump power for $\alpha_{SF} = 0$ and $\alpha_{SF} = 0.7\,\text{dB/cm}$. Peak-to-peak ripple and bandwidth contour maps are the same with and without the low loss $(\alpha_{SF} = 0.7\,\text{dB/cm})$. The pumps are set at 1512.5 nm and 1587.950 nm.

It is seen in Figure 4-5 that using a 0.450-nm pump detuning for the single-pass cascaded SFG + DFG device, peak-to–peak ripple less than 0.2 dB and 3-dB bandwidths greater than 98 nm with waveguide lengths shorter than 3-cm can be achieved. For a 3-cm long waveguide, -10-dB mean efficiency is achievable for the pump powers of 99 mW and 133 mW when $\alpha_{SF} = 0$ and $\alpha_{SF} = 0.7\,\text{dB/cm}$, respectively, which proves the need for the 34 mW supplementary power to compensate the loss. The increase in the loss-compensating extra power obtained in Figure 4-5

(e.g., 34 mW) compared to what is achieved from Figure 4-3 (e.g., 26 mW) is due to the use of pump detuning to flatten the efficiency response.

Furthermore, Figure 4-5 gives good information for the design of the lengths of single-pass cascaded SFG + DFG wavelength converters, and the exact assignment of total pump powers. To obtain the bandwidth with the desired efficiency and ripple, one should choose the length and input power on the intersection of the ripple and efficiency curves of the contour maps.

4.2.2.2 Step-chirped grating

A technique for flattening the ripple of efficiency response in the single-pass cascaded SFG + DFG is achieved by applying just a small shift in the period of the grating so that the new uniform grating period is $\Lambda' = \Lambda_{\mathrm{SFG}} + \delta\Lambda$. In this case the new phase-mismatch conditions are $\Delta k'_{\mathrm{SFG}} = \beta'_{\mathrm{SF}} - \beta_{\mathrm{p1}} - \beta_{\mathrm{p2}} - 2\pi/\Lambda'$ and $\Delta k'_{\mathrm{DFG}} = \beta'_{\mathrm{SF}} - \beta_{\mathrm{s}} - \beta'_{\mathrm{c}} - 2\pi/\Lambda'$ for the SFG and DFG, respectively. Thus, the phase-mismatch differences for the SFG and DFG are $\delta k_{\mathrm{SFG}} = \beta'_{\mathrm{SF}} - \beta_{\mathrm{SF}} - 2\pi(1/\Lambda' - 1/\Lambda_{\mathrm{SFG}})$ and $\delta k_{\mathrm{DFG}} = \beta'_{\mathrm{SF}} - \beta_{\mathrm{SF}} - \beta'_{\mathrm{c}} + \beta_{\mathrm{c}} - 2\pi\,(1/\Lambda' - 1/\Lambda_{\mathrm{SFG}})$, respectively. When the period shift $(\delta\Lambda)$ is decreased, the sum frequency wavelength is detuned such that $\lambda'_{\mathrm{SF}} > \lambda_{\mathrm{SF}}$. Thus, the reduction of β_{SF} to β'_{SF} is more than that of β_{c} to β'_{c} which leads to $\delta k_{\mathrm{SFG}} \approx \delta k_{\mathrm{DFG}} < 0$. For the cascaded single-pass SFG + DFG when $\delta\Lambda = 0$, the conditions for signals between the two pumps is $\Delta k_{\mathrm{SFG}} = 0$ and $\Delta k_{\mathrm{DFG}} > 0$. With a small nanometer-resolution decrease of period shift $(\delta\Lambda < 0)$, Δk_{SFG} and Δk_{DFG} are reduced. However, the efficiencies near the pumps are decreased resulting in a response flattening with acceptable ripple for a critical period shift.

Figure 4-6 illustrates the conversion efficiency responses of the single-pass cascaded SFG + DFG having uniform gratings for several $\delta\Lambda$ with the minimum resolution of 1-nm when the pumps are at 1512.5 nm and 1587.5 nm $(\Delta\lambda_p = 75\,\mathrm{nm})$. The QPM period of SFG (Λ_{SFG}), total pump power, signal power and length are as same as Figure 4-4 and the SF loss is 0.7 dB/cm. It is seen that a slight decrease of period shift when $\delta\Lambda < 0$ leads to decreasing the ripple of responses. However, it decreases the mean efficiency so that it has dropped around 3.6 dB for a critical period shift $(\delta\Lambda = -5\,\mathrm{nm})$ compared with $\delta\Lambda = 0$ although the bandwidth of 90 nm can be

achieved. Nevertheless, the mean efficiency penalty and bandwidth penalty are 1.5 dB and 8 nm more than those with a 0.450-nm pump detuning in Figure 4-4.

Nonetheless, using a few-section SCG, we can take advantage of response flattening of the single-pass cascaded SFG + DFG while the mean efficiency may be kept the same as the one with uniform gratings. An SCG structure similar to Figure 2-1 is proposed. To obtain the output converted signal and efficiency, we can consider p sections with uniform grating. The calculations begin and cascade from the first section with the length L_1 to the last one with the length L_p, in which we use Equations (4-1) to (4-5) to describe the single-pass cascaded SFG + DFG in lossy waveguides with a full model of pump and SF wave depletion. Here, the period shift is defined as the difference between the first section period and the QPM period of the SFG, $\delta\Lambda = \Lambda_1 - \Lambda_{\mathrm{SFG}}$.

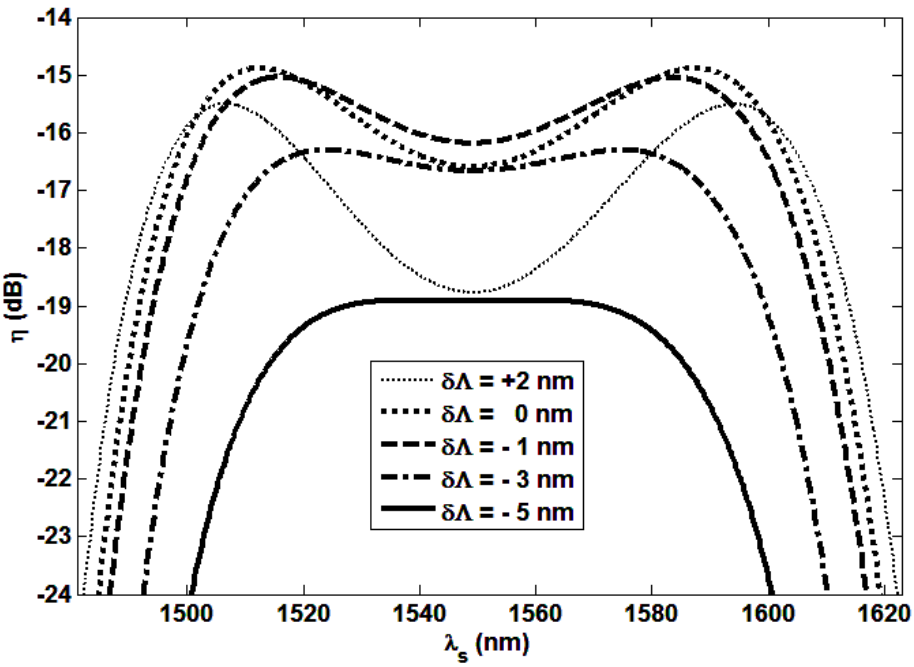

Figure 4-6 : Conversion efficiency of the single-pass cascaded SFG + DFG with uniform grating versus signal wavelength for different period shifts when pumps are at 1512.5 and 1587.5 nm ($\Delta\lambda_p = 75$ nm) and $\alpha_{\mathrm{SF}} = 0.7$ dB/cm.

Figure 4-7(a) and (b) depict the conversion efficiency of the single-pass cascaded SFG + DFG versus the signal wavelength for the 2- and 4-section SCG for various period shifts $\delta\Lambda$ with a minimum resolution of 0.5-nm and for two chirp steps $\Delta\Lambda = -1\,\text{nm}$ and $-4\,\text{nm}$ when pumps are at 1512.5 nm and 1587.5 nm $(\Delta\lambda_p = 75\,\text{nm})$. Furthermore, the waveguide length, loss, QPM period of the SFG, total pump power and signal power are the same with Figure 4-6.

In Figure 4-7(a), for the simplest SCG including 2 sections, the flatness of conversion efficiency response is affected by a nanometer-resolution change in the period shift $\delta\Lambda$, so that it is possible to find an appropriate critical period shift (e.g., $\delta\Lambda = -1.5\,\text{nm}$) to achieve a flat response with a peak-to-peak ripple less than 0.2 dB for a given chirp step (e.g., $\Delta\Lambda = -1\,\text{nm}$) wherein a bandwidth of around 98 nm with maximum efficiency of -16.5 dB can be achieved. Although it is apparent that the large chirp step (absolute value) reduces the bandwidth and efficiency, a flat response for $\Delta\Lambda = -4\,\text{nm}$ and $\delta\Lambda = +3\,\text{nm}$ can still be achieved.

To obtain higher efficiency, it is possible to use more sections. For a 4-section device with $\Delta\Lambda = -1\,\text{nm}$ and $\delta\Lambda = +1.0\,\text{nm}$, a bandwidth of 95 nm with maximum efficiency of -16 dB can be achieved which shows 0.5 dB increase in efficiency in comparison with a 2-section device; see solid thick lines in Figure 4-7(a) and Figure 4-7(b). Also, a large chirp step leads to smaller efficiency and bandwidth as it is seen in Figure 4-7(b). For a 4-section device when $\Delta\Lambda = -4\,\text{nm}$ and $\delta\Lambda = +2\,\text{nm}$, the conversion efficiency is reduced more than the uniform structure with the critical period shift in Figure 4-6 (see solid line). It means that the conversion efficiency of a 4-section SCG with $\Delta\Lambda = -4\,\text{nm}$ is no longer suitable. Therefore, to achieve both efficient and flat broadband devices we should use a small chirp step around -1 nm whilst more sections may be advantageous to get higher efficiency.

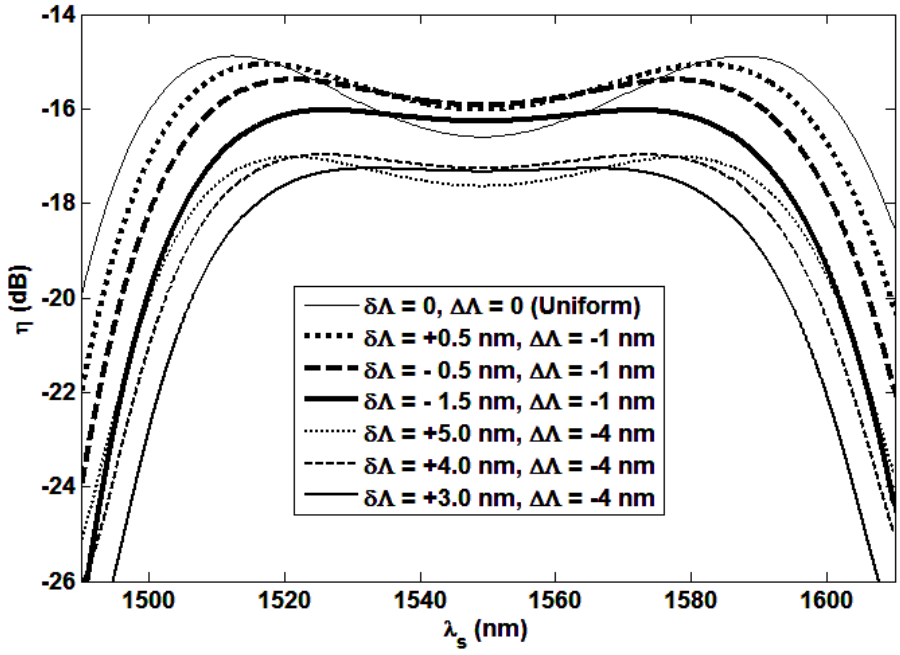

(a)

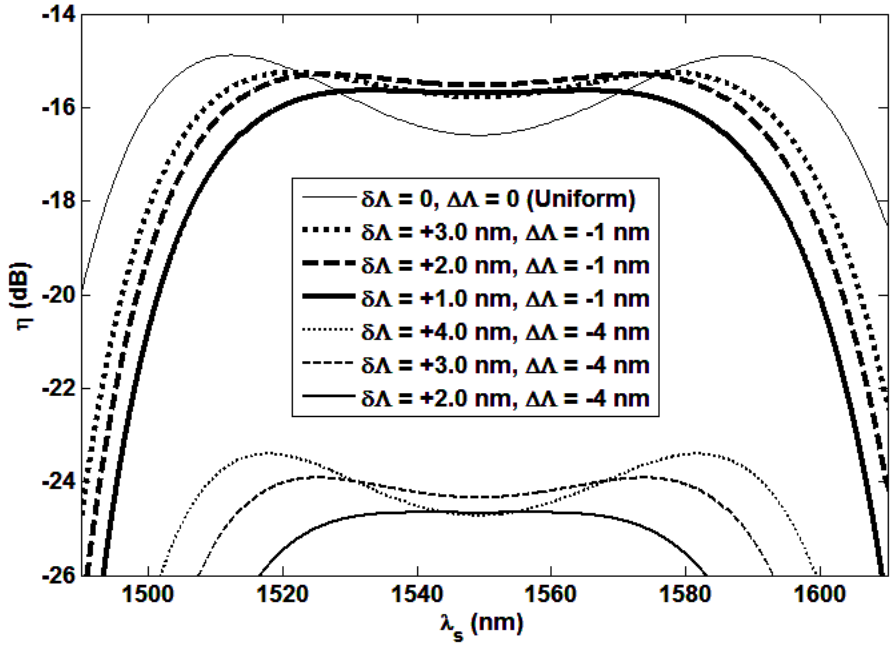

(b)

Figure 4-7 : Conversion efficiency of single-pass cascaded SFG + DFG versus signal wavelength for (a) 2-section SCG and (b) 4-section SCG, for different period shifts and chirp steps when pumps are at 1512.5 and 1587.5 nm and $\alpha_{SF} = 0.7\,\text{dB/cm}$.

Figure 4-8 shows the influence of the number of sections on the conversion efficiency and bandwidth of the single-pass cascaded SFG + DFG device using the SCG with the same length. The efficiency is plotted when the critical period shift with half a nm resolution is adopted to obtain a flat response with peak-to-peak ripple around 0.2 dB. The conversion efficiency of the SCG with -1-nm chirp step is improved for the same waveguide length when the number of sections is enhanced up to 4 sections and then decreases. Nonetheless, the enhancement in efficiency with more sections is still possible but it may need a smaller chirp step (sub-nanometer size), which makes the fabrication difficult as the device gradually moves toward a linear-chirped grating.

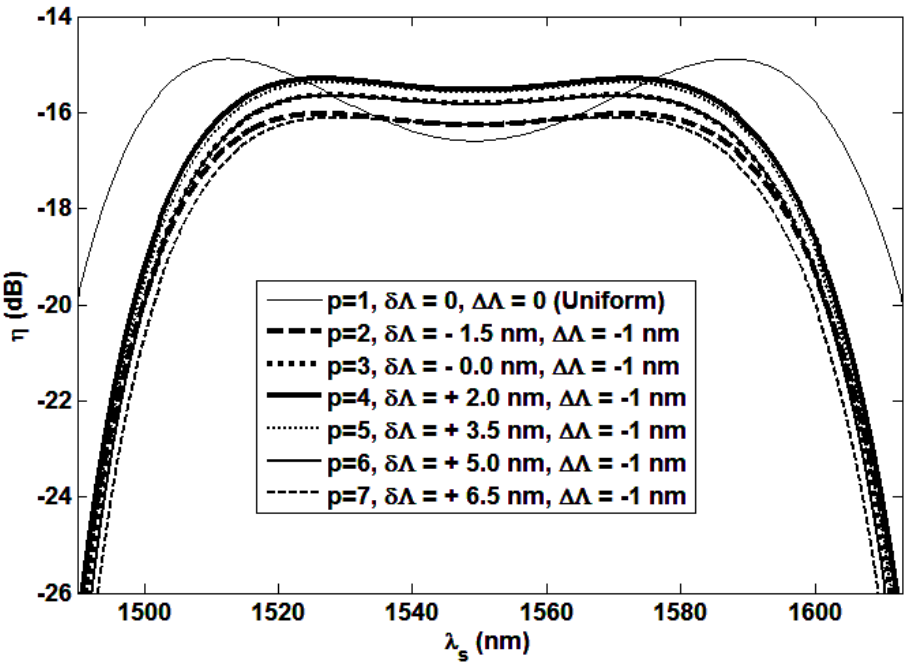

Figure 4-8 : Conversion efficiency of a 3-cm-long single-pass cascaded SFG + DFG versus signal wavelength for 2- to 7-section SCG using -1-nm chirp step with their critical period shifts when pumps are at 1512.5 and 1587.5 nm and $\alpha_{SF} = 0.7\,\text{dB/cm}$.

Figure 4-9 illustrates the design diagram contour maps of efficiency, peak-to-peak ripple and bandwidth of 4-section SCG-based single-pass cascaded SFG + DFG devices versus waveguide length and total pump power where the pumps are set at wavelengths of 1512.5 nm and 1587.5 nm. Also, we assume $\Lambda_1 = 14275\,\text{nm}$ and $\Delta\Lambda = -1\,\text{nm}$. Figure 4-9 shows that an almost constant bandwidth and low ripple can be achieved using a constant length and more flattening of the ripples can be achieved for shorter lengths. Hence, the criteria are presented on the design diagram and the designer can select the proper length and power for a flattop response. For instance, a bandwidth of 95 nm with less than 0.2-dB peak-to-peak ripple is achieved for a 3-cm long waveguide and efficiency greater than -5 dB is only possible for the pump powers greater than 187 mW.

4.2.2.3 Uniform grating (with or without pump detuning) versus 4-section SCG

The optimized value of first period and pump detuning, and resultant maximum and mean conversion efficiency, peak-to-peak ripple, and signal bandwidth for the number of sections are quantified in Table 4-1 when the pumps are at 1512.5 nm and 1587.5 + $\Delta\lambda_{p2}$ nm. For the uniform grating with the pump detuning ($\Delta\lambda_{p2} = 0.450\,\text{nm}$), the mean conversion efficiency and maximum bandwidth are -17.9 dB and 98 nm, respectively. However, almost the same bandwidth and ripple with the mean conversion efficiency of -15.9 dB can be achieved for the 4-section SCG device which shows 2-dB enhancement in efficiency compared to that of the uniform grating with 0.450-nm pump detuning.

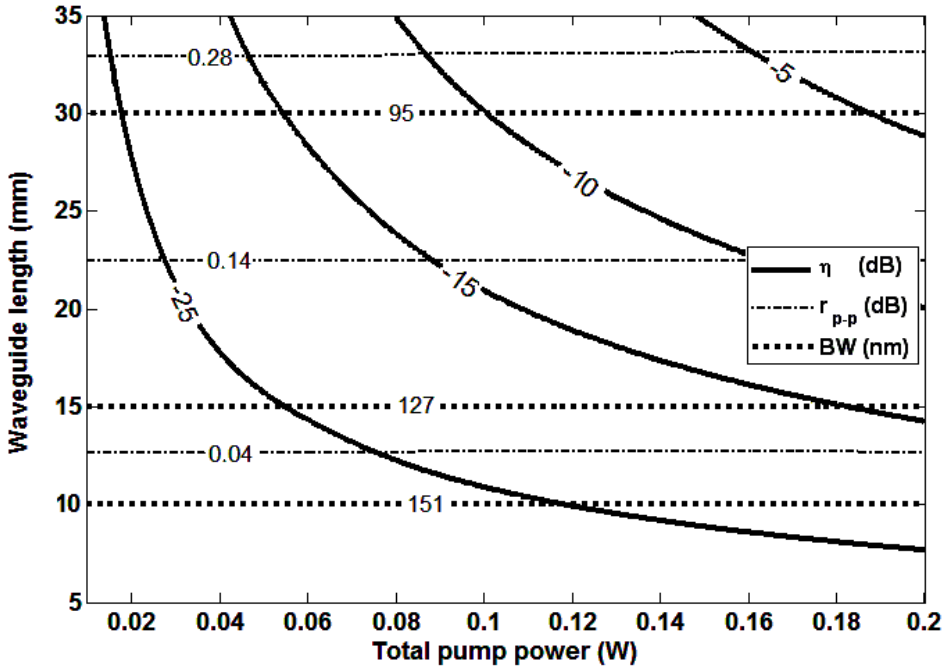

Figure 4-9 : Contour maps of conversion efficiency, bandwidth and ripple of the single-pass cascaded SFG + DFG based device for a 4-section SCG with -1-nm chirp step and 2-nm critical period shift when pumps are at 1512.5 and 1587.5 nm.

Table 4-1 : First period, chirp step, pump detuning, maximum and mean efficiency, peak-to-peak ripple, signal bandwidth; for uniform grating with and without pump detuning (p = 1) and SSG (p = 4) in single-pass cascaded SFG + DFG when the pumps are at 1512.5 nm and 1587.5 + $\Delta\lambda_{p2}$ nm. The total pump power and length are 50 mW and 3 cm for all cases.

Sections (p)	Λ_1 (nm)	$\Delta\Lambda$ (nm)	$\Delta\lambda_{p2}$ (nm)	η_{max} (dB)	η_{mean} (dB)	$r_{p\text{-}p}$ (dB)	$\Delta\lambda_s$ (nm)
1	14273.0	0	0	-14.9	-15.8	1.72	118
			0.450	-17.1	-17.9	0.18	98
4	14275.0	-1	0	-15.3	-15.9	0.20	95

4.3 Conclusion

In summary, we have numerically evaluated the properties of the single-pass cascaded SFG + DFG and single-pass cascaded SHG + DFG and showed that for the same length, the adoption of the single-pass cascaded SFG + DFG device further improves the bandwidth with a small efficiency reduction and some increased ripple, which can be easily compensated for by increasing the input pump power. Moreover, we showed that the increased wavelength detuning of a pump by a small amount to a longer wavelength in the single-pass device, removes the ripple with a penalty on the mean efficiency. Further, introducing few-section SCG with proper design provides almost the same bandwidth and flatness with much less mean efficiency penalty compared to the counterpart pump-detuned device. For each case, we also presented the criteria for selection of the waveguide length and pump powers on design diagrams to obtain the required efficiency, ripple and bandwidth. If the *ripple is tolerable* ($r_{p\text{-}p} < \sim 2$ dB), the design diagram for uniform grating without pump detuning in Figure 4-3 is chosen. Otherwise for the design of a *flattop response* ($r_{p\text{-}p} < \sim 0.2$ dB), the diagram for uniform grating with pump detuning in Figure 4-5 for higher bandwidth, or the diagram for 4-section SCG without pump detuning in Figure 4-9 for higher efficiency may be used.

CHAPTER 5
ENHANCEMENT OF CONVERSION EFFICIENCY BY DOUBLE-PASS CASCADED SFG + DFG AND RESPONSE FLATENNING USING PUMP TUNING AND SCG

5.1 Overview

The mean conversion efficiency of the cascaded single-pass SFG + DFG depends on the wavelengths of the pumps and is decreased by increasing the pump wavelength difference to achieve broader bandwidth. To overcome the mean efficiency reduction, the double-pass cascaded SFG + DFG scheme has been proposed, which is also able to filter out the residual pump wavelengths at the output [109]. Although the double-pass cascaded SFG + DFG scheme has been principally investigated [110]-[113], research on the improvement of conversion properties including flattening of the response still remains and is of immense importance. Two diverse solutions to remove efficiency variations using the detuning of pump wavelength and using the step-chirped grating are proposed. It is demonstrated that if a pump wavelength is increased slightly or alternatively the period of a few-section SCG is shifted by a few nanometers, they lead to flattening of the response variations.

In this Chapter, we evaluate and compare numerically the properties of the double-pass cascaded SHG + DFG and double-pass cascaded SFG + DFG schemes. We also propose that for the same length with or without waveguide loss, the adoption of the double-pass cascaded SFG + DFG, increases the bandwidth but with a large ripple, and reduces the mean efficiency significantly. We show that for the double-pass cascaded SFG + DFG, using pump detuning or alternatively SCG, reduces the ripple to obtain a flat response. In addition, we demonstrate that for the same length of the double-pass cascaded SFG + DFG device, using an SCG instead of pump detuning further improves the mean efficiency performance to achieve almost the same bandwidth and

ripple. The efficiency reduction may also be compensated by increasing the input pump power. Additionally, it is verified that for the same waveguide length and power, the efficiency *enhancement* expected due to the use of the double-pass device instead of the single-pass one is finally lost if the waveguide loss increases above a certain value. Further, well below this loss value, to achieve almost the same flatness of efficiency response using pump detuning or an SCG, the reduction in mean efficiency is smaller for the double-pass device compared to the single-pass one for the same loss. Moreover, we present the design diagrams of optimized double-pass devices for selection of the waveguide length and pump powers to obtain the required efficiency, ripple and bandwidth.

5.2 Double-pass cascaded SFG + DFG

The use of single-pass cascaded SFG + DFG wavelength converters to set the pumps wavelengths out of the optical window, which is at least 75 nm for practical applications e.g., in WDM systems, was discussed in Chapter 4. For higher efficiency, a double-pass device provides a good solution besides filtering out the pump wavelengths and is presented in this Chapter. The scheme of wavelength conversion based on the double-pass cascaded SFG + DFG in a PPLN waveguide is shown in Figure 5-1.

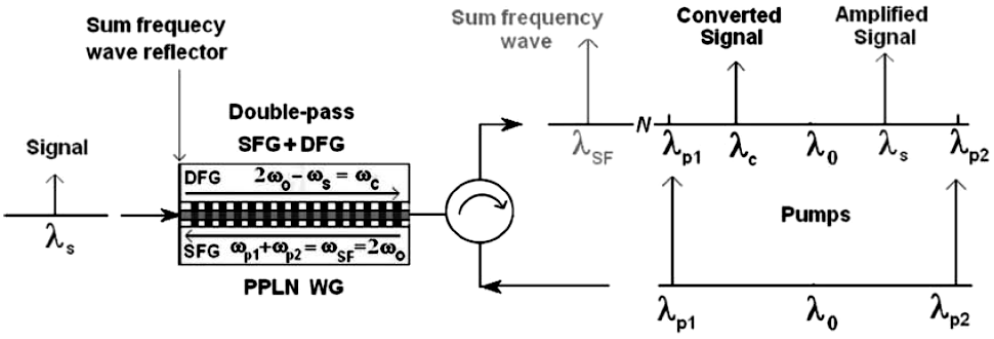

Figure 5-1 : Schematic description of the double-pass cascaded SFG + DFG.

Here, the double-pass device is modeled and theoretically investigated and compared with the single-pass one. Having a reflective coating at a wavelength $\lambda_{SF} \approx \lambda_0 / 2$, assuming no wavelength-dependent phase shifts upon reflection [112], maximizes the SFG before starting the DFG, where λ_0 is approximately the mean wavelength of the two pumps. For the double-pass cascaded SFG + DFG, the SFG process can be described by the three coupled equations [105]

$$\frac{d}{dx} A_{p1}(x) = -j\omega_{p1}\kappa_{SFG} A_{p2}^{*}(x) A_{SF}(x) \exp(-j\Delta k_{SFG} x) - \tfrac{1}{2}\alpha_{p1} A_{p1}(x), \tag{5-1}$$

$$\frac{d}{dx} A_{p2}(x) = -j\omega_{p2}\kappa_{SFG} A_{p1}^{*}(x) A_{SF}(x) \exp(-j\Delta k_{SFG} x) - \tfrac{1}{2}\alpha_{p2} A_{p2}(x), \tag{5-2}$$

$$\frac{d}{dx} A_{SF}(x) = -j\omega_{SF}\kappa_{SFG} A_{p1}(x) A_{p2}(x) \exp(j\Delta k_{SFG} x) - \tfrac{1}{2}\alpha_{SF} A_{SF}(x), \tag{5-3}$$

and the DFG process is also expressed as

$$\frac{d}{dx} A'_{SF}(x) = -j\omega_{SF}\kappa_{DFG} A_s(x) A_c(x) \exp(j\Delta k_{DFG} x) - \tfrac{1}{2}\alpha_{SF} A'_{SF}(x), \tag{5-4}$$

$$\frac{d}{dx} A_s(x) = -j\omega_s\kappa_{DFG} A'_{SF}(x) A_c^{*}(x) \exp(-j\Delta k_{DFG} x) - \tfrac{1}{2}\alpha_s A_s(x), \tag{5-5}$$

$$\frac{d}{dx} A_c(x) = -j\omega_c\kappa_{DFG} A'_{SF}(x) A_s^{*}(x) \exp(-j\Delta k_{DFG} x) - \tfrac{1}{2}\alpha_c A_c(x), \tag{5-6}$$

where A_{SF} and A'_{SF} are the amplitudes of sum frequency in forward and backward propagation directions. As before, the equations describing the double-pass cascaded SFG + DFG are solved numerically with a full model of depleted pumps and sum frequency waves. In the double-pass case, first for the forward propagation direction, Equations (5-1) to (5-3), (only SFG), are solved followed by Equations (5-4) to (5-6), (including DFG) for the backward propagation direction. The conversion efficiency is defined as the power ratio of the output converted signal to the input signal or $\eta = |A_c(L)|^2 / |A_s(0)|^2$ where L is the waveguide length including gratings. Also, for a double-pass device we assume a constant 95% reflectivity at the SF wavelength. Throughout this Chapter, $\alpha_{p1} = \alpha_{p2} = \alpha_s = \alpha_c = 0.35\,\text{dB/cm}$ and $\alpha_{\text{SF}} = 0.7\,\text{dB/cm}$ are assumed for low-loss waveguides in the 1550-nm and 775-nm band, respectively [105], unless otherwise stated.

5.2.1 Enhancement of conversion efficiency

Figure 5-2 depicts the conversion efficiency of a 3-cm double-pass cascaded SFG + DFG based device versus signal wavelength for lossless ($\alpha_{\text{SF}} = 0$) and lossy ($\alpha_{\text{SF}} = 0.7\,\text{dB/cm}$) waveguides for wavelength differences of the pumps of $\Delta\lambda_p = 0$ and $\Delta\lambda_p = 75\,\text{nm}$ for which the QPM poling periods are calculated to be $14.286\,\mu\text{m}$ and $14.273\,\mu\text{m}$, respectively. Also, the total pump powers and signal power are 50 mW and 1 mW, respectively. For both $\Delta\lambda_p = 0$ and $\Delta\lambda_p = 75\,\text{nm}$, the SFG is perfectly phase-matched whilst for $\Delta\lambda_p = 0$, the DFG is phase-matched only at $\lambda_s = 1550\,\text{nm}$. For $\Delta\lambda_p = 75\,\text{nm}$, the DFG is phase-matched only at $\lambda_s = 1512.5\,\text{nm}$ and $\lambda_s = 1587.5\,\text{nm}$. For $\Delta\lambda_p = 0$ (shown with fine lines in Figure 5-2), we have the case with and without loss in which the two pump wavelengths are identical and set to $\lambda_{p1} = \lambda_{p2} = 1550\,\text{nm}$, resulting in an SF wave at $\lambda_{\text{SF}} = 775\,\text{nm}$. Thus, the double-pass cascaded SFG + DFG in this condition is similar to double-pass cascaded SHG + DFG. This means that as the two pump powers of the cascaded SFG + DFG are equal, each required pump power for cascaded SFG + DFG is half that for cascaded SHG + DFG to achieve the same conversion efficiency. Figure 5-2 shows that the conversion bandwidth is enhanced (i.e., 28 nm) by setting the pumps farther apart but the efficiency curve develops a large ripple (i.e., 2.5 dB). Moreover, assuming the loss

($\alpha_{SF} = 0.7\,\text{dB/cm}$), the mean efficiency drops considerably by 4.1 dB while the bandwidth and response variation remains almost the same for both the $\Delta\lambda_p = 0$ and $\Delta\lambda_p = 75\,\text{nm}$ cases. Therefore, the loss consideration in double-pass schemes is very important for a realistic design as even the low-loss waveguide may drastically reduce the efficiency. However, in both cases, the efficiency curves show ripples.

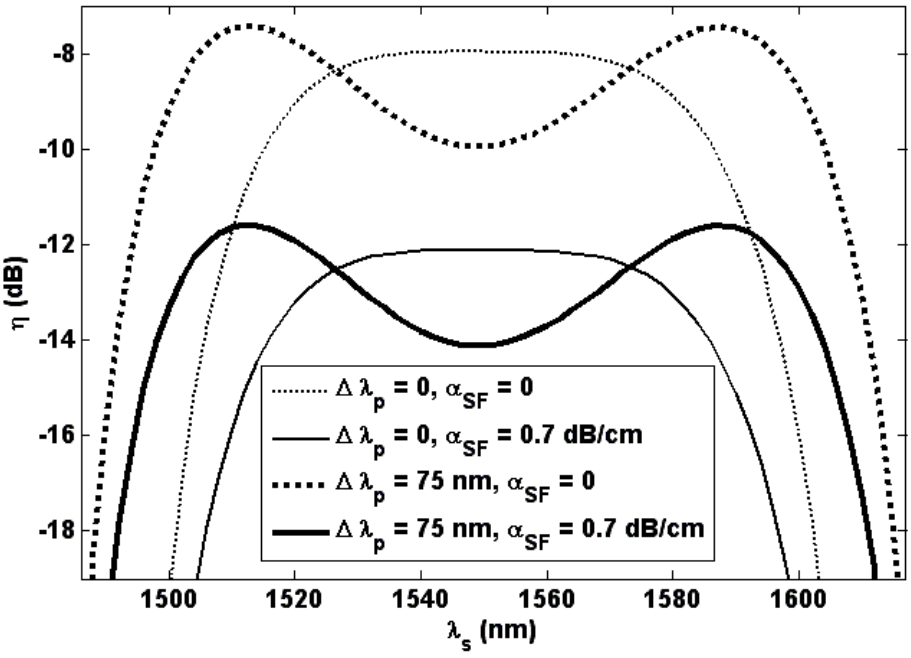

Figure 5-2 : Efficiency of double-pass SFG + DFG device versus signal wavelength with a waveguide length of 3 cm and 50-mW total pump powers for $\Delta\lambda_p = 0$ and $\Delta\lambda_p = 75\,\text{nm}$ with and without loss.

Figure 5-3 depicts the contour maps of efficiency, peak-to-peak ripple and bandwidth of the double-pass cascaded SFG + DFG device versus waveguide length and total pump powers in which the pumps are set at 1512.500 nm and 1587.500 nm. The efficiency decreases considerably for $\alpha_{SF} = 0.7\,\text{dB/cm}$ compared to $\alpha_{SF} = 0$ especially for long devices while the peak-to-peak

ripple and bandwidth contour maps are almost the same with or without loss. Figure 5-3 also shows that almost the constant bandwidth and ripple can be achieved using a fixed length and further reduction in the ripple can be achieved for shorter waveguides. In Figure 5-3, for a 3-cm long waveguide, the bandwidth of 110 nm with less than 2-dB ripple is achieved in which a -10-dB mean efficiency is possible for pump powers of 45 mW and 69 mW when $\alpha_{SF} = 0$ and $\alpha_{SF} = 0.7\,\text{dB/cm}$, respectively. This shows the need for a supplementary 24 mW of power for the same efficiency to compensate for the loss. It is also seen that to achieve the higher efficiency for the same length, the amount of the extra power to compensate the loss increases which can be easily predicted using the contour maps.

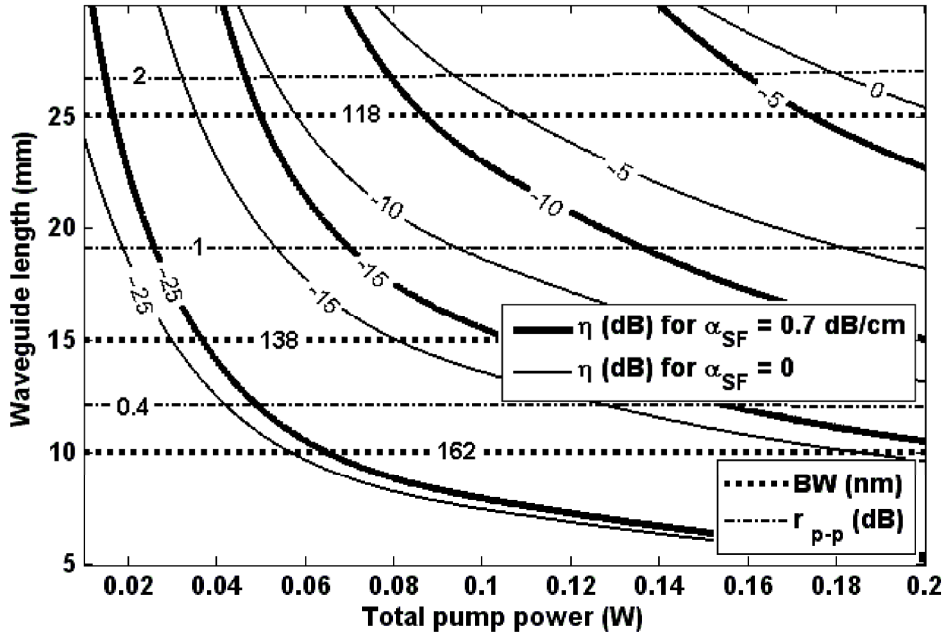

Figure 5-3 : Contour maps of efficiency, peak-to-peak ripple and bandwidth of the cascaded double-pass SFG + DFG device versus length and total power for the SF loss of 0.70 dB/cm when the pumps are set at 1512.5 nm and 1587.5 + $\Delta\lambda_{p2}$ nm for $\Delta\lambda_{p2}$ = 0.

5.2.2 Response flattening

5.2.2.1 Pump detuning

The problem with the double-pass cascaded SFG + DFG scheme for $\Delta\lambda_p = 75\,\text{nm}$ is the huge ripple in the responses even though it is possible to achieve higher efficiencies compared to the single-pass cascaded SFG + DFG. To overcome the non-uniform response, we again use increasing detuning of the pumps for the double-pass cascaded SFG + DFG scheme for a small reduction in the bandwidth and mean efficiency.

Figure 5-4 illustrates the conversion efficiency of a 3-cm-long double-pass cascaded SFG + DFG device versus signal wavelength assuming lossless $(\alpha_{\text{SF}} = 0)$ and low-loss $(\alpha_{\text{SF}} = 0.7\,\text{dB/cm})$ waveguides for $\Delta\lambda_{p2} = 0$ and $\Delta\lambda_{p2} = 0.225\,\text{nm}$ where $\Delta\lambda_{p2}$ is a small increase in the wavelength of the second pump. Also, we consider again $\Delta\lambda_p = 75\,\text{nm}$, a total pump power of 50 mW and signal power of 1 mW. For the double-pass device, since the SFG and DFG processes are independent, only the variation of the two DFG phase-matched points contributing to the two peaks in the efficiency curve converge rapidly toward $2\lambda_{\text{SF}}$ as the second pump is detuned to $\Delta\lambda_{p2} = 0.225\,\text{nm}$. In this case, the peak-to-peak ripple in the efficiency reduces from 2.5 dB to 0.25 dB with a mean efficiency and bandwidth penalty of about 0.7 dB and 20 nm, respectively, for both low-loss and lossless waveguides. Moreover, the loss $(\alpha_{\text{SF}} = 0.7\,\text{dB/cm})$ decreases only the mean efficiency by around 4.1 dB for both $\Delta\lambda_{p2} = 0$ and $\Delta\lambda_{p2} = 0.225\,\text{nm}$.

Comparison of Figure 5-2 and Figure 5-4 for both the lossless and low-loss waveguides shows that using the double-pass cascaded SFG + DFG device with a pump wavelength difference $(\Delta\lambda_p = 75.225\,\text{nm})$ instead of the double-pass cascaded SHG + DFG one $(\Delta\lambda_p = 0)$ increases the flattop bandwidth by about 8 nm for a mean efficiency penalty of around 0.7 dB, which can be easily compensated for by increasing the input pump power. Although there are advantages using the double-pass cascaded SFG + DFG wavelength conversion technique instead of the double-pass SHG + DFG one, the drawbacks may be the need for a tunable laser, combiner and additional components.

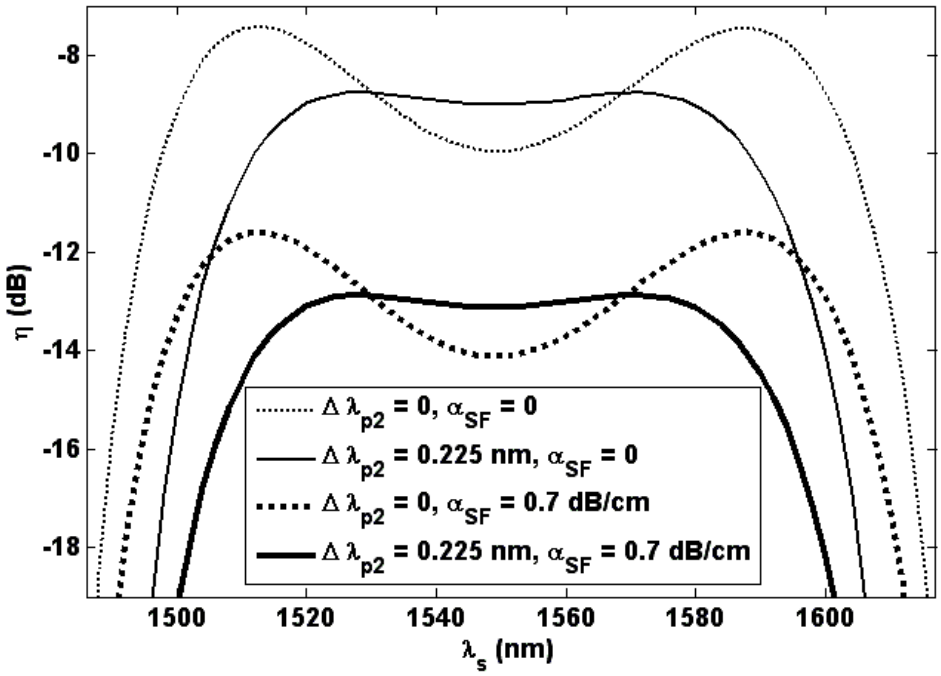

Figure 5-4 : Efficiency of double-pass cascaded SFG + DFG device versus signal wavelength for a 3-cm long lossless and low-loss waveguides when the pumps are set at 1512.5 nm and $1587.5 + \Delta\lambda_{p2}$ nm and the total power of the two pumps is 50 mW.

On the other hand, from the comparison of Figure 4-4 and Figure 5-4, to achieve the same flatness in lossy waveguides, the reduction in mean efficiency is smaller and the mean efficiency is almost 4.3 dB higher for the double-pass cascaded SFG + DFG scheme in comparison with the single-pass cascaded SFG + DFG. The reason for higher mean efficiency in the double-pass device is that the signal and pumps are counter-injected in the waveguide and the available waveguide length is used twice.

Figure 5-5 illustrate the contour maps of efficiency, peak-to-peak ripple and bandwidth of the double-pass SFG + DFG device versus waveguide length and total pump power where the pumps are set at wavelengths of 1512.5 nm and 1587.5 + $\Delta\lambda_{p2}$ nm, for a detuning of $\Delta\lambda_{p2} = 0.225\,\text{nm}$.

Figure 5-5 also shows that almost a constant bandwidth and ripple can be achieved using a constant length and more flattening of the ripples can be achieved using the shorter length. It is

seen in Figure 5-5 that for waveguide lengths shorter than 3-cm, using a 0.225-nm pump detuning for the double-pass cascaded SFG + DFG device, peak-to–peak ripple less than 0.25 dB and 3-dB bandwidths greater than 90 nm can be achieved. For a 3-cm long waveguide, -10-dB mean efficiency is achievable for the pump powers of 45 mW and 75 mW when $\alpha_{SF} = 0$ and $\alpha_{SF} = 0.7\,\text{dB/cm}$, respectively, which shows the need for the 30 mW supplementary power to compensate the loss. The increase in the loss-compensating extra power obtained in Figure 5-5 (e.g., 30 mW) compared to what is achieved from Figure 5-3 (e.g., 24 mW) is due to the use of pump detuning to flatten the efficiency response.

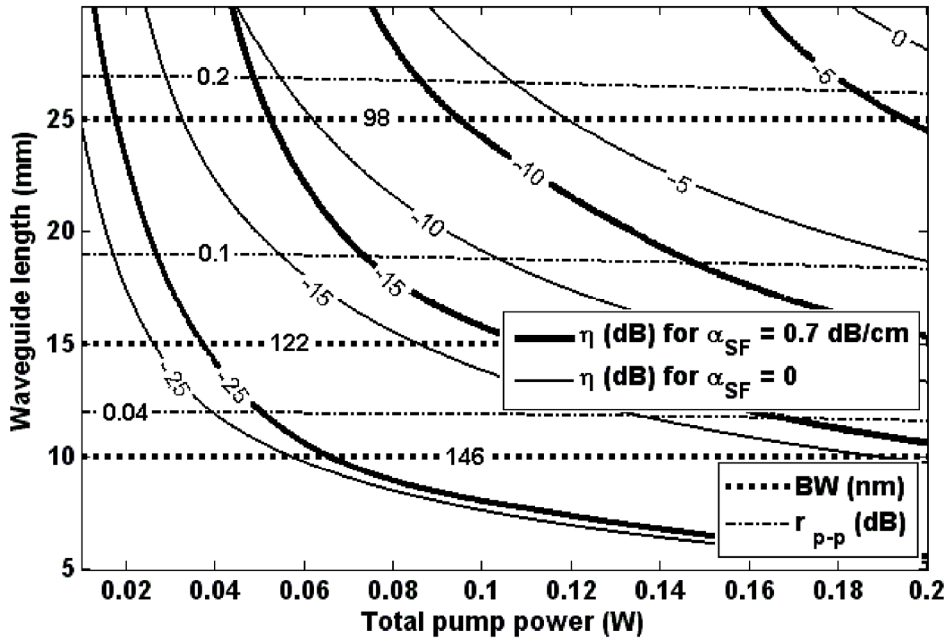

Figure 5-5 : Contour maps of efficiency, peak-to-peak ripple and bandwidth of the cascaded double-pass SFG + DFG device versus length and total power for the SF loss of 0.70 dB/cm when the pumps are set at 1512.5 nm and 1587.5 + $\Delta\lambda_{p2}$ nm for $\Delta\lambda_{p2}$ = 0.225 nm.

5.2.2.2 Step-chirped grating

Another technique for flattening the ripple was presented in Section 4.2.2.2. By applying just a small shift in the period of the uniform grating, the efficiencies near the pumps are decreased resulting in a response flattening with acceptable ripple for a critical period shift where the new grating period is $\Lambda' = \Lambda_{SFG} + \delta\Lambda$. Figure 5-6 illustrates the conversion efficiency responses of the double-pass cascaded SFG + DFG having uniform grating for several $\delta\Lambda$'s with a 1-nm resolution when the pumps are at 1512.5 nm and 1587.5 nm ($\Delta\lambda_p = 75\,\text{nm}$). The QPM period of SFG (Λ_{SFG}), powers and length are the same as Figure 5-4 and the SF loss is 0.7 dB/cm.

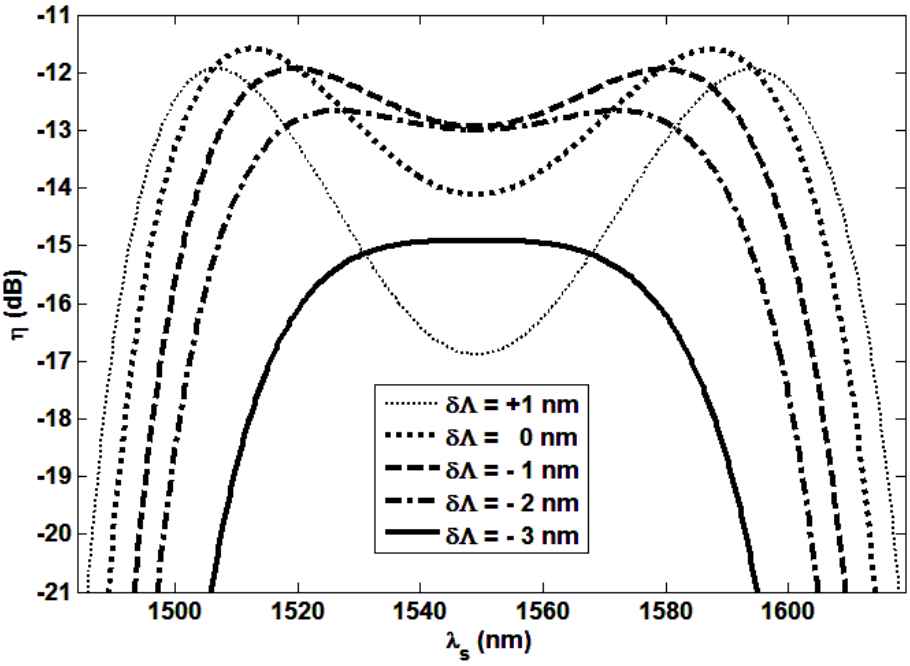

Figure 5-6 : Conversion efficiency of the double-pass cascaded SFG + DFG with uniform grating versus signal wavelength for different period shifts when pumps are at 1512.5 and 1587.5 nm ($\Delta\lambda_p = 75$ nm) and $\alpha_{SF} = 0.7\,\text{dB/cm}$.

It is seen that a slight decrease in period shift when $\delta\Lambda < 0$ leads to a decrease of the ripple in the responses. However, it decreases the mean efficiency as well, so that it has dropped by around 3.3 dB for a critical period shift ($\delta\Lambda = -3\,\text{nm}$) compared with $\delta\Lambda = 0$, although a bandwidth of 76 nm can be achieved. Also, the mean efficiency penalty and bandwidth penalty are 2 dB and 14 nm more than those with a 0.225-nm pump detuning in Figure 5-4 (see solid thick lines). However, with the help of the SCG, we can take advantage of both high efficiency and flat wide bandwidth of the double-pass cascaded SFG + DFG. Figure 5-7 shows the conversion efficiency responses of the double-pass cascaded SFG + DFG using the SCG with the same length for different number of sections. The efficiency is plotted when the critical period shift with a nm resolution is adopted to obtain a flat response with peak-to-peak ripple of less than 0.2 dB.

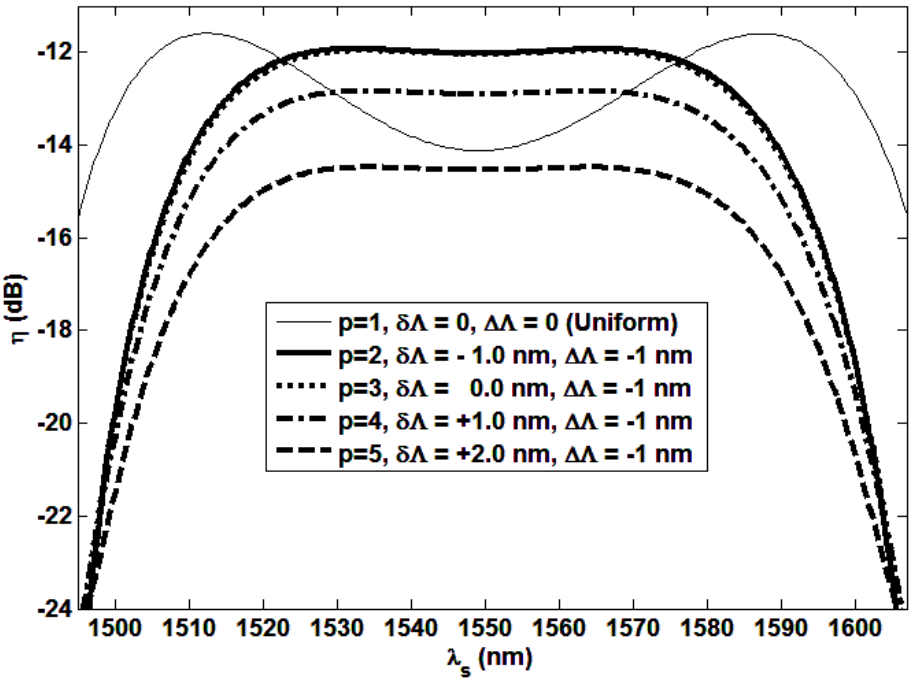

Figure 5-7 : Conversion efficiency of a 3-cm-long double-pass cascaded SFG + DFG versus signal wavelength for 2- to 5-section SCG with -1-nm chirp step with their critical period shifts when pumps are at 1512.5 and 1587.5 nm and $\alpha_{SF} = 0.7\,\text{dB/cm}$.

The conversion efficiency of the SCG with -1-nm chirp step is improved for the same waveguide length when the number of sections is enhanced up to 2 sections, and then decreases for more sections. Nevertheless, the enhancement in efficiency with more sections is still possible but it may need a smaller chirp step which is not desirable for fabrication.

Figure 5-8 illustrates the contour maps of efficiency, peak-to-peak ripple and bandwidth of 2-section SCG-based double-pass cascaded SFG + DFG devices versus waveguide length and total pump power where the pumps are set at wavelengths of 1512.5 nm and 1587.5 nm. Also, we assume $\Lambda_1 = 14\,272\,\text{nm}$ and $\Delta\Lambda = -1\,\text{nm}$.

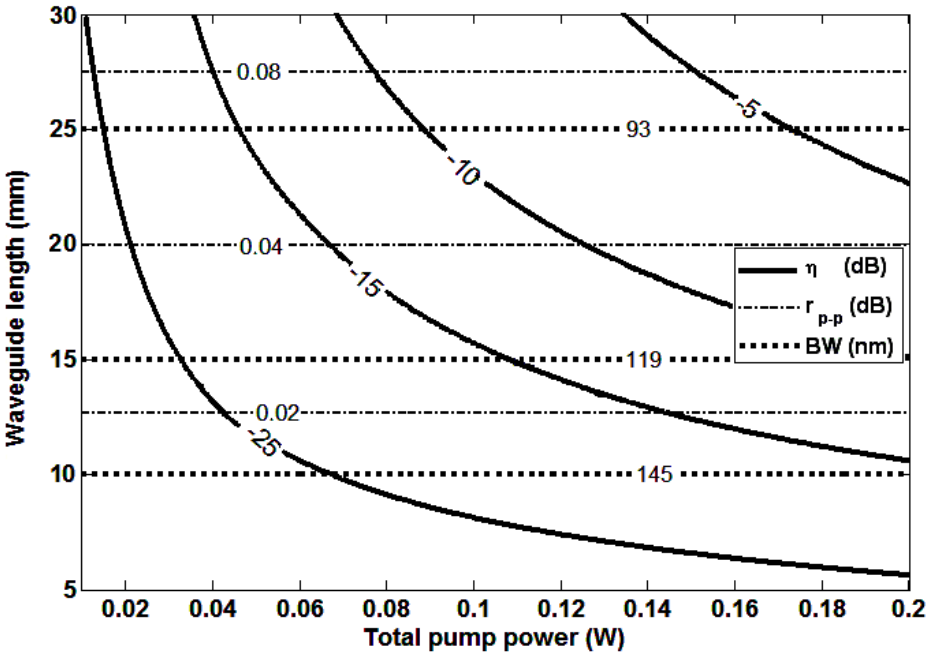

Figure 5-8 : Contour maps of conversion efficiency, bandwidth and ripple of double-pass cascaded SFG + DFG based device for a 2-section SCG with -1-nm chirp step and -1-nm critical period shift when pumps are at 1512.5 and 1587.5 nm.

Figure 5-8 shows that an almost constant bandwidth and low ripple can be achieved using a constant length and further flattening of the ripples can be achieved for shorter lengths. Hence, the criteria are presented on the design diagram and the designer can select the proper length and pump power for a flattop response. For instance, a bandwidth of 87 nm with less than 0.1-dB peak-to-peak ripple is achieved for a 3-cm long waveguide and conversion efficiency greater than -10 dB is only possible for the pump powers greater than 67 mW. However, this minimum power is smaller than that for the pump-detuned device with the same length achieved from Figure 5-5 (75 mW).

5.2.2.3 Uniform grating (with pump detuning) versus 2-section SCG

The optimized value of first period and pump detuning, and resultant maximum and mean conversion efficiency, peak-to-peak ripple, and signal bandwidth for the number of sections are quantified in Table 5-1 for the double-pass cascaded SFG + DFG when the pumps are at 1512.5 nm and 1587.5 nm.

Table 5-1 : First period, chirp step, pump detuning, maximum and mean efficiency, peak-to-peak ripple, signal bandwidth; for uniform grating with and without pump detuning (p = 1) and SSG (p = 2) in double-pass cascaded SFG + DFG when the pumps are at 1512.5 nm and 1587.5 + $\Delta\lambda_{p2}$ nm. The total pump power and length are 50 mW and 3 cm for all cases.

Sections (p)	Λ_1 (nm)	$\Delta\Lambda$ (nm)	$\Delta\lambda_{p2}$ (nm)	η_{max} (dB)	η_{mean} (dB)	$r_{p\text{-}p}$ (dB)	$\Delta\lambda_s$ (nm)
1	14273.0	0	0	-11.6	-12.8	2.52	110
			0.225	-12.9	-13.5	0.25	90
2	14272.0	-1	0	-11.9	-12.3	0.11	87

For the uniform grating with pump detuning ($\Delta\lambda_{p2} = 0.225\,\text{nm}$), the mean conversion efficiency and maximum bandwidth are -13.5 dB and 90 nm, respectively. However, almost the same bandwidth and ripple with the mean conversion efficiency of -15.8 dB can be achieved for the 2-section SCG device with $\Lambda_1 = 14\,272\,\text{nm}$ and $\Delta\Lambda = -1\,\text{nm}$ which shows 1.2-dB enhancement in efficiency compared to that of the uniform grating with 0.225 nm pump detuning, as shown in Table 5-1.

5.3 Comparison of double-pass and single-pass configurations

5.3.1 Efficiency versus waveguide loss

Figure 5-9(a) shows the cascaded SFG + DFG conversion efficiency of pump-detuned single-pass ($\Delta\lambda_{p2} = 0.450\,\text{nm}$) and double-pass ($\Delta\lambda_{p2} = 0.225\,\text{nm}$) devices for different losses when the total pump power and the waveguide length is 100 mW and 2.5 cm, respectively. As the loss increases, the efficiency is much reduced for the double-pass device compared with the single-pass one and therefore their efficiencies become the same for a certain loss. For instance, the efficiency *enhancement* of double-pass scheme compared to single-pass one, drops from almost 5.5 dB to 4 dB showing a 1.5 dB decrease when the SF loss increases from 0 to 0.7 dB/cm in Figure 5-9(a). That is because the SF effective path is twofold in the double-pass device compared to the single-pass one. Nonetheless, it is evident that in this case, using a double-pass structure to enhance the efficiency is only feasible when the SF loss is smaller than 2.6 dB/cm. To achieve the efficiency enhancement in double-pass devices with greater SF loss, it is possible to use smaller waveguide lengths with increased pump powers. Figure 5-9(b) shows the conversion efficiency of the single- and double-pass devices for the different SF loss when the total pump power is 400 mW and the waveguide length is 1.25 cm to achieve almost the same efficiency responses in Figure 5-9(a). In this case, the efficiency enhancement based on the double-pass scheme tolerates the same 1.5-dB decrease for an SF loss of 1.4 dB/cm, as shown in Figure 5-9(b). Also, the efficiency enhancement is only available until the SF loss exceeds 5.2 dB/cm. Thus, using shorter waveguides with higher input power is more suited to high-loss double-pass devices.

Similar results can be obtained for SCG-based single-pass and double-pass devices. Figure 5-10(a) shows the conversion efficiency of 3-section SCGs as single- and double-pass devices which lead to maximum efficiency for different losses when the total pump power and the waveguide length is 100 mW and 2.5 cm, respectively. However, using a double-pass structure to enhance the efficiency is only possible when the SF loss is smaller than 2.6 dB/cm. Figure 5-10(b) shows the conversion efficiency of the 3-section SCG as single- and double-pass devices for the different SF loss when the total pump power and the waveguide length is 400 mW and 1.25 cm to achieve almost the same efficiency responses in Figure 5-10(a). Similar to Figure 5-9(b), the efficiency enhancement is only available for SF loss smaller than 5.2 dB/cm. Nevertheless, for the same length and power, the efficiency enhancement expected due to the use of the double-pass device instead of the single-pass one is finally cut off when the single-pass SF loss is 6.5-dB.

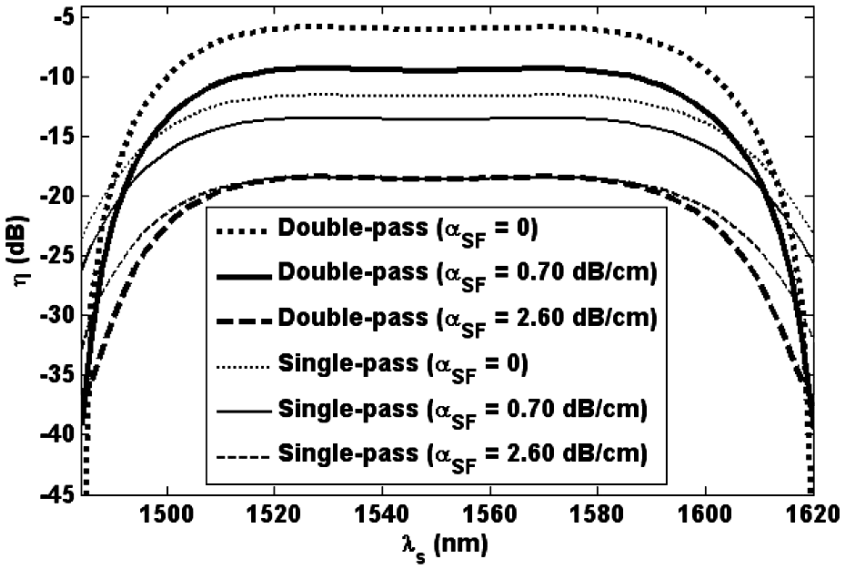

(a)

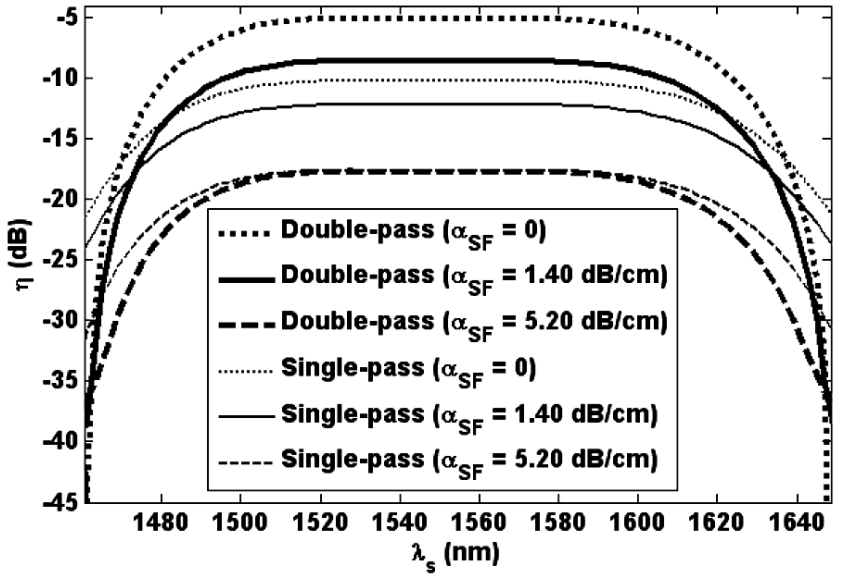

(b)

Figure 5-9 : Conversion efficiency of wavelength detuned single-pass ($\Delta\lambda_{p2}$ = 0.450 nm) and double-pass ($\Delta\lambda_{p2}$ = 0.225 nm) cascaded SFG + DFG based device versus signal wavelength for different loss when the length and total pump power are (a) 2.5 cm and 100 mW and (b) 1.25 cm and 400 mW.

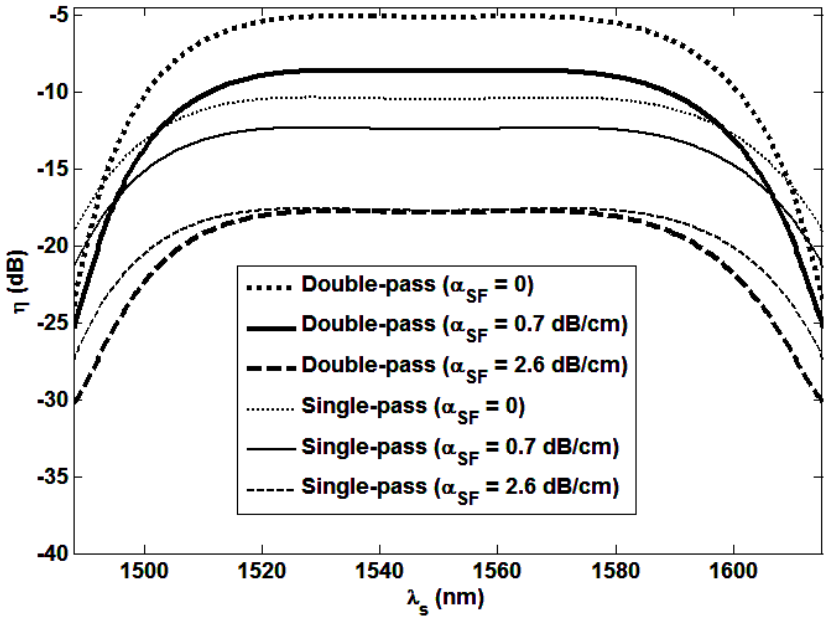

(a)

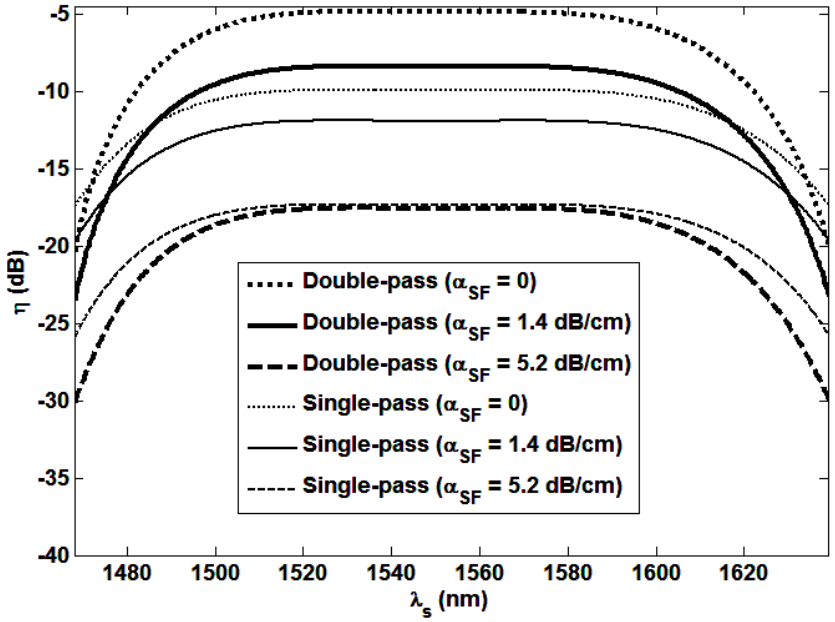

(b)

Figure 5-10 : Conversion efficiency of 3-section SCG-based single-pass and double-pass cascaded SFG + DFG versus signal wavelength for different loss when $\Delta\Lambda = -1\,\text{nm}$, $\delta\Lambda = 0$ and the length and total pump power are (a) 2.5 cm and 100 mW and (b) 1.25 cm and 400 mW.

5.3.2 Uniform-grating device (with pump detuning) versus 3-section SCG device

Table 5-2 gives efficiency, ripple and bandwidth comparison among 3-cm-long devices with uniform grating (with and without pump detuning) and 3-section SCG with the same starting period of 14273 nm (without pump detuning), using single-pass and double-pass schemes in cascaded SFG + DFG with 50 mW and 1 mW pump and signal power, respectively. It shows that using the SCG and double-pass configuration leads to higher efficiency with an insignificant bandwidth penalty. It also proves that the increased wavelength detuning of one of the pumps or alternatively using the 3-section SCG in the double-pass device, removes the ripple in the conversion response with less penalty on the mean efficiency in comparison with the single-pass device to achieve almost the same flatness.

Table 5-2 : Comparison of the mean efficiency, ripple and bandwidth; for uniform grating with and without pump detuning (p = 1) and SCG (p = 3) of single-pass and double-pass cascaded SFG + DFG schemes when the pumps are at 1512.5 nm and 1587.5 + $\Delta\lambda_{p2}$ nm. The total pump power and length are 50 mW and 3 cm for all cases.

SFG + DFG	Sections (p)	$\Delta\Lambda$ (nm)	$\Delta\lambda_{p2}$ (nm)	η_{mean} (dB)	$r_{\text{p-p}}$ (dB)	BW (nm)
Double-pass	1	0	0	-12.8	2.52	110
			0.225	-13.5	0.25	90
	3	-1	0	-12.4	0.07	84
Single-pass	1	0	0	-15.8	1.72	118
			0.450	-17.9	0.18	98
	3	-1	0	-16.1	0.17	94

5.4 Conclusion

In summary, we numerically evaluated the properties of the double-pass SFG + DFG device and showed that the increased detuning of one pump by a small amount to a longer wavelength removes the ripple further and flattens the efficiency response. Alternatively using a few-section step-chirped grating with nanometer chirp step has a similar effect. Additionally, we showed that for the same length of the double-pass cascaded SFG + DFG device, using the SCG instead of the pump detuning further improves the mean efficiency performance to achieve almost the same bandwidth and ripple. We also demonstrated that for the same length, the efficiency enhancement expected due to the use of the double-pass device instead of the single-pass one is reduced for a lossy waveguide while the conversion efficiency profile has almost the same shape with or without low loss. Moreover, it was shown that for the same length and power, the efficiency enhancement advantage expected due to the use of the double-pass device instead of the single-pass one is finally lost for a waveguide loss above a certain value. Also, the criteria for selection of the waveguide length and pump powers to obtain the desired efficiency, ripple and bandwidth are presented for each case. Using a double-pass device, the higher efficiency and almost the same ripple, with a small bandwidth penalty compared to the single-pass device can be achieved. Thus, the proper length and input power can be selected on the intersection of the ripple and efficiency contour maps of the double-pass design diagram. If the *ripple is acceptable* ($r_{p\text{-}p} < \sim 2$ dB), Figure 5-3 (uniform grating without pump detuning) is chosen. Otherwise for a *flattop response* ($r_{p\text{-}p} < \sim 0.2$ dB), Figure 5-5 (uniform grating with pump detuning) for higher bandwidth may be used, or Figure 5-8 (2-section SCG without pump detuning) for higher efficiency can be used.

CHAPTER 6
CONCLUSIONS

6.1 Thesis overview

There has been increasing interest in broadband wavelength converters based on quasi-phase matched SHG in LN waveguides as there are several applications in ultrafast optical signal processing, optical communication, sensing, displays and so on. Nonetheless, the problem associated with quasi-phase matched wavelength conversion is the narrowband nature of SHG, as the bandwidth is dependent on the inverse of the uniform grating length. Although, a chirped grating has been theoretically proposed to broaden the bandwidth by chirping the pitch of the inverted domains as a function of length, three problems impede its realization.

The first problem for realizing of such a broadband device is the smallness of chirp step in the LCG which is typically about 100 picometers or less for a converter with tens of nanometers of bandwidth. For the first time, we proposed the engineering of the SCG with large chirp step (>1 nm) for the convenience of fabrication in low-loss LN waveguide. The bandwidth and efficiency, which were found to be almost linearly proportional to the length and FH power, remain almost the same for the SCG in comparison to the LCG. It was shown that if the chirp step changes to one-tenth and the sections increased tenfold, the results are approximately the same. A design formula was also presented for the first time to determine the maximum segments one should use as a design rule dependent on the required bandwidth, using a full depletion model for FH pump.

The second problem is the obvious ripple (> 3-dB peak-to-peak) on the efficiency curves of the LCG and SCG. We considered an effective method to apodize and flatten the SH bandwidth by considering increasing and decreasing patterns of inverted domains into the gratings in low-loss Ti:LN waveguides. Using apodization, the efficiency curve of ALCG and ASCG can be dramatically smoothed and flattened with the ripples being reduced (< 0.1-dB peak-to-peak) and the spectral ears can be significantly suppressed at the cost of longer apodization lengths.

Additionally, to achieve the same bandwidth and efficiency for the same length, using fewer sections but with more segments, the ASCG can use larger chirp steps and duty-factor change (desirable for fabrication) in comparison to the ALCG. Moreover, it was demonstrated that by increasing the minimum line width (inverted domain) in a broadband (>50 nm) few-section ASCG designed for fabrication in MgO-doped LN, it is possible to attain almost the same efficiency response with a small price of a slight increase in the non-uniformity of conversion efficiency response.

The third problem is related to the reduction in the SHG efficiency using the ASCG. Two new techniques, namely small-effective-cross-section waveguides with or without resonant structures, were proposed for the first time to overcome the reduced SHG efficiency of the ASCG. By designing of a broadband SHG device with the ASCG using the smaller effective-cross-section (~4 times) APE waveguides in LN, the efficiency was increased (5.5 dB) compared to that of the same length and input FH power in Ti:LN waveguide. Also, by proposing a singly pump-resonant waveguide with the ASCG, we have found that the conversion efficiency envelope of resonant axial modes for quasi-continuous FH increases substantially with the same bandwidth, for low loss waveguides. The optimized values of back-facet reflectivity and input power to achieve the maximum efficiency, for several waveguide loss parameters have also been presented. For a 5-cm-long waveguide with the ASCG using singly pump-resonance, having 1-dB FH loss and the optimized back-facet reflectivity of 0.65, a maximum efficiency of about -1.8 dB (over almost the same bandwidth without resonance) is obtained for a 21-dBm input FH power. Moreover, resonant devices with the larger bandwidth can be simply designed using the ASCG with fewer segments.

There is also a great need for the development of wide waveband wavelength converters. Broadband cascaded SFG + DFG devices, working in the 1.55-μm wavelength transmission window for WDM systems, offer good solutions. However, the problem in the SFG + DFG device is that for the wide pump wavelength difference, the SFG is perfectly phase-matched whilst the DFG phase-mismatch is large when the signal is far from the pump. Thus, it increases the variation of conversion response for larger pump wavelength difference, converting equal-power signal channels unevenly. In this dissertation, two different solutions to this problem were proposed firstly using detuning of a pump wavelength and secondly, using an SCG. It was shown

that, if a pump wavelength is increased slightly, or alternatively periods of a few-section SCG are shifted with nanometer resolution accuracy, the SFG phase-mismatch is decreased slightly and the DFG phase-mismatch is also reduced which leads to flattening of response variation.

For the first time, the improved single-pass and double-pass configurations for flattop efficient broadband wavelength conversion based on cascaded SFG + DFG in LN waveguide was analyzed numerically with a full depletion model of pumps and sum frequency waves. We evaluated and compared the properties of the cascaded SFG + DFG when the pump wavelength difference is 75 nm and 0 nm. It is also proposed that for the same length with or without waveguide loss, the adoption of the cascaded SFG + DFG, increases the bandwidth with a small efficiency reduction which can be easily compensated by increasing the input pump power. We also showed that for the cascaded SFG + DFG devices, using the pump detuning and alternatively SCG, improves the efficiency response to achieve almost a flat bandwidth. Additionally, we verified that for the same length of the cascaded SFG + DFG devices, using SCG instead of pump detuning further improves the mean efficiency performance to achieve almost the same bandwidth and ripple.

We also demonstrated that for the same length, the efficiency enhancement due to the use of the double-pass device instead of the single-pass one is reduced for the lossy waveguide. However, the conversion efficiency profile is unaffected with almost the same shape with or without low loss. For the first time, it was shown that for the same length and power, the efficiency enhancement advantage due to the use of the double-pass device instead of the single-pass one is finally terminated for a waveguide loss above a certain value. In addition, it was confirmed that replacing a pump-detuned or alternatively a few-section SCG-based single-pass scheme with a double-pass scheme in low-loss LN waveguide, improves the efficiency. This replacement also offers a means for removing the ripples with a smaller efficiency penalty which can be compensated easily with a smaller increase of the total pump power. We obtained reasonable pump powers and waveguide lengths to achieve lossless or even amplified broadband single-pass and double-pass devices, suitable for designs of wide waveband wavelength converters operating in the 1.55-μm optical window. For each case the selection criteria for the waveguide length and pump powers to obtain the desired efficiency, ripple and bandwidth were presented on the design diagrams.

6.2 Direction for future work

In WDM systems, all-optical bidirectional broadband wavelength converters will play a significant role in the future to avoid wavelength blocking and improve the use of signal wavelengths [119]. Nonetheless, for multi-wavelength systems including metro/access networks, it will be necessary to use both the 1300-nm and the 1550-nm low-loss transmission windows. Currently, wavelength conversion between the two bands is done by semiconductor optical amplifiers (SOA). However, it is very difficult to realize broadband up-conversion with such large wavelength hopping in SOAs and the converted signal suffers from high absorption loss; and signal-to-noise ratio of output beam is drastically degraded on the shorter wavelengths [120]-[125]. Thus, there is a need for a replacement all-optical bidirectional broadband wavelength converter (i.e., 1550 nm <=>1300 nm).

Although we have explored wide flattop waveband conversion using cascaded SFG + DFG within the 1550-nm transmission window, a novel and innovative technique is proposed for future work to broaden the conversion bandwidth within both the 1300-nm and 1550-nm transmission windows. This is developed on the concept of cascaded SFG + DFG and can be realized by chirping the pitch of the grating as a function of length using careful design of the poled regions in LN. The design should follow our work on the ASCG. By apodization or altering the design of the grating, one can also change the wide spectral shape (>100 nm) to a desired one. The design is aimed at reducing the complexity of the ALCG so that the fabrication process can be eased by reducing the number of sections. This complex problem needs to be solved by careful numerical analysis, as apodization has to be designed into the grating as well. Moreover, using a double-pass structure for the same device can provide higher efficiency.

There is much to be done using the proposed ideas we have in this thesis, and it is rich area for exploitation. We expect to see many of the ideas implemented and perhaps mass produced. For applications in temperature-insensitive devices, some of the ideas will lead to compact all optical signal processing. Using these converters also addresses the issue of cost and ease of manufacturing for numerous application in communications and sensing systems.

REFERENCES

[1] R. W. Boyd, Nonlinear optics, Academics Press, 2003.

[2] J.-M. Liu, Photonic Device, Cambridge University Press, 2005.

[3] P. A. Franken, A. E. Hill, C. W. Peters, and G. Weinreich "Generation of optical harmonics", Phys. Rev. Lett., vol. 7, no. 4, pp. 118-120, 1961.

[4] J. A. Armstrong, N. Bloembergen, J. Ducuing, and P. S. Pershan, "Interactions between light waves in a nonlinear dielectric", Phys. Rev., vol. 127, no. 6, pp. 1918-1939, 1962.

[5] N. Bloembergen, and A. J. Sievers, "Nonlinear optical properties of periodic laminar structures," Appl. Phys. Lett., vol. 17, no. 11, pp. 483-486, 1970.

[6] B. Jaskorzynska, G. Arvidsson, and F. Laurell, "Periodic structures for phase-matching in second harmonic generation in titanium lithium niobate waveguides," SPIE vol. 651, pp. 221-8, Integrated Optical Circuit Engineering III, Innsbruck, Austria, 1986.

[7] M. M. Fejer, G. A. Magel, D. H. Jundt, and R. L. Byer, "Quasi-phase-matched second harmonic generation: tuning and tolerances," IEEE J. Quantum Electron., vol. 28. no. 11, pp. 2631-2654, 1992.

[8] M. Asobe, Y. Nishida, O. Tadanaga, H. Miyazawa, and H. Suzuki, "Wavelength conversion using quasi-phase matched $LiNbO_3$ waveguides," IEICE Transactions on Electronics, vol. E88-C, no. 3, pp. 335-41, 2005.

[9] M. Yamada, N. Nada, M. Saitoh, and K. Watanabe, "First-Order Quasi-Phase Matched $LiNbO_3$ Waveguide Periodically Poled by Applying an External Field for Efficient Blue Second-Harmonic Generation," Appl. Phys. Lett., vol. 62, no. 5, pp. 435-436, 1993.

[10] H. Nishihara, M. Haruna, T. Suhara, Optical Integrated Circuits, Mc-Graw Hill, 1989.

[11] T. Suhara and M. Fujimura: Waveguide Nonlinear-Optic Devices, Springer Verlag, Berlin, 2003.

[12] M. L. Bortz, M. Fujimura, and M.M. Fejer, "Increased acceptance bandwidth for quasi-phasematched second harmonic generation in $LiNbO_3$ waveguides," Elec. Lett., vol. 30, no. 1, pp. 34-5, 1994.

[13] T. Suhara, and H. Nishihara, "Theoretical analysis of waveguide second-harmonic generation phase matched with uniform and chirped gratings," IEEE J. Quantum Electron., vol. 26, no. 7, pp. 1265-1276, 1990.

[14] F. Lu, Y. Chen, J. Zhang, W. Lu, X. Chen and Y. Xia, "Broadcast wavelength conversion based on cascaded $\chi^{(2)}$ nonlinearity in MgO-doped periodically poled $LiNbO_3$," Elec. Lett., vol. 43, no. 25, pp. 1446-1447, 2007.

[15] J. Zhang, Y. Chen, F. Lu, and X. Chen, "Flexible wavelength conversion via cascaded second order nonlinearity using broadband SHG in MgO-doped PPLN," Opt. Express, vol. 16, no. 10, pp. 6957-6962, 2008.

[16] N. E. Yu, J. H. Ro, M. Cha, S. Kurimura and T. Taira, "Broadband quasi-phase-matched second-harmonic generation in MgO-doped periodically poled $LiNbO_3$ at the communications band," Opt. Lett., vol. 27, no. 12, pp. 1046-1048, 2002.

[17] N. E. Yu, S. Kurimura and K. Kitamura, "Broadband second harmonic generation with simultaneous group-velocity matching and quasi-phase matching," Jpn. J. Appl. Phys. vol. 42, no. 7B, pp. L821–L823, 2003.

[18] J. Huang, X. P. Xie, C. Langrock, R. V. Roussev, D. S. Hum, and M. M. Fejer, "Amplitude modulation and apodization of quasiphase-matched interactions," Opt. Lett., vol. 31, no. 5, pp. 604-606, 2006.

[19] R. Das and K. Thyagarajan, "Broadening of the phase-matching bandwidth in quasi-phase-matched second-harmonic generation using GaN-based Bragg reflection waveguide," Opt. Lett., vol. 32, no. 21, pp. 3128-3130, 2007.

[20] R. Das and K. Thyagarajan, "SHG in Bragg reflection waveguides for enhanced bandwidth applications," Opt. Commun., vol. 270, no. 1, pp. 79–84, 2007.

[21] K. Mizuuchi, K. Yamamoto, M. Kato, and H. Sato, "Broadening of the phase-matching bandwidth in quasi-phase-matched second-harmonic generation," IEEE J. Quantum Electron., vol. 30, no. 7, pp. 1596-604, 1994.

[22] S. Gao, C. Yang, and G. Jin, "Flat broad-band wavelength conversion based on sinusoidally chirped optical superlattices in lithium niobate," IEEE Photonics Technol. Lett., vol. 16, no. 2, pp. 557-9, 2004.

[23] Y. L. Lee ,Y. Noh, C. Jung, T. Yu, D. Ko, J. Lee, "Broadening of the second-harmonic phase-matching bandwidth in a temperature-gradient-controlled periodically poled Ti:$LiNbO_3$ channel waveguide," Opt. Exp., vol. 11, no. 22, pp. 2813-2819, 2003.

[24] Z. Xianglong, C. Xianfeng, W. fei, C. Yuping, X. Yuxing and C. Yingli, "Second-harmonic generation with broadened flattop bandwidth in aperiodic domain-inverted gratings," Opt. Commun., vol. 204, no. 1-6, pp. 407-411, 2002.

[25] K. Mizuuchi, and K. Yamamoto, "Waveguide second-harmonic generation device with broadened flat quasi-phase-matching response by use of a grating structure with located phase shifts," Opt. Lett., vol. 23, no. 24, pp. 1880-2, 1998.

[26] B.-Y. Gu, B.-Z. Dong, Y. Zhang, and G.-Z. Yang, "Enhanced harmonic generation in aperiodic optical superlattices," Appl. Phys. Lett., vol. 75, no. 15, pp. 2175-2177, 1999.

[27] S.-N. Zhu, Y.-Y. Zhu, Y.-q. Qin, H.-F. Wang, C.-Z. Ge, and N.-B. Ming, "Experimental realization of second harmonic generation in a Fibonacci optical superlattice of $LiTaO_3$," Phys. Rev. lett., vol. 78, no. 14, pp. 2752-2755, 1997.

[28] J. Wu, T. Kondo, R. Ito, "Optimal design for broadband quasi-phase-matched second-harmonic generation using simulated annealing," J. of Lightwave Technol., vol. 13, no. 3, pp. 456-60, 1995.

[29] S.-D. Yang and A. M. Weiner, K. R. Parameswaran, and M. M. Fejer, "400-photon-per-pulse ultrashort pulse autocorrelation measurement with aperiodically poled lithium niobate waveguides at 1.55 μm," Opt. Lett., vol. 29, no. 17, pp. 2070-2072, 2004.

[30] S.-D. Yang and A. M. Weiner, K. R. Parameswaran, and M. M. Fejer, "Ultrasensitive second-harmonic generation frequency-resolved optical gating by aperiodically poled $LiNbO_3$ waveguides at 1.5 μm," Opt. Lett., vol. 30, no. 16, pp. 2164-2166, 2005.

[31] S.-D. Yang, H. Miao, Z. Jiang, A. M. Weiner, K. R. Parameswaran, and M. M. Fejer, "Ultrasensitive nonlinear measurements of femtosecond pulses in the telecommunications band by aperiodically poled $LiNbO_3$ waveguides," Applied Optics, vol. 46, no. 27, pp. 6759-69, 2007.

[32] A. Galvanauskas, M. A. Arbore, M. H. Chou, and M. M. Fejer., "Chirped-pulse-amplification circuits for fiber amplifiers, based on chirped-period quasi-phase-matching gratings", Opt. Lett., vol. 23, no. 21, pp. 1695-1697, 1998.

[33] M. Charbonneau-Lefort and M. M. Fejer, and B. Afeyan, "Tandem chirped quasi-phase-matching grating optical parametric amplifier design for simultaneous group delay and gain control," Opt. Lett., vol. 30, no. 6, pp. 634-636, 2005.

[34] Y. L. Lee, Y.-C. Noh, C. Jung, T. J. Yu, B.-A. Yu, J. Lee, D.-K. Ko and K. Oh, "Reshaping of a second-harmonic curve in periodically poled Ti:$LiNbO_3$ channel waveguide by a local-temperature-control technique," Appl. Phys. Lett., vol. 86, no. 1, pp. 011104 (1-3), 2005.

[35] S. Gao, C. Yang, X. Xiao, G. Jin, "Broadband and multiple-channel visible laser generation by use of segmented quasi-phase-matching gratings," Optics Communications, vol. 233, no. 1-3, pp. 205-209, 2004.

[36] Z. Zheng, A. M. Weiner, K. R. Parameswaran, M. Chou, M. M. Fejer, "Femtosecond second-harmonic generation in periodically poled lithium niobate waveguides with simultaneous strong pump depletion and group-velocity walk-off," *J. Opt. Soc. Am. B*, vol. 19, no. 4, pp. 839-48, 2002.

[37] G. Imeshev, M. A. Arbore, M. M. Fejer, A. Galvanauskas, M. Fermann, D. Harter, "Ultrashort-pulse second-harmonic generation with longitudinally nonuniform quasi-phase-matching gratings: pulse compression and shaping," *J. Opt. Soc. Am. B*, vol. 17, no. 2, , pp. 304-18, 2000.

[38] A. Tehranchi, and R. Kashyap, "Design of novel unapodized and apodized step-chirped quasi-phase matched gratings for broadband frequency converters based on second harmonic

generation," IEEE J. Lightwave Technology, IEEE J. Lightwave Technol., vol. 26, no. 3, pp. 343-49, 2008.

[39] A. Tehranchi, and R. Kashyap, "Engineered gratings for flat broadening of second-harmonic phase-matching bandwidth in MgO-doped lithium niobate waveguides," Optics Express, vol. 16, no. 23, pp. 18970-75, 2008.

[40] A. Tehranchi, and R. Kashyap, "Novel designs for efficient broadband frequency doublers using singly pump-resonant waveguide and engineered chirped gratings," IEEE J. Quantum Electronics, vol. 45, no. 2, pp. 187-94, 2009.

[41] T. Suhara, M. Fujimura and M. Uemukai, "Waveguide nonlinear-optic wavelength conversion devices and their applications," in Photonics Based on Wavelength Integration and Manipulation, IPAP Books 2, pp. 137–150, 2005.

[42] S. J. B. Yoo, "Wavelength conversion technologies for WDM network applications," IEEE J. Lightwave Technol., vol. 14, no. 6, pp. 955-66, 1996.

[43] C. Langrock, S. Kumar, J. E. McGeehan, A. E. Willner, and M. M. Fejer, "All-optical signal processing using $\chi^{(2)}$ nonlinearities in guided-wave devices," J. Lightwave Technol. vol. 24, no. 7, pp. 2579-2592, 2006.

[44] T. Vo-Dinh, Biomedical Photonics Handbook, CRC Press, 2002.

[45] J. M. Schmitt "Optical coherence tomography (OCT): a review," IEEE J. Select. Topics Quantum Electron., vol. 5, no. 4, pp. 1205-15, 1999.

[46] H. Wang and A. M. Rollins, "Optimization of dual-band continuum light source for ultrahigh-resolution optical coherence tomography," Appl. Opt., vol. 46, no. 10, pp. 1787-94, 2007.

[47] Chinn S. R. and Swanson E. A., "Blindness limitations in optical coherence domain reflectometry," Electron. Lett., vol. 29, no. 23, pp. 2025–2027, 1993.

[48] K. Mizuuchi, H. Ohta, K. Yamamoto, and M. Kato, "Second-harmonic generation with a high-index-clad waveguide," *Opt. Lett.*, vol. 22, no. 16, pp. 1217-1219, 1997.

[49] R. Kashyap, "Phase-matched second-harmonic generation in periodically poled optical fibers," *Appl. Phys. Lett.*, vol. 58, no. 12, pp. 1233-5, 1991.

[50] R. Kashyap, "Phase-matched periodic electric-field-induced second-harmonic generation in optical fibers," *J. Opt. Soc. Am. B*, vol. 6, no. 3, pp. 313-28, 1989.

[51] R. Kashyap, "Design of step-chirped fibre Bragg gratings," *Opt. Commun.,* vol. 136, no. 5-6, pp. 461-9, 1997.

[52] R. Kashyap, Fiber Bragg Gratings, Academic Press, 1999.

[53] V. Y. Shur, E. L. Rumyantsev, E. V. Nirolaeva, E. I. Shishkin, O. V. Fursov, R. G. Batchko, L. A. Eyres, M. M. Fejer, and R. L. Byor, "Nanoscale backswitched domain patterning in lithium niobate," *Appl. Phys. Lett.*, vol. 76, no. 2, pp. 143–145, 2000.

[54] V. Y. Shur, "Domain engineering in lithium niobate and lithium tantalate: domain wall motion," *Ferroelectrics*, vol. 340, no. 1, pp. 3-16, 2006.

[55] M. H. Chou, K. R. Parameswaran, M. M. Fejer, and I. Brener, "Multiple-channel wavelength conversion by use of engineered quasi-phase-matching structures in $LiNbO_3$ waveguides," Opt. Lett., vol. 24, no. 16, pp. 1157-1159, 1999.

[56] M. Asobe, O. Tadanaga, H. Miyazawa, Y. Nishida, and H. Suzuki, "Multiple quasi-phase-matched $LiNbO_3$ wavelength converter with a continuously phase-modulated domain structure," Opt. Lett., vol. 28, no. 7, pp. 558-560, 2003.

[57] M. Asobe, O. Tadanaga, H. Miyazawa, Y. Nishida, and H. Suzuki, "Multiple quasi-phase-matched device using continuous phase nodulation of $\chi^{(2)}$ grating and its application to variable wavelength conversion," IEEE J. Quantum Electron., vol. 41, no. 12, pp. 1540-1547, 2005.

[58] M. Asobe, T. Umeki, O. Tadanaga, K. Yoshino, E. Yamazaki and A. Takada, "Low crosstalk and variable wavelength conversion using multiple QPM $LiNbO_3$ waveguide module," Electron. Lett., vol. 45, no. 10, pp. 519-521, 2009.

[59] T. Umeki, M. Asobe, Y. Nishida, O. Tadanaga, K. Magari, T. Yanagawa, and H. Suzuki, "Widely tunable 3.4 μm band difference frequency generation using apodized $\chi^{(2)}$ grating," Opt. Lett., vol. 32, no. 9, pp. 1129-31, 2007.

[60] A. Ashkin, G. D. Boyd, and J. M. Dziedzic, “Resonant optical second harmonic generation and mixing," IEEE J. of Quantum Electron., vol. 2, no. 6, pp. 109-124. 1966.

[61] R. G. Smith, "Theory of intracavity optical second-harmonic generation,” IEEE J. of Quantum Electron., vol. 6, no. 4, pp. 215-23, 1970.

[62] W. J. Kozlovsky, C. D. Nabors, and R. L. Byer, “Efficient second harmonic generation of a diode-laser-pumped CW Nd:YAG laser using monolithic MgO:$LiNbO_3$ external resonant cavities,” IEEE J. of Quantum Electron., vol. 24, no. 6, pp. 913-19, 1988.

[63] R. Paschotta, P. Kürz, R. Henking, S. Schiller, and J. Mlynek, “82% efficient continuous-wave frequency doubling of 1.06 μm with a monolithic MgO:$LiNbO_3$ resonator,” Opt. Lett., vol. 19, no. 17, pp. 1325-7, 1994.

[64] W. P. Risk, T. R. Gosnell, and A. V. Nurmikko, Compact Blue-Green Lasers, Cambridge University Press, 2003.

[65] R. Regener, and W. Sohler, “Efficient second-harmonic generation in Ti:$LiNbO_3$ channel waveguide resonators,” JOSA B, vol. 5, no. 2, pp. 267-77, 1988.

[66] K. Shinozaki, Y. Miyamoto, H. Okayama, T, Kamiioh, and T. Nonaka, “Second-harmonic generation device with integrated periodically domain-inverted regions and distributed Bragg reflector in a $LiNbO_3$ channel waveguide,” Appl. Phys. Lett., vol. 58, no. 18, pp. 1934-1936, 1991.

[67] Z. Weissman, A. Hardy, M. Katz, M. Oron, and D. Eger, “Second-harmonic generation in Bragg-resonant quasi-phase-matched periodically segmented waveguides,” Opt. Lett., vol. 20, no. 7, pp. 674-6, 1995.

[68] T. Suhara, M. Fujimura, K. Kintaka, H. Nishihara, P. Kurz, and T. Mukai, “Theoretical analysis of squeezed-light generation by second-harmonic generation,” IEEE J. of Quantum Electron., vol. 32, no. 4, pp. 690-700, 1996.

[69] M. Fujimura, T. Suhara, and H. Nishihara, “Theoretical analysis of resonant waveguide optical second harmonic generation devices,” J. Lightwave Technol., vol. 14, no. 8, pp. 1899-906, 1996.

[70] M. Fujimura, M. Sudoh, K. Kintaka, T. Suhara, and H. Nishihara, "Enhancement of SHG efficiency in periodically poled $LiNbO_3$ waveguide utilising a resonance effect," Electron. Lett., vol. 32, no. 14, p. 1283-1284,1996.

[71] M. Fujimura, M. Sudoh, K. Kintaka, T. Suhara, and H. Nishihara, "Resonant waveguide quasi-phase-matched SHG devices with electrooptic phase-modulator for tuning," IEEE J. Selected Topics in Quantum Electron., vol. 2, no. 2, pp. 396-400, 1996.

[72] C. Q. Xu, K. Shinozaki, H. Okayama, T. Kamijoh, "Second-harmonic generation using a fiber ring resonator with a $LiNbO_3$ waveguide and a semiconductor optical amplifier," Appl. Phys. Lett., vol. 69, no. 15, pp. 2154-6, 1996.

[73] D. J. L. Birkin, E.U. Rafailov, G. S. Sokolovskii, W.Sibbett, G. W. Ross, P. G. R. Smith, D. C. Hanna, "3.6 mW blue light by direct frequency doubling of a diode laser using an aperiodically poled lithium niobate crystal," Appl. Phys. Lett., vol. 78, no. 21, pp. 3172, 2001.

[74] R. Regener and W. Sohler, "Loss in low-finesse Ti:$LiNbO_3$ optical waveguide resonators," *Appl. Phys. B*, vol. 36, no. 3, pp. 143–147, 1985.

[75] C. Q. Xu, H. Okayama, K. Shinozaki, K. Watanabe, and M. Kawahara, "Wavelength conversions ~1.5 μm by difference frequency generation in periodically domain-inverted LiNbO3 channel waveguides," Appl. Phys. Lett., vol. 63, no. 9, pp. 1170–1172, 1993.

[76] M. H. Chou, J. Hauden, M. A. Arbore, and M. M. Fejer, "1.5-μm-band wavelength conversion based on difference-frequency generation in $LiNbO_3$ waveguides with integrated coupling structures," Opt. Lett., vol. 23, no. 13, pp. 1004-1006, 1998.

[77] D. Hofmann, G. Schreiber, C. Haase, H. Herrmann, W. Grundkotter, R. Ricken, and W. Sohler, "Quasi-phase-matched difference-frequency generation in periodically poled Ti:$LiNbO_3$ channel waveguides," Opt. Lett., vol. 24, no. 13, pp. 896-898, 1999.

[78] X. Liu, H. Zhang, and Y. Guo, "Theoretical analyses and optimizations for wavelength conversion by quasi-phase-matching difference frequency generation," IEEE J. Lightwave Technol., vol. 19, no. 11, pp. 1785-92, 2001.

[79] W. Liu, J. Sun, and J. Kurz, "Bandwidth and tunability enhancement of wavelength conversion by quasi-phase-matching difference frequency generation," Opt. Commun., vol. 216, no. 1-3, pp. 239-46, 2003.

[80] S. Gao, C. Yang, and G. Jin, "Conventional-band and long-wavelength-band efficient wavelength conversion by difference-frequency generation in sinuoidally chirped optical superlattice waveguides," Opt. Commun., vol. 239, no. 4-6, pp. 333-38, 2004.

[81] O. Tadanaga, T. Yanagawa, Y. Nishida, K. Magari, T. Umeki, M. Asobe, and H. Suzuki, "Widely tunable 2.3 μm-band difference frequency generation in quasiphase-matched $LiNbO_3$ ridge waveguide using index dispersion control," J. Appl. Phys., vol. 102, no. 3, pp. 033102 (1-5), 2007.

[82] K. Gallo, G. Assanto, and G. Stegeman, "Efficient wavelength shifting over the erbium amplifier bandwidth via cascaded second order processes in lithium niobate waveguides," Appl. Phys. Lett., vol. 71, no. 8, pp. 1020-1022, 1997.

[83] K. Gallo, and G. Assanto, "Analysis of lithium niobate all-optical wavelength shifters for the third spectral window," J. Opt. Soc. Amer. B, vol. 16, no. 5, pp. 741-753, 1999.

[84] M. H. Chou, I. Brener, M. M. Fejer, E. E. Chaban, and S. B. Christman, "1.5-μm-Band Wavelength Conversion Based on Cascaded Second-Order Nonlinearity in LiNbO3 Waveguides," IEEE Photon. Technol. Lett., vol. 11, no. 6, pp. 653-655, 1999.

[85] I. Brener, M. H. Chou, D. Peale, and M. M. Fejer, "Cascaded $\chi^{(2)}$ wavelength converter in $LiNbO_3$ waveguides with counter-propagating beams," Elec. Lett., vol. 35, no. 14, pp. 1155-1157, 1999.

[86] G. Schreiber, H. Suche, Y. L. Lee, W. Grundkotter, V. Quiring, R. Ricken and W. Sohler, "Efficient cascaded difference frequency conversion in periodically poled Ti:$LiNbO_3$ waveguides using pulsed and cw pumping," Appl. Phys. B, vol. 73, no. 5-6, pp. 501-504, 2001.

[87] Junqiang Sun, and Wei Liu, "Multiwavelength generation by utilizing second-order nonlinearity of $LiNbO_3$ waveguides in fiber lasers," Opt. Commun., vol. 224, no. 1-3, pp. 125-130, 2003.

[88] G. S. Kanter, P. Kumar, K. R. Parameswaran, and M. M. Fejer, "Wavelength-selective pulsed all-optical switching based on cascaded second-order nonlinearity in a periodically poled lithium-niobate waveguide," IEEE Photon. Tech. Lett., vol. 13, no. 4, pp. 341-343, 2001.

[89] X. Tang, Z. Wu, and P. Urquhart, "Temperature optimization for broad-band quasi-phase-matched difference frequency generation," IEEE J. of Lightwave Technol., vol. 22, no. 6, pp. 1622-1627, 2004.

[90] Y. L. Lee, H. Suche, Y. H. Min, J. H. Lee, W. Grundkötter, V. Quiring, and W. Sohler, "Wavelength- and time-selective all-optical channel dropping in periodically poled Ti:$LiNbO_3$ channel waveguides," IEEE Photon. Tech. Lett., vol. 15, no. 7, pp. 978-980, 2003.

[91] X. Liu and Y. Li, "Optimal design of DFG-based wavelength conversion based on hybrid genetic algorithm," Opt. Exp., vol. 11, no. 14, pp. 1677-1688, 2003.

[92] Y. L. Lee, C. Jung, Y.-C. Noh, I. Choi, D.-K. Ko, and J. Lee, H.-Y. Lee and H. Suche, "Wavelength selective single and dual-channel dropping in a periodically poled Ti:$LiNbO_3$ waveguide," Opt. Exp., vol. 12, no. 4, pp. 701-7, 2004.

[93] A.-C. Chiang, T.-D. Wang, Y.-Y. Lin, C.-W. Lau, Y.-H. Chen, B.-C. Wong, Y.-C. Huang, J.-T. Shy, Y.-P. Lan, Y.-F. Chen, and P.-H. Tsao, "Pulsed optical parametric generation, amplification, and oscillation in monolithic periodically poled lithium niobate crystals," IEEE J. OF Quantum Electron., vol. 40, no. 6, pp. 791-800, 2004.

[94] X. Liu, H. Zhang, Y. Guo, and Y. Li, "Optimal design and applications for quasi-phase-matching three-wave mixing," IEEE J. OF Quantum Electron., vol. 38, no. 9, pp. 1225-1233, 2002.

[95] Y. L. Lee, C. Jung, Y.-C. Noh, M. Y. Park, C. C. Byeon, D.-K. Ko, and J. Lee, "Channel-selective wavelength conversion and tuning in periodically poled Ti:$LiNbO_3$ waveguides," Opt. Exp., vol. 12, no. 12, pp. 2649-2655, 2004.

[96] M. Asobe, I. Yokohama, H. Itoh, and T. Kaino, "All-optical switching by use of cascading of phase-matched sum-frequency-generation and difference-frequency-generation processes in periodically poled $LiNbO_3$," Opt. Lett., vol. 22, no. 5, pp. 274-6, 1997.

[97] I. Yokohama, M. Asobe, A. Yokoo, H. Itoh, and T. Kaino, "All-optical switching by use of cascading of phasematched sum-frequency generation and difference-frequency generation processes," J. Opt. Soc. Am. B, vol. 14, no. 12, pp. 3368-3377, 1997.

[98] S. Gao , C. Yang, X. Xiao, Y. Tian, Z. You, and G. Jin, "Bandwidth enhancement and response flattening of cascaded sum- and difference-frequency generation-based wavelength conversion," Opt. Commun., vol. 266, no. 1, pp. 296-301, 2006.

[99] Y. Wang, B. Chen and C.-Q. Xu, "Polarisation-insensitive QPM wavelength converter with out-of-band pump," Electron. Lett., vol. 40, no. 3, pp. 189-91 , 2004.

[100] C.-Q. Xu and B. Chen, "Cascaded wavelength conversions based on sum-frequency generation and difference-frequency generation," Opt. Lett., vol. 29, no. 3, pp. 292-4, 2004.

[101] Y. L. Lee, B. Yu, C. Jung, Y. Noh, J. Lee, and D. Ko, "All-optical wavelength conversion and tuning by the cascaded sum- and difference frequency generation (cSFG/DFG) in a temperature gradient controlled Ti:PPLN channel waveguide," Opt. Exp., vol. 13, no. 8, pp. 2988-93, 2005.

[102] J. Wang, J. Q. Sun, C. H. Luo, and Q. Z. Sun, "Experimental demonstration of wavelength conversion between ps-pulses based on cascaded sum- and difference frequency generation (SFG+DFG) in $LiNbO_3$ waveguides," Opt. Exp., vol. 13, no. 19, pp. 7405–14, 2005.

[103] H. Furukawa, A. Nirmalathas, N. Wada, S. Shinada, H. Tsuboya, and T. Miyazaki, "Tunable all-optical wavelength conversion of 160-Gb/s RZ optical signals by cascaded SFG-DFG generation in PPLN waveguide," IEEE Photon. Technol. Lett., vol. 19, no. 6, pp. 384-6, 2007.

[104] J. Wang, J. Sun, J. R. Kurz, and M. M. Fejer, "Tunable wavelength conversion of ps-pulses exploiting cascaded sum- and difference frequency generation in a PPLN-fiber ring laser," IEEE Photon. Technol., Lett., vol. 18, no. 20, pp. 2093-5, 2006.

[105] S. Gao, C. Yang, X. Xiao, Y. Tian, Z. You, and G. Jin, "Performance evaluation of tunable channel-selective wavelength shift by cascaded sum- and difference-frequency generation in periodically poled lithium niobate waveguides," IEEE J. Lightwave Technol., vol. 25, no. 3, pp. 710-8, 2007.

[106] J. Wang, J. Sun, X. Zhang, D. Huang, and M. M. Fejer, "All-optical format conversions using periodically poled lithium niobate waveguides," IEEE J. Quantum Electron., vol. 45, no. 2, pp. 195-205, 2009.

[107] J. Wang, J. Sun, X. Zhang, D. Liu, D. Huang, "Proposal and simulation for all-optical format conversion between differential phase-shift keying signals based on cascaded second-order nonlinearities," Opt. Commun., vol. 281, no. 19, pp. 5019-24, 2008.

[108] J. Sun, H. Li, Y. Cheng, J. Li, "Tunable wavelength conversion of picosecond pulses based on cascaded sum and difference-frequency generation in quasi-phase-matched $LiNbO_3$ waveguides," Opt. Commun., vol. 281, no. 23, pp. 5874-83, 2008.

[109] B. Chen, and C.-Q. Xu, "Analysis of novel cascaded $\chi^{(2)}$ (SFG+DFG) wavelength conversions in quasi-phase-matched waveguides," IEEE J. Quantum Electron., vol. 40, no. 3, pp. 256-61, 2004.

[110] S. Yu, and W. Gu, "Wavelength conversions in quasi-phase matched $LiNbO_3$ waveguide based on double-pass cascaded $\chi^{(2)}$ SFG+DFG interactions," IEEE J. Quantum Electron., vol. 40, no. 11, pp. 1548-54 , 2004.

[111] S. Yu and W. Gu, "A tunable wavelength conversion and wavelength add/drop scheme based on cascaded second-order nonlinearity with double-pass configuration," IEEE J. Quantum Electron., vol. 41, no. 7, pp. 1007-11, 2005.

[112] G. Imeshev, M. Proctor, and M. M. Fejer, "Phase correction in double-pass quasi-phase-matched second-harmonic generation with a wedged crystal," Opt. Lett., vol. 23, no. 3, pp. 165-7, 1998.

[113] S. Yu, Y. J. Zhang, H. Zhang, W. Gu, "A tunable wavelength-interchanging cross-connect scheme utilizing two periodically poled $LiNbO_3$ waveguides with double-pass configuration," Opt. Commun., vol. 272, no. 2, pp. 480-3, 2007.

[114] A. Tehranchi, and R. Kashyap, "Response flattening of efficient broadband wavelength converters based on cascaded sum- and difference frequency generation in periodically poled lithium niobate waveguides," IEEE J. Quantum Electronics, vol. 45, no. 9, pp. 1114-20, 2009.

[115] A. Tehranchi, and R. Kashyap, "Efficient wavelength converters with flattop responses based on counterpropagating cascaded SFG and DFG in low-loss QPM $LiNbO_3$ waveguides," Optics Express, vol. 17, no. 21 , pp. 19113-19119, 2009.

[116] A. Tehranchi, and R. Kashyap, "Improved cascaded sum and difference frequency generation-based wavelength converters in low-loss quasi-phased-matched lithium niobate waveguides," Applied Optics, vol. 48, no. 31, pp. G143-7, 2009.

[117] A. Tehranchi, and R. Kashyap, "Wideband wavelength conversion using double-pass cascaded $\chi^{(2)}$: $\chi^{(2)}$ interaction in lossy waveguides," Opt. Commun., vol. 283, no. 7, pp. 1485-1488, 2010.

[118] H. Y. Shen, H. Xu, Z. D. Zeng, W. X. Lin, R. F. Wu, and G. F. Xu, "Measurement of refractive indices and thermal refractive-index coefficients of $LiNbO_3$ crystal doped with 5 mol. % MgO," Appl. Opt., vol. 31, no. 31, pp. 6695-97, 1992.

[119] B. Ramamurthy and B. Mukherjee, "Wavelength conversion in WDM networking," IEEE J. Selected Areas Commun., vol. 16, no. 7, pp. 1061-1073, 1998.

M. Matsuura, N. Kishi, and T. Miki, "Ultrawideband wavelength conversion using cascaded SOA-based wavelength converters," J. Lightwave Technol., vol. 25, no. 1, pp. 38-45, 2007.

[120] M. Matsuura, N. Kishi, and T. Miki, "All-optical wavelength conversion with large wavelength hopping by utilizing multistage cascaded SOA-based wavelength converters," IEEE Photon. Technol. Lett., vol. 18, no. 8, pp. 926-28, 2006.

[121] T. Durhuus, B. Mikkelsen, C. Joergensen, S. L. Danielsen, and K. E. Stubkjaer, "All-optical wavelength conversion by semiconductor optical amplifiers," J. Lightwave Technol., vol. 14, no. 6, pp. 942-954, 1996.

[122] P. E. Barnsley and P. J. Fiddyment, "Wavelength conversion from 1.3 to 1.55 μm using split contact optical amplifiers," IEEE Photon. Technol. Lett., vol. 3, no. 3, pp. 256-258, 1991.

[123] T. J. Morgan, R. S. Tucker, and J. P. R. Lacey, "All-optical wavelength translation over 80 nm at 2.5 Gb/s using four-wave mixing in a semiconductor optical amplifier," IEEE Photon. Technol. Lett., vol. 11, no. 8, pp. 982–984, 1999.

[124] A. Bilenca, R. Alizon, V. Mikhelashhvili, D. Dahan, G. Eisenstein, R. Schwertberger, D. Gold, J. P. Reithmaier, and A. Forchel, "Broadband wavelength conversion based on cross-gain modulation and fourwave mixing in InAs-InP quantumdash semiconductor optical amplifiers operating at 1550 nm," IEEE Photon. Technol. Lett., vol. 15, no. 4, pp. 563-565, 2003.

[125] J. P. R. Lacey, G. J. Pendock, and R. S. Tucker, "All-optical 1300-nm to 1550-nm wavelength conversion using cross-phase modulation in a semiconductor optical amplifier," IEEE Photon. Technol. Lett., vol. 8, no. 7, pp. 885-887, 1996.